THE ANNALS OF "DUNAREA DE JOS" UNIVERSITY OF GALATI

Fascicle IX
METALLURGY AND MATERIALS SCIENCE

Table of Content

THE ANNALS OF "DUNAREA DE JOS" UNIVERSITY OF GALATI
FASCICLE IX. METALLURGY AND MATERIALS SCIENCE
Nº. 3 - 2015, ISSN 1453 – 083X

ALUMINA INFLUENCE ON THE CORROSION RESISTANCE OF Ni-P-Al$_2$O$_3$COMPOSITE LAYERS

Tamara RADU

"Dunarea de Jos" University of Galati, Romania
e-mail: tradu@ugal.ro

ABSTRACT

This paper aims to analyze the corrosion resistance of composite layers based on Ni-P matrix and disperse phase alumina of 10 µm size, present in amounts of 5, 10 and 20 g / L in the nickel plating bath. The influence of alumina on the corrosion resistance of Ni-P-Al$_2$O$_3$ composite layers was tested in 0.1N hydrochloric acid solution compared to Ni-P layers with different phosphorus contents. The samples immersed in the corrosive environment were weighed every 7 days for 4 weeks. The corrosion rate was appreciated considering the loss of mass per area in time. Mass loss was calculated considering the total time of corrosion and the mass lost each week for determining the kinetics of the process. The variation curves of the corrosion rate are presented, depending on the chemical composition of the analyzed layers and the corrosion time.

KEYWORDS: Ni-P-Al$_2$O$_3$, composite coatings, corrosion rate, HCl 0.1N

1. Introduction

Ni-P-Al$_2$O$_3$ composite layers are an improved version of Ni-P coatings. Ni-P layers are obtained by electroless method, a method based on an autocatalytic reducing process.

Phosphorus is supplied by the reductant used, respectively sodium hypophosphite, and the content in the layer depends on the pH of the nickel bath. When the pH of the nickel plating bath is low (4-5%P), the phosphorus content is higher in the coating layer [1-3].

Ni-P layers have a different corrosion behavior depending on the content of phosphorus.

Thus coatings with high phosphorus content (9-12%) have best corrosion resistance, in diverse environments [4, 5]. Coatings with low-phosphorus content have good corrosion resistance in basic environments [1].

Ni-P layers were developed especially for high hardness and wear resistance, practically comparable to hard chrome layers. This characteristic was improved by achieving composite structures with disperse phases: SiC, WC, Al$_2$O$_3$ etc. [6 7]. The influence of these particles on corrosion resistance was also investigated as well as the influence of other particles such as TiO$_2$, Zr O$_2$, SiO$_2$ etc. [8, 9].

The influence of alumina on the corrosion resistance of Ni-P-Al$_2$O$_3$ composite layers is the subject of many research studies in the field, presenting different opinions and results [4, 10-14]. Some authors reported an increase of the corrosion resistance in the presence of alumina and another insignificant or even negative influence. These different results are given by the particles size and the amount of alumina introduced into the electroless nickel bath.

This paper aims to analyze the corrosion resistance of Ni-P matrix composite layers and disperse 10 µm size phase alumina, present in amounts of 5, 10 and 20 g/L in the nickel plating bath.

2. Experimental research

The experimental research studies aimed to obtain Ni-P coatings with different phosphorus content and composite layers by including in the Ni-P matrix alumina particles of 10 µm size for different quantities of alumina from the nickel-plating bath, respectively 5 g/L; 10 g/L and 20 g/L. This study also aimed to verify some controversial or insufficiently explained aspects, presented in literature, regarding Al$_2$O$_3$ influence on corrosion resistance. The composite and Ni-P layers were performed on samples with sizes of 30x60 mm, made of 0.4 mm thick steel sheet, with low carbon content. The strip surface was prepared by:

- chemical degreasing, at 80-90 ℃, followed by washing in warm (80-90 ℃) and cold water;
- hydrochloric acid 20%, pickling and washing in warm water (85-90 ℃).

The Ni-P coating was obtained in a solution of 25% nickel sulfate and 23% sodium hypophosphite. The sodium acetate was used as the complexion agent and the lead acetate was used for bath stabilizing. Working temperature was 85 °C. To vary the phosphorus content in the coating layer, the pH of the solution was varied, respectively, pH=3.64, for a high phosphorus content (9-10% P), pH=4.87 for the medium phosphorus content (7-8% P), and pH=6.60 for the low-phosphorus (5-6% P) content.

To obtain layers with similar thicknesses, the influence of pH on this parameter was taken into consideration (at the increase of the pH, the layer thicknesses increases) and the immersion duration was varied. The plated samples at pH=3.64 were kept in the solution for 15 minutes. The plated samples at pH = 4.87 were kept in the solution for 20 minutes and the plated samples at pH = 3.64 were kept in the solution for 25 minutes.

To remove the hydrogen a stirring at 200 rot./min. was imposed. To obtain composite layers in Ni-P matrix and alumina as disperse phase, the same solution was used in which was introduced alumina powder of 10 μm size in amounts of 5 g/L, 10 g/L and 20 g/L. The applied working parameters were: bath temperature - 85 °C, duration - 20 min, and pH = 4.83 and magnetic stirring 500 rot./min. to maintain the alumina in suspension. The samples were analyzed considering surface quality and were selected for corrosion process.

The corrosion resistance was made according to standard G31/2004. The test was conducted for a period of four weeks and the samples were weighed at every seven days.

The corrosion rate was calculated in $g/m^2 h$ depending on the total time of corrosion and each week to determine the kinetics of the process [15].

3. Results and discussion

The alumina influence on the corrosion resistance of the $Ni-P-Al_2O_3$ layers was examined in comparison with the Ni-P layers with different phosphorus contents. Figure 1 shows the corrosion rate of Ni-P layers. It was observed that after 168 h, 336 h and 504 h, the layers obtained at the lowest pH, which has the highest content of phosphorus, have had the best corrosion behavior. After 672 h, the corrosion rate of these layers is very similar to the corrosion of layers obtained at pH=4.87. The layers obtained at pH = 6.6 present the highest corrosion rate. These layers have the lowest content of phosphorus. The results confirm data from the literature.
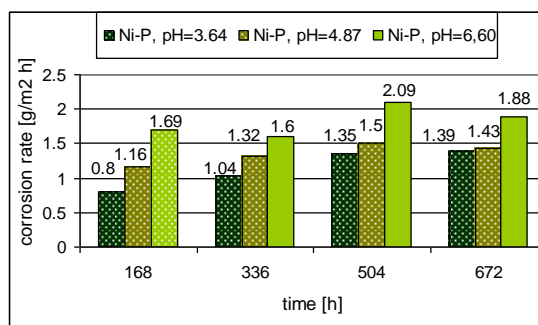
Fig. 1. *Corrosion rate of Ni- P layers in 0.1N HCl solution*

Figure 2 shows the kinetics of the corrosion process of the Ni-P layers every week. It was observed that layers with high phosphorus (pH=3.64) and medium (pH=4.87) content have similar behavior respectively the corrosion rate increases until week 3 and decreases in week 4 (due to the formation of the corrosion products on the surface). The layers with low phosphorus corroded more slowly in the 2nd week and very fast in week three, when corrosion products were formed that reduced the corrosion rate in week 4.

Figure 3 presents the results of the corrosion test for composite layers obtained in nickel plating bath with different content of alumina. The results show a very good corrosion behavior of the composite layers with Ni-P matrix and 10 μm size disperse phase alumina obtained in nickel bath with 20 g/L alumina.

The corrosion rate of these layers is almost twice lower than the other composite layers that behave comparably. This behavior is explained by the passivation of the surface by the alumina particles. Increasing the amount of particles, a larger area will be occupied by alumina which will ensure a higher resistance to corrosion.
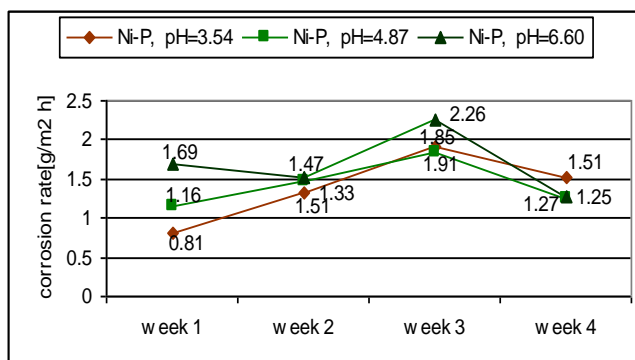
Fig. 2. Kinetics of the corrosion process of the Ni-P layers
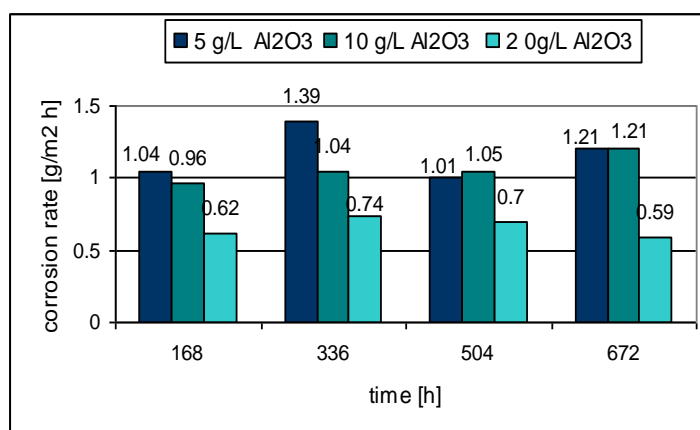
Fig. 3. Corrosion rate of Ni-P-Al₂O₃ layers in 0.1N HCl solution

The kinetics of the process presented in Figure 4 shows that in all weeks the layers obtained with 20 g/L alumina in the bath have the lowest rate of corrosion. Increasing the corrosion rate in week 2 is explained by the surface morphology of these layers. Because alumina is not a catalytic support for Ni, it causes the formation of dimples on the surface, resulting in a rough surface with nickel in relief and alumina in dimples (Figure 5). So the corrosion rate increases in week 2 through the preferential corrosion of nickel and in week 3 the surface is passive due to alumina and the corrosion rate decreases. In week 4 a higher quantity of alumina in the layers obtained in nickel bath with 20 g/L provides high resistance to corrosion compared to other layers that continue to corrode with higher rates.
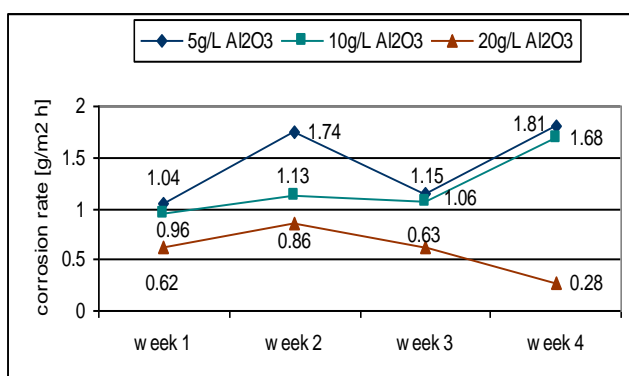
Fig. 4. Kinetics of the corrosion process for Ni-P-Al₂O₃ layers
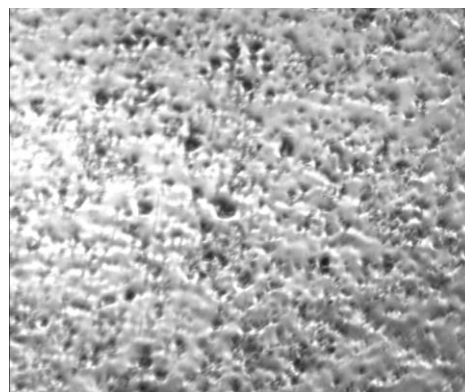
Fig. 5. Surface aspect of the Ni-P-Al₂O₃ composite layers

In Figure 6 is compared the corrosion behavior of Ni-P layers with high phosphorus content obtained at pH = 3.54 and of the composite layer of Ni-P-Al_2O_3 with different Al_2O_3 content depending on the amount of particles of alumina in the electrolyte. It can be noticed that all composite layers show a higher resistance to corrosion compared to Ni-P layers.
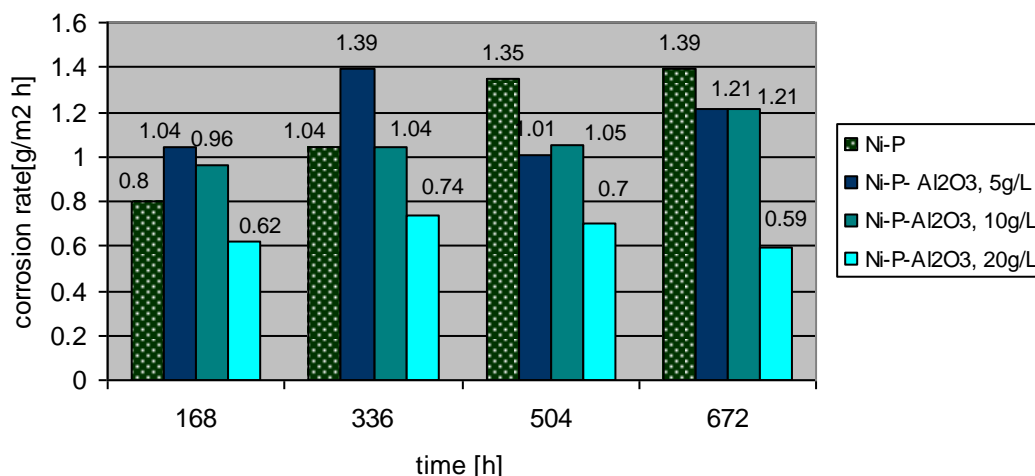
Fig. 6. *Comparative corrosion rate for the Ni-P layers and composite layers*

The different corrosion behavior of the layer is explained by the different kinetics of the corrosion process on the time intervals analyzed as shown in Figure 7. The Ni-P layers were subject to continuous corrosion until week 3 vs. the composite layers at which the process of corrosion slows in week 3.
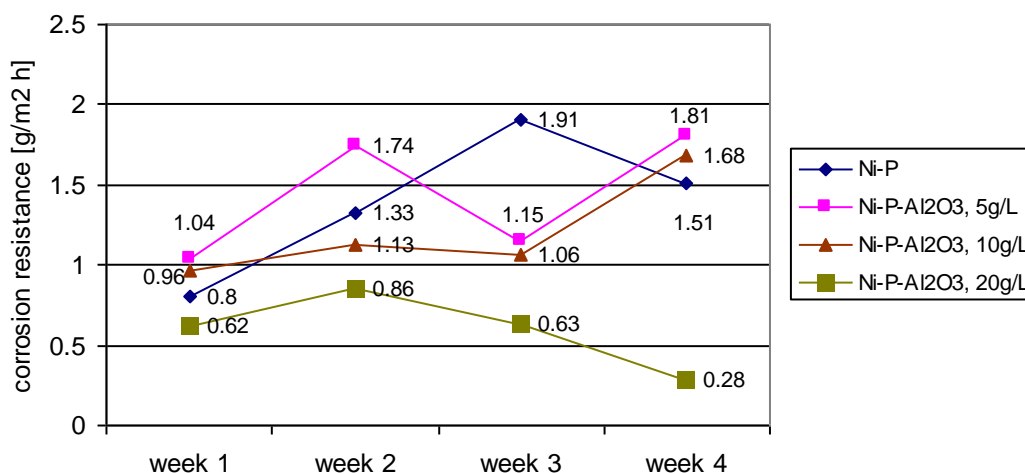
Fig. 7. *Comparative analysis of the kinetics of the corrosion process
for the Ni-P and Ni- P-Al_2O_3 layers*

4. Conclusions

The research has shown better corrosion behavior in 0.1N HCl for composite Ni-P-Al_2O_3 layers compared to Ni-P layers.

The presence of alumina of 10 μm size as disperse phase in Ni-P matrix leads to increased corrosion resistance in 0.1N HCl.

The highest corrosion resistance was shown by the layers obtained in nickel bath with 20 g/L alumina, respectively 0.59 g/m^2h;

The different kinetics of the corrosion process for Ni-P layers and composite layers explains the different behavior of corrosion. Because alumina is not a catalytic support for Ni, it forms dimples on the surface resulting in rough surfaces with nickel in relief and alumina in dimples. This surface structure will lead initially to a higher corrosion rate of the

composite layers. The surface leveling and passivation effect given by the alumina will ensure thereafter a lower corrosion rate of these layers.

References

[1]. **Glenn O. Mallory, Juan B. Hajdu**, *Electroless Plating: Fundamental and Applications*, International Headquarters in Orlando, Florida, Reprint Edition, available online, 2008.

[2]. **S. I. Balint, S. Constantinescu, L. Balint**, *Influence of heat treatment on the characteristics of Ni-P-Al$_2$O$_3$ composite layers,* SGEM Proceeding, vol. 1 p. 99, 2015.

[3]. **G. G. Istrate, S. I. Balint, A. Ciocan, V. Dragan**, *Influence of technological parameters on layer thickness to obtain Ni-P electroless coatings*, SGEM Proceeding, vol. 1, p. 113, 2015.

[4]. **T. Radu, M. Vlad, F. Potecasu, G. G. Istrate**, *Preparation and characterisation of electroless Ni-P-Al$_2$O$_3$ nanocomposite coatings*, Digest Journal of Nanomaterials and Biostructures Vol. 10, no. 3, p. 1055-1065, 2015.

[5]. **Z. Abdel Hamid, S. A. El Badry, A. Abdel Aal**, Surf. *&* Coat. Technol., 201, 2007.

[6]. **B. Elsener, M. Crobu, M. A. Scorciapino, A. Rossi**, Journal of Applied Electrochemistry, 38, (7), 2008.

[7]. **G. Jiaqiang, et al.**, Materials Letters, 59, (2-3), 2005.

[8]. **J. N. Balaraju, C. Anandan, K. S. Rajam,** Surf. *&* Coat. Technol., 200, (12-13), 2006.

[9]. **C. Li, Y. Wang, Z. Pan**, Materials and Design, 47, 2013.

[10]. **S. A Froukhteh, C. Dehghanian, M. Emamy**, Progres in Nature Science: Materials International, 22, (4), 2012.

[11]. **P. Gadhari, P. Sahoo**, Procedia Materials Science, 5, 2014.

[12]. **A. S. Hamdy, M. A. Shoeib, H. Hady, O. F. Abdel Salam**, Surf. & Coat., Technol, 202, 2007.

[13]. **L. K. Hari Krishnan, S. John, K. N. Srinivasan, J. Praveen, M. Ganesan, P. M. Kavimani**, Metallurgical and Materials Transactions A, vol. 37A, 2006.

[14]. **J. N. Balaraju, K. S. Rajam,** Surface & Coatings Technology, 200, p. 3933-3943, 2006.

[15]. **T. Radu, S. Constantinescu, L. Balint,** *Materiale metalice rezistente la coroziune*, Editura Ştiinţifică F. M. R., ISBN:973-8151-31-7, 2004.

INFLUENCE OF THE ANODIC OXIDATION TREATMENT ON THE CORROSION BEHAVIOUR OF ALUMINIUM AND ALUMINIUM ALLOYS

Valentin DUMITRAŞCU, Lidia BENEA*

Research (Competences) Centre: Interfaces-Tribocorrosion and Electrochemical Systems (CC-ITES),
Engineering Faculty, Dunărea de Jos University of Galati, 47 Domnească Street, RO-800008, Galati, Romania
*Corresponding author
e-mail: Lidia.Benea@ugal.ro

ABSTRACT

This paper deals with the effect of anodic oxidation treatment on the corrosion behaviour of 6061 aluminium alloy in natural sea water. Anodic oxidation treatment leads to the formation of an amorphous oxide layer on the top surface of 6061 aluminium alloy as shown by optical microscopy results. The corrosion behaviour was investigated in natural sea water, harvested from the Black Sea, Mangalia harbour. The study was done by in situ electrochemical methods such as: open circuit potential (OCP), electrochemical impedance spectroscopy (EIS), potentiodynamic polarization (PD) and cyclic voltammetry polarization (CV). The results show that the untreated 6061 aluminium alloy undergoes severe corrosion in natural sea water in comparison with anodized 6061 aluminium alloy. The results obtained by different electrochemical methods were in good agreement with each other and showed an improved corrosion resistance of the anodic oxide layer formed on aluminium alloy in natural sea water. The results were confirmed by optical microscopy.

KEYWORDS: anodic oxidation, aluminium, corrosion, aluminium alloy

1. Introduction

Materials with unusual combination of properties like low densities, strength, stiffness and impact resistance and which are not easily corroded are needed for aerospace, underwater and transportation applications and all of these conditions cannot be met by metals, conventional metallic alloys, ceramics and polymeric materials [1].

The nanocomposite and nanostructured materials can be fabricated by different physico-chemical methods such as chemical vapour deposition, sol-gel deposition, electrodeposition, electroless deposition. Electrodeposition and anodic oxidation are bottom-down methods to fabricate functional surfaces with nanoscale structures.

Aluminium alloys are widely employed within the spacecraft industry and they provide the required mechanical and corrosion properties, the choice of alloy series depending on application [2].

The surface modifications of aluminium alloy are generally performed by anodic oxidation, chemical oxidation, coatings, electroplating, etc. In order to improve the mechanical and electrochemical performance of aluminium alloys for corrosion protection, anodic structured oxide layers are always preformed before their application in automobile, marine and construction industries [3].

The development and application of anodic oxidation technology is the most rapid and versatile. Anodic films, composed of amorphous alumina, are formed by application of an anodic potential to aluminium that is immersed in a suitable electrolyte. For slightly alkaline electrolytes or those close to neutrality, when the solubility of the oxide is low, compact oxides (barrier–type films) are usually generated. In contrast, in electrolytes in which the solubility of the oxide is increased, porous oxides can be formed. The porous oxides are very important for industrial applications [4].

The major topics for corrosion research in relation to aluminium alloys have included localised corrosion of aluminium alloys containing magnesium, stress corrosion cracking of alloys used in aerospace applications, galvanic corrosion of aluminium in atmospheric and automotive applications, corrosion

inhibition and most recently the filiform corrosion of aluminium sheet [5].

The structural characteristics of the anodic oxide film formed on the aluminium surface and the intensity of corrosion attack are influenced by (i) the chemical composition of the exposed alloys, (ii) the presence and distribution of micro-defects (vacancies, voids, etc.) as well as macro-defects (inclusion, second phase particles) and (iii) by electrolyte composition (pH, halide concentration, temperature). In general, pitting on the aluminium alloy surface takes place in the presence of an electrolyte within a 4.5–8.5 pH range and tends to increase with an increase in temperature, concentration of aggressive ions and stagnation of the electrolyte [6].

Different types of aluminium alloy present different corrosion behaviour in marine environment due to the distribution of the intermetallic phases. The presence of different alloying elements can promote the formation of corrosion micro-cells and initiates the local corrosion process [7].

However, the corrosion behaviour of the aluminium alloys is poor in marine environmental and tends to localized corrosion, pitting corrosion, intergranular corrosion, etc. which can affect the service life of aluminium alloy components.

The anodic oxide film on the surface of 6061 Aluminium alloy was generated in sulphuric acid anodization bath. The aim of this work was to evaluate and compare the corrosion behaviour of 6061 aluminium alloy before and after the anodic oxidation process, in sea water harvested from the Black Sea, Mangalia harbour by electrochemical methods.

2. Experimental procedure

2.1. Materials

The tested material selected for study is 6061 aluminium alloy. The composition of the 6061 aluminium alloy specimens is given in Table 1.
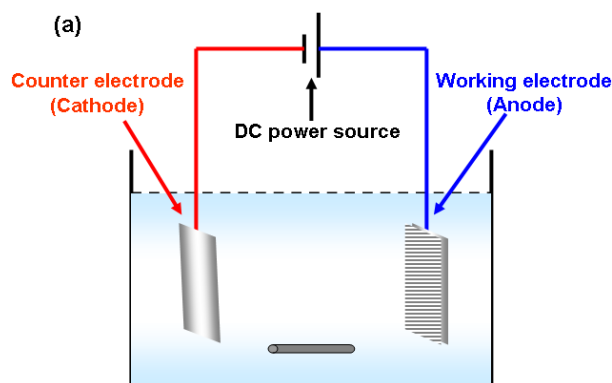
Table 1. *Composition of the 6061 aluminium specimens (% by weight)*

Element	Composition (%)
Si	0.4
Fe	0.2
Cu	0.15
Mn	0.15
Mg	0.8
Cr	0.04
Zn	0.25
Ti	0.15
Al	Balance

2.2. Preparation of anodic films

Before the anodization process, the samples of 6061 aluminium alloy with rectangular shape of 20x20x2 mm were connected with a copper wire and isolated with epoxy resin to delimit the active surface. The samples were degreased with acetone, rinsed with deionized water and dried at room temperature.

The electrochemical cell set-up used in anodization process, shown in Fig. 1 (a), consists of two electrodes, the first one being the sample of 6061Aluminium alloy used as working electrode (anode) and the other one being the counter electrode (cathode). The anodizing process was carried out in 300 mL electrolyte of 1M H_2SO_4 to which 1 gL^{-1} of $Al_2(SO_4)_3 \cdot 18H_2O$ was added. The temperature was maintained at 25 ± 1 ºC.

After the anodization process, the samples were washed with deionized water and boiled in deionized water for 5 min. at 95 ºC in order for the pores to be sealed.
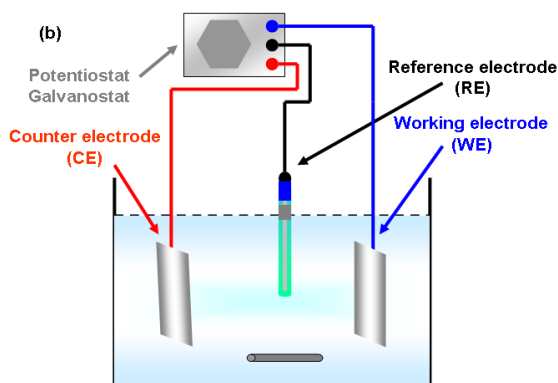
Fig. 1. *(a) The anodization cell set-up and (b) the electrochemical cell set-up for corrosion tests*

2.3. Characterization methods

The comparative corrosion behavior was tested in natural sea water, harvested from the Black Sea, Mangalia harbor. The characteristics of sea water are presented in Table 2.

Table 2. *Characteristics of sea water*

pH	Conductivity [mS]	Salinity [ppt]
7.63	21	12.4

The surface morphology of anodized 6061 aluminium alloy was compared with that of polished metal surface using the optical microscope OPTIKA XDS-3 MET.

The optical microscope images were recorded to establish the interaction of sea water environment with the surface of 6061 aluminium alloy. After the immersion of untreated and anodized 6061 aluminium alloy in natural sea water, the surface morphology was compared to the images recorded before immersion.

Electrochemical tests were carried out using a VoltaLab PGZ 100 potentiostat/galvanostat. It was used a conventional three-electrode cell shown in Fig. 1 (b) consisting of 6061 aluminium sample as working electrode (WE), an Ag/AgCl (saturated solution of KCl, E=199 mV vs. Standard Hydrogen Electrode) as reference electrode (RE) and Pt-Rh grid as counter electrode (CE). The surface area exposed to the electrolyte was about 1.7 cm^2. The electrochemical methods applied were: open circuit potential, potentiodynamic polarization and cyclic voltammetry.

3. Results and discussion

3.1. Surface characterization of the coatings before and after anodic oxidation

Fig. 2. displays the comparative surfaces morphologies of untreated 6061 aluminium alloy and 6061 aluminium alloy after the anodic oxidation treatment.

From Fig. 2 (a) it can be observed that the surface of untreated 6061 aluminium alloy is characterized by irregular shape with no homogenous distribution. Fig. 2 (b) shows the typical surface of 6061 aluminium alloy after the anodic oxidation in 1M H_2SO_4 to which 1g/L $Al_2(SO_4)_3 \cdot 18H_2O$ was added for 45 min at a constant current density of 15 mA/cm^2. Anodizing time, current density and electrolytes are important parameters in determining the film thickness of porous alumina. The specified parameters are established after many experiments regarding the current density and time of the anodizing process.

After oxide film formation, the samples were boiled in deionised water for 5 min. at 95°C to obtain a real barrier oxide layer with closed pores. From Fig. 2 (b) it can be observed that the anodized aluminium surface presents a rough surface. The anodic film generated on the 6061 aluminium alloy appears to be more regular, with relatively straight pores and continuous cell walls. This occurs because the oxidation of the major alloying element, magnesium, proceeds immediately with aluminium and does not induce oxygen generation within the barrier layer and consequent lateral porosity [8].
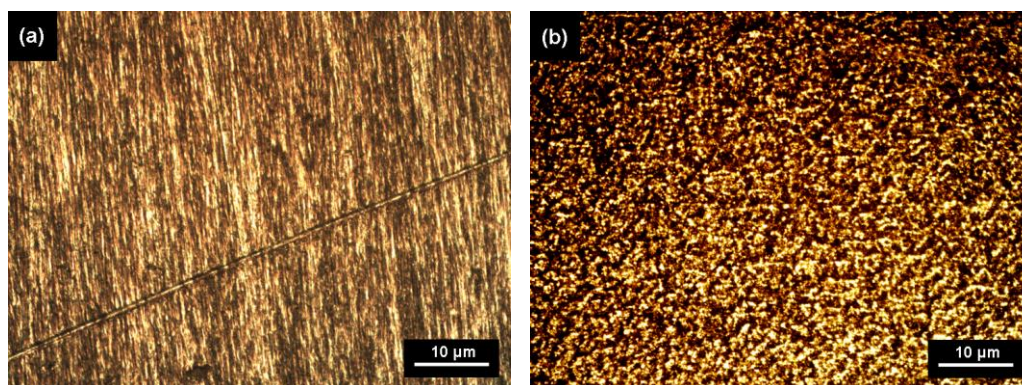
Fig. 2. *Optical micrograph of 6061 aluminium alloy (a) before and (b) after the anodic treatment*

3.2. Evolution of open circuit potential (OCP)

When an electrically conductive material is immersed in an electrolyte, a potential difference called electrode potential appears at the solution material interface. The analysis of the potential versus time offers useful information about the behavior of material in contact with a wet corrosive environment. In Fig. 3. is shown the evolution of the open circuit

potential (OCP) of untreated 6061 aluminium alloy and anodized 6061 aluminium alloy.
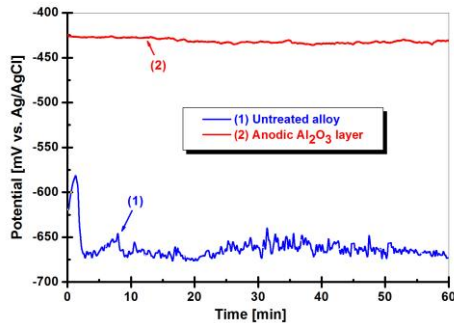
Fig. 3. *Evolution of open circuit potential for: (1——) untreated and (2——) anodic oxidized 6061 aluminium alloy in sea water*

From Fig. 3 it can be observed that the potential of anodic aluminium oxide layer is stable around -425 mV vs. Ag/AgCl. After the immersion of untreated 6061 aluminium alloy in sea water it can be observed that the potential initially decreased rapidly because of dissolution of air-formed aluminium oxide and after that, the potential is stabilized around 660 mV vs. Ag/AgCl. This trend was observed also by F.J. Garcia-Garcia *et al.* [9] when they studied the influence of Ni on corrosion behaviour for 1050 aluminium alloy.

The open circuit behaviour during immersion time indicates that the anodized 6061 aluminium alloy shows more noble and stable corrosion potential value compared to the untreated aluminium alloy. This behaviour of ennoblement of corrosion potential by controlled oxide film formation was also observed by L. Benea *et al.* [10] when they studied the influence of anodic oxidation on the corrosion behaviour of Ti-6Al-4V alloy in physiological fluids.

3.3. Potentiodynamic polarization

The diagrams I = f(E) (intensity-potential curves) shown in Fig. 4 were recorded in a range of potentials starting from -1.2 V to +0.2 V vs. Ag/AgCl at a scan rate of 5 mV/s. Corrosion current density is an important parameter to evaluate the kinetics of the corrosion reactions [11].

The polarization curves were performed to assess the polarization domains for the untreated and anodized 6061 aluminium alloy after immersion in the natural sea water. If the passive state covers a higher potential domain and the passivation current value is smaller, then the metal or alloy shows a high corrosion resistance.

From Fig. 4 it can be observed that for both of the studied surfaces, the cathodic domain is not present. For anodized 6061 aluminium alloy, the passive current density is very low, being close to zero, indicating a good corrosion resistance for the entire studied domain. For untreated 6061 aluminium alloy, the passive domain is ranged between -1.2 V vs. Ag/AgCl and -0.4 V vs. Ag/AgCl and after that the transpassive domain is observed, where the current density increases since this is a transpassive dissolution. In this domain, the passive film is dissolved and loses its protective properties and even disappears at high potential values.
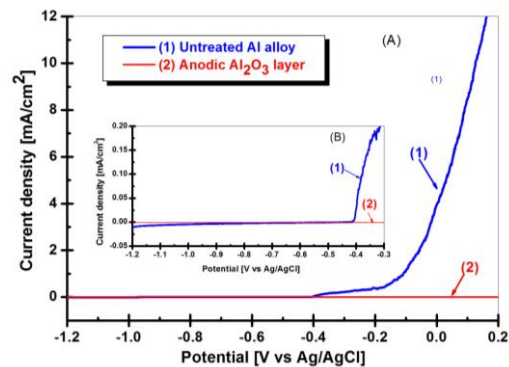
Fig. 4. *Potentiodynamic diagrams for: (1——) untreated and (2——) anodic oxidation 6061 aluminium alloy. Layer (A) gives the entire potential domain scanned while layer (B) provides the zoom of recorded diagrams in the passive domain.*

From the polarization diagrams by applying the Stern Geary formula (Equation 1) there were calculated the polarization resistances and corrosion current densities. For simple corrosion systems, the corrosion reactions are strictly controlled by charge transfer and the corrosion current density (i_{corr}) can be correlated with the polarization resistance (R_p) by Equation (1).

$$i_{cor} = \frac{B}{R_p} \qquad (1)$$

Where: the corrosion rate (i_{corr}) is expressed as corrosion current density in A / cm^2 and B is a constant related to the system material environment given by the relation:

$$B = \frac{b_a |b_c|}{2,303(b_a + b_c)} \qquad (2)$$

Where: b_a and b_c are the Tafel slopes for anodic and cathodic reactions.

The increase of polarization resistance means the decrease of corrosion current density, therefore the decrease of corrosion rate.

From the polarization diagrams, the values of corrosion current densities and polarization resistance for both surfaces are presented in Table 3.

Table 3. *The values of corrosion current densities and polarization resistance*

Nr crt	Type of surface	Polarization resistance [$kohm \cdot cm^2$]	Corrosion current density [$\mu A / cm^2$]
1	Untreated Al alloy	17.2	0.5
2	Anodized Al alloy	3160	0.0016

The polarization resistance increases from 17.2 $kohm \cdot cm^2$ for untreated 6061 aluminium alloy to 3.16 $Mohm \cdot cm^2$ for anodized aluminium alloy. The corrosion current density decreases from 0.5 $\mu A/cm^2$ for untreated 6061 aluminium alloy to 0.0016 $\mu A/cm^2$ for anodized aluminium alloy.

3.4. Cyclic voltammetry

The cyclic voltammograms (Fig. 5) of untreated and anodized 6061 aluminium alloy were recorded in the potential range of -1.2 V vs. Ag/AgCl to +0.2 V vs. Ag/AgCl at a scan rate of 5 mV/s and then reversed with the same scan rate till the starting potential to form one complete cycle.

The highlighted areas with localized corrosion susceptibility can be seen very well due to the specific hysteresis aspect, in the presence of chloride ions, which presents the anodic transpassivation part of the untreated 6061 aluminium alloy curves [6]. The specific hysteresis aspect indicates that untreated 6061 aluminium alloy is susceptible to pitting and crevice corrosion in marine environment. In comparison with untreated aluminium alloy, anodized aluminium does not reveal pitting corrosion susceptibility behaviour, since the specific hysteresis aspect is completely missing [12].

From Fig. 5 it can be observed that upon the onset of the transpassive region, the current still raises up until the potential is reversed in the case of untreated 6061 aluminium alloy immersed in seawater, indicating a susceptibility to pitting corrosion. On the other hand, for anodized 6061 aluminium alloy, the potential remains constant on the entire studied range of potential.
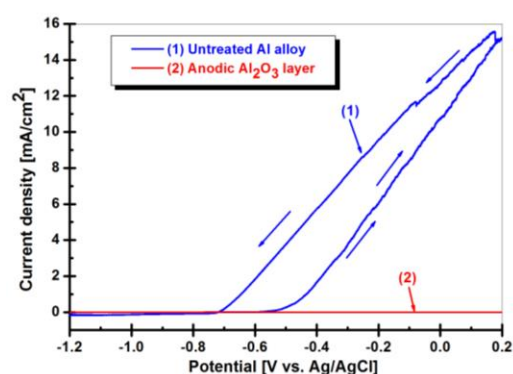
Fig. 5. *Cyclic voltammetry for: (1——) untreated and (2——) anodic oxidation 6061 aluminium alloy untreated and anodized 6061 aluminium alloy*

3.5. Surface morphology after corrosion tests

The optical microscopy images of freshly polished surface of 6061 aluminium alloy are given in Fig. 2 (a), which shows a polished surface with a few scratches because of polishing and anodized surface of 6061 aluminium alloy in Fig. 2 (b).
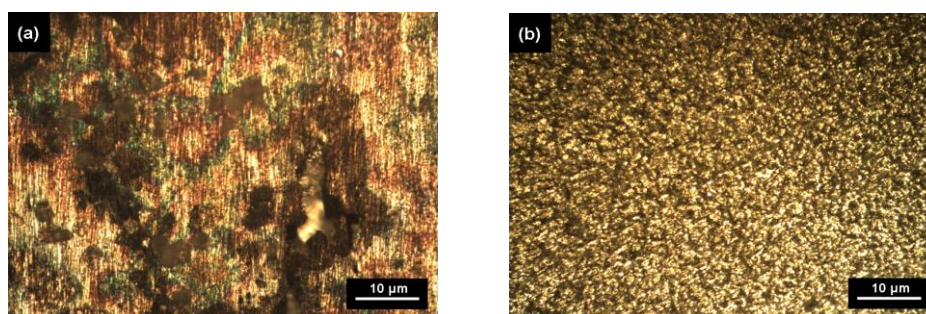
Fig. 6. *Optical microscopy after corrosion in sea water for: (a) untreated 6061 aluminium alloy; (b) anodized 6061 aluminium alloy*

After the corrosion tests, the surface morphologies of untreated and anodized 6061 aluminium alloy was recorded and are given in Fig. 6 (a). and Fig. 6 (b).

The image of corroded sample presented in Fig. 6 (a) shows the degradation of untreated 6061 aluminium alloy with more and less uniform attack in natural sea water. From Fig. 6 (b) it can be observed that the anodic oxide layer formed after anodic treatment does not undergo any corrosion attack.

4. Conclusion

In this work, the corrosion resistance of untreated and anodized 6061 aluminium alloy was studied by electrochemical methods. The electrochemical methods and surface morphology characterization showed that the anodic oxidation treatment enhanced the corrosion resistance due to the formation of a continuous adherent alumina layer on the aluminium alloy surface.

Electrochemical methods for corrosion resistance evaluation are ideal tools for obtaining detailed information about the characteristics of the anodized aluminium alloy compared to the untreated alloy. They can quantify the changes of the barrier layer with immersion time.

The polarization resistance increases from 17.2 $kohm \cdot cm^2$ for untreated 6061 aluminium alloy to 3.16 $Mohm \cdot cm^2$ for anodized aluminium alloy.

The corrosion rate decreases from 0.5 $\mu A/cm^2$ for untreated 6061 aluminium alloy to 0.0016 $\mu A/cm^2$ for anodized aluminium alloy.

From the cyclic voltammograms of both studied surfaces it can be observed that the untreated 6061 aluminium alloy presents the specific hysteresis which indicates the susceptibility to pitting and crevice corrosion in comparison with anodized aluminium alloy.

The better corrosion resistance of anodized oxide layer formed on aluminium alloy results is confirmed by the optical microscopy images obtained after corrosion tests.

Acknowledgements

References

[1]. **K. R. Padmavathi, R. Ramakrishnan,** *Tribological behaviour of aluminium hybrid metal matrix composite*, Procedia Engineering, 97, p. 660-667, 2014.

[2]. **R. Grilli, M. A. Baker, J. E. Castle, B. Dunn, J. F. Watts,** *Corrosion behaviour of a 2219 aluminium alloy treated with chromate conversion coating exposed to a 3.5% NaCl solution*, Corrosion Science, 53, p. 1214-1223, 2011.

[3]. **J. Y. Wang, C. Li, C. Y. Yin, Y. H. Wang, S. L. Zheng,** *Ultrasmall nanopores obtained by electric field enhance one-step anodization of aluminium alloy*, Surface & Coatings Technology, 258, p. 615-623, 2014.

[4]. **M. Curioni, P. Skeldon, G. E. Thompson**, *Chapter 5– Anodized anti-corrosion coatings for aluminium using rare earth metals*, from *Rare-earth based corrosion inhibitors*, Edited by: *M. Forsyth and B. Hinton*, Woodhead Publishing Series in Metals and Surface Engineering, ISBN: 978-0-85709-347-9, 2014.

[5]. **N. Birbilis, B. Hinton**, *Chapter 19 – Corrosion and corrosion protection of aluminium*, from Fundamentals *of aluminium metallurgy – production, processing and applications*, Edited by: R. Lumley, Woodhead Publishing Series in Materials, ISBN: 978-0-85709-025-6, 2011.

[6]. **H. Ezuber, A. El-Houd, F. El-Shawesh**, A *study on the corrosion behaviour of aluminium alloys in seawater*, Materials and Design, 29, p. 801-805, 2008.

[7]. **J. Ryl, J. Wysocka, M. Jarzynka, A. Zielinsky, J. Orlikowski, K. Darowicki**, *Effect of native air-formed oxidation on the corrosion behaviour of AA 7075 aluminium alloys*, Corrosion Science, 87, p. 150-155, 2014.

[8]. **M. Garcia-Rubio, P. Ocon, M. Curioni, G.E. Thompson, P. Skeldon, A. Lavia, I. Garcia**, *Degradation of the corrosion resistance of anodic oxide films through immersion in the anodizing electrolyte*, Corrosion Science, 52, p. 2219-2227, 2010.

[9]. **F. J. Garcia-Garcia, P. Skeldon, G. E. Thompson, G. C. Smith**, *The effect of nickel on alloy microstructure and electrochemical behaviour of AA1050 aluminium alloy in acid and alkaline solutio*ns, Electrochimica Acta, 75, p. 229-238, 2012.

[10]. **L. Benea, E. Mardare-Danaila, M. Mardare, J. P. Celis**, *Preparation of titanium oxide and hydroxyapatite on Ti–6Al–4V alloy surface and electrochemical behaviour in bio-simulated fluid solution*, Corrosion Science, 80, p. 331-338, 2014.

[11]. **M. Mubarak Ali, V. Raj**, *Formation and characterization of ceramic nanocomposite crystalline coatings on aluminium by anodization*, Journal of Materials Science & Technology, 29(7), p. 595-602, 2013.

[12]. **B. Zaid, D. Saidi, A. Benzaid, S. Hadji**, *Effects of pH and chloride concentration on pitting corrosion of AA6061 aluminium alloy*, Corrosion Science, 50, p. 1841-1847, 2008.

INFLUENCE OF SECONDARY REFINING TREATMENTS ON THE QUALITY OF HIGH-GRADE STEEL USED IN OIL AND GAS INDUSTRY

Anisoara CIOCAN

"Dunarea de Jos" University of Galati, 111, Domnească Street, 800201, Galaţi, Romania
e-mail: aciocan@ugal.ro

ABSTRACT

Steel is the most important alloy used in oil and gas industry from production and processing to the distribution of refined products. In this research is analyzed the production technology of steel intended for long pipeline used in conveying gas and oil in the natural gas and oil industries. Data from 14 melts were analyzed. The basic oxygen furnace (BOF) is used for steelmaking. The secondary refining processes were conducted at the ladle furnace station by forming an active ladle slag and using the mixing of bath with argon. Steel degassing is conducted in RH vacuum degassing equipment. The variation of chemical composition, especially the content of carbon, oxygen, and hydrogen, was analyzed according to parameters of industrial technology.

KEYWORDS: steel, pipeline, oil and gas industry, secondary refining treatments

1. Introduction

High grade steels with special properties must be utilized in oil and gas industry [1, 2]. These steels are produced in the basic oxygen furnace (BOF) and then mill rolled. The thick sheets of steel are obtained in order to make pipes that work in adverse temperature conditions to transport oil and natural gas in oil and gas industry.

The cleanness assessment of high quality steels is provided through refining treatments developed in secondary steelmaking steps. These treatments are performed in ladle furnaces (LF) and in RH vacuum degassing units, pieces of equipment typically used in the mass production of high-purity steel in integrated steel mills plants. The most important functions of secondary refining are final desulphurization, degassing gas components such as oxygen, nitrogen, hydrogen, etc., removal of inclusions and final decarburization (for ultra-low carbon steel) [3-6].

In this research the refined treatments applied to molten steel before continuous casting were conducted in a ladle furnace. Moreover, the vacuum treatment is performed in a RH degassing station.

2. Experimental research

The chemical composition and mechanical properties of the steel suitable for long pipeline used in conveying gas and oil in the natural gas and oil industries in accordance with API SPEC 5L specification of standard [7] are given in Tables 1 and 2.

Table 1. Chemical composition of X65 steel grade (wt.%)

C	Si	Mn	P	S	Al	Ti	V	Mo	Nb	Ca	H₂ *	N₂ *
0.06 – 0.09	0.25 – 0.35	1.40 – 1.55	0.018	0.006	0.02 – 0.05	0.01 – 0.016	0.04 – 0.055	0.07 – 0.010	0.04 – 0.06	0.002	max. 3.0	max. 0.0070
* ppm												

The specific temperatures of X65 steel grade are the following: liquidus temperature 1521 ºC; optimum tapping temperature 1546 ºC; maximum casting temperature 1580 ºC. The steel was made in a basic oxygen furnace (BOF). The primary raw materials were pre-desulfured liquid hot metal (S =

0.006%) and steel scrap in balance. A ladle furnace (LF) with the capacity of 180 t of steel was used for refining molten steel. Data from 14 melts were analyzed. In the LF the steel was reheated.

Table 2. *Mechanical properties of X65 steel grade*

R_c, [MPa]	$R_{p0.5}$, [MPa]	R_m, [MPa]	A, [%]	Charpy V - notch values at test temperature -51 ºC, [J]
≥ 240	≥ 448	≥ 531	19 – 23	18

The temperature was properly adjusted depending on requirements. An active ladle slag with basic characteristics and physical properties adapted to the temperature close to the liquidus temperature of steel was used for liquid steel coverage during treatment. The literature recommends for carbon aluminum-killed steels the slag of the system CaO – Al_2O_3 – SiO_2: 45 – 60% CaO, <10% MgO, 25-40 Al_2O_3, <20% SiO_2, <0.5% (FeO+MnO) [8-10].

During treatment, argon is continuously stirred in liquid steel. So the metallurgical reactions such as deoxidation, desulphurization and removal of oxide-inclusions can be managed. All these steps have allowed to precisely adjust the final chemical composition and to obtain the quality required for the steel.

To remove hydrogen and nitrogen from molted steel, RH vacuum unit was used. Before degassing, the reactor was cleaned to remove crusts and then preheated to over 1000 ºC. The ladle freeboard was of about 600 mm. To achieve a homogeneous bath temperature and composition, the steel in the ladle is stirred by means of argon gas bubbling. The volume of argon stirring gas varied in the range of 3.5 – 6.7 Nm^3/t. The recirculation of liquid steel started when a vacuum of 20-30 torr was reached. After 6-8 minutes when the 1 torr depression was reached, the addition of microalloying and deoxidizing materials has been initiated. The materials addition procedure lasted for 8-10 minutes. In the end, the molten steel temperature and the chemical composition were homogenized for a period of 5 minutes.

3. Results and discussion

The chemical composition of the steel after tapping from BOF and in LF is given in Table 3, respectively in Table 4. Adding alloy additives in the form of ferroalloys into steel is one of the most important stages of secondary metallurgy. During LF treatment the chemical composition was corrected by Ti, V, Nb Mo.

Table 3. *Chemical composition of steel after tapping from BOF (wt.%)*

No. melt	C	Mn	P	S	Si	Al	Mo
1	0,04	1.18	0.011	0.012	0.12	0.005	-
2	0.04	1.24	0.011	0.010	0.30	0.008	0.077
3	0.03	0.90	0.010	0.010	0.25	0.006	0.070
4	0.03	1.14	0.010	0.012	0.23	0.006	0.084
5	0.03	0.58	0.008	0.010	0.12	0.003	0.072
6	0.03	1.08	0.009	0.010	0.19	0.008	0.085
7	0.04	0.75	0.008	0.009	0.20	0.013	0.080
8	0.04	0.84	0.008	0.012	0.18	0.005	0.080
9	0.03	1.13	0.009	0.010	0.20	0.010	0.084
10	0.04	1.29	0.008	0.010	0.21	0.006	0.083
11	0.04	1.24	0.009	0.012	0.29	0.008	0.083
12	0.06	1.35	0.009	0.011	0.21	0.006	0.083
13	0.03	1.07	0.007	0.010	0.15	0.005	0.073
14	0.03	1.10	0.008	.008	0.17	0.006	0.074

***Table 4.** Chemical composition of steel in the LF station, (wt.%)*

No. melt	Chemical composition (wt.%)										
	C	Si	Mn	P	S	Al	Ti	V	Mo	Nb	Ca
1	0.08	0.27	1.49	0.017	0.005	0.024	0.005	-	0.068	0.030	-
2	0.07	0.33	1.45	0.019	0.009	0.026	0.017	0.027	0.083	0.035	-
3	0.08	0.26	1.52	0.013	0.010	0.044	0.011	0.033	0.073	0.040	0.0008
4	0.07	0.33	1.45	0.017	0.009	0.054	0.019	0.032	0.085	0.040	-
5	0.05	0.26	1.43	0.010	0.010	0.054	0.015	0.027	0.074	0.035	-
6	0.05	0.33	1.50	0.017	0.008	0.044	0.010	0.032	0.090	0.039	0.0030
7	0.06	0.289	1.38	0.015	0.007	0.035	0.019	0.025	0.083	0.030	0.00018
8	0.07	0.25	1.50	0.017	0.012	0.020	-	0.025	0.080	0.033	0.0010
9	0.07	0.26	1.49	0.014	0.009	0.037	0.012	0.032	0.085	0.040	0.0005
10	0.07	0.25	1.50	0.011	0.008	0.036	0.012	0.032	0.083	0.036	0.0005
11	0.07	0.28	1.59	0.011	0.010	0.046	0.014	0.032	0.083	0.037	0.0005
12	0.07	0.26	1.50	0.011	0.009	0.050	0.013	0.032	0.083	0.042	0.0001
13	0.07	0.37	1.57	0.016	0.007	0.033	-	0.029	0.077	0.037	0.0004
14	0.08	0.33	1.44	0.013	0.007	0.021	0.019	0.024	0.075	0.034	0.0002

***Table 5.** Aluminium and oxygen contents of steel after RH refining*

No.	Al [%]	Oxygen [ppm]
1	0.034	2.5
2	0.049	2.9
3	0.048	2.1
4	0.042	2.2
5	0.040	2.4
6	0.043	2.9
7	0.037	2.4
8	0.040	3.0
9	0.035	2.5
10	0.041	3.1
11	0.045	2.5
12	0.043	2.4
13	0.038	2.6
14	0.033	2.5

***Table 6.** Hydrogen content during refining treatment, in ppm*

No.	Time of the test				
	In LF		In RH		
	Initial H content at tapping from BOF	Final H content at output from LF	Initial H content after feeding into RH station	Final H content at output from RH station	H content at continuous casting machine
1	6.2	6.5	6.5	1.4	1.4
2	6.7	7.0	7.0	1.7	1.7
3	7.1	7.3	7.3	2.3	2.3
4	7.0	7.4	7.4	2.4	2.4
5	6.6	6.9	6.9	1.9	1.9
6	10.1	10.6	10.6	3.5	3.5
7	6.8	7.1	7.1	2.2	2.2
8	6.7	7.0	7.0	2.3	2.3
9	6.4	6.8	6.8	1.7	1.7
10	6.9	7.0	7.0	2.1	2.1
11	6.3	6.6	6.6	2.0	2.0
12	6.2	6.5	6.5	1.7	1.7
13	6.7	6.9	6.9	2.1	2.1
14	6.5	6.8	6.8	1.8	1.8

The deoxidizing agents SiCa and Al have been added to the melt and blowed argon was used to stir liquid steel.

The ferroalloy purity has influence on the quality of steel. This is obvious as the ferroalloy additives are added at the final stage of steel melting. High total oxygen content in ferroalloys inevitably affects the purity of steel [11]. For oxygen removal a supplementary treatment is efficient. So, after refining, the molten steel was transported to RH vacuum degassing unit for secondary refining. Particles of Al were added in the RH station for the final deoxidation. So the oxygen content was reduced (Table 5).

The degassing under vacuum leads to a decrease in hydrogen content by 50 - 70% (Table 6).

The chemical composition of the steels after RH treatment is shown in Table 7.

Table 7. Chemical composition of steel after RH refining process, (wt.%)

No.	C	Si	Mn	P	S	Al	Ti	V
1	0.09	0.29	1.53	0.018	0.005	0.034	0.014	0.001
2	0.07	0.30	1.45	0.018	0.008	0.038	0.010	0.030
3	0.08	0.26	1.52	0.013	0.010	0.044	0.011	0.033
4	0.07	0.30	1.43	0.016	0.009	0.040	0.012	0.032
5	0.07	0.26	1.48	0.011	0.008	0.040	0.014	0.028
6	0.06	0.32	1.47	0.015	0.007	0.030	0.014	0.031
7	0.06	0.32	1.40	0.012	0.009	0.038	0.011	0.025
8	0.07	0.25	1.45	0.015	0.009	0.035	0.010	0.027
9	0.07	0.26	1.49	0.014	0.009	0.037	0.012	0.032
10	0.07	0.25	1.50	0.011	0.008	0.036	0.012	0.032
11	0.07	0.28	1.59	0.011	0.010	0.046	0.014	0.032
12	0.07	0.26	1.50	0.011	0.009	0.050	0.013	0.032
13	0.08	0.33	1.50	0.014	0.009	0.032	0.012	0.030
14	0.07	0.31	1.40	0.010	0.008	0.040	0.010	0.025

Table 7. Chemical composition of steel after RH refining process, (wt.%) (continuation)

No.	Cu	Ni	Cr	Mo	Nb	N	Ca
1	0.010	0.010	0.020	0.070	0.035	0.0054	0.0015
2	0.010	0.025	0.030	0.085	0.036	0.0075	0.001
3	0.015	0.010	0.020	0.070	0.040	0.0100	0.0001
4	0.005	0.005	0.030	0.085	0.039	0.0066	0.0001
5	0.010	0.010	0.015	0.076	0.037	0.0063	0.0007
6	0.010	0.010	0.010	0.085	0.034	0.0068	0.0001
7	0.010	0.010	0.010	0.080	0.032	0.0076	0.0020
8	0.005	0.005	0.015	0.080	0.33	0.0067	0.0001
9	0.005	0.005	0.010	0.085	0.040	0.0085	0.0005
10	0.005	0.005	0.015	0.085	0.036	0.0080	0.0005
11	0.005	0.005	0.015	0.083	0.037	0.0069	0.0005
12	0.010	0.010	0.010	0.083	0.042	0.0095	0.0001
13	0.010	0.010	0.015	0.074	0.035	0.0080	0.0001
14	0.010	0.010	0.010	0.075	0.033	0.0062	0.0001

The steel is discharged from the overheated converter. Ferroalloys and fluxes added to the steel in the LF and RH station affect its temperature.

Also the steel tapping and transport of ladle for further treatment lead to heat losses (Table 8 and Figure 1).

Table 8. *Temperature of the molten steel at different locations (ºC)*

No.	after tapping from BOF	in the LF station	after RH refining
1	1617	1586	1570
2	1595	1565	1600
3	1638	1601	1573
4	1632	1603	1580
5	1619	1597	1572
6	1608	1620	1594
7	1579	1590	1569
8	1591	1620	1592
9	1619	1599	1571
10	1618	1633	1597
11	1575	1616	1584
12	1570	1601	1576
13	1610	1600	1578
14	1604	1595	1569
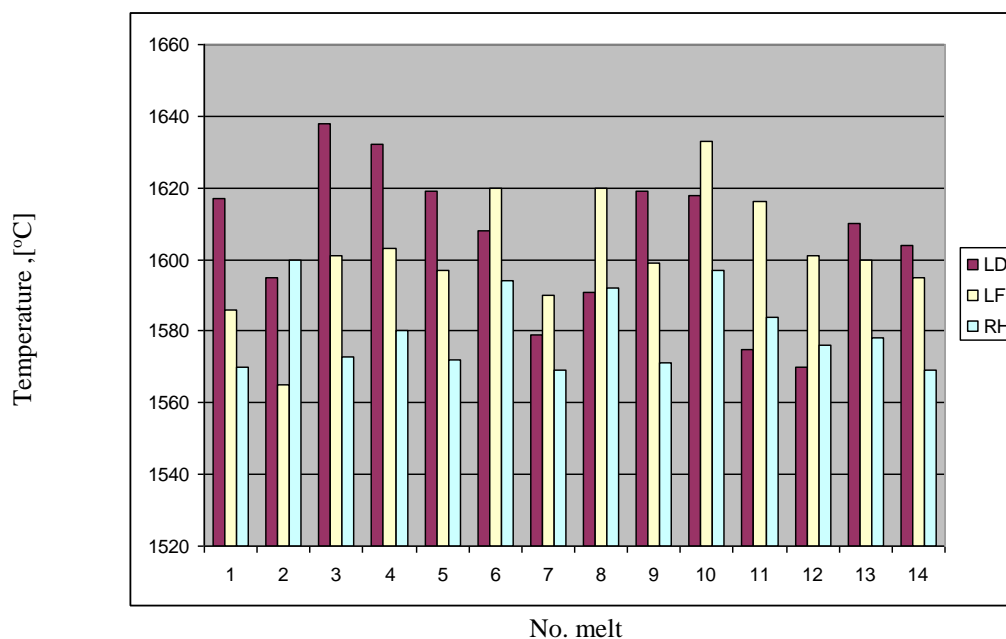
Fig. 1. *Temperature variation of molten steel during treatments*

At tapping from BOF, the carbon content of steel was below the values from standard specification (0.06 – 0.09%). The addition of a large amount of alloys in LF leads to an increase of carbon (Figure 2).

This allows for the additions of ferroalloys in the next stages of treatment without exceeding the prescribed final concentration.

Additional decarburization was carried out in the vacuum vessel.

The carbon is removed as carbon monoxide according to the reaction $[C] + [O] \rightarrow \{CO\}$.

So, oxygen and carbon contents are simultaneously reduced.
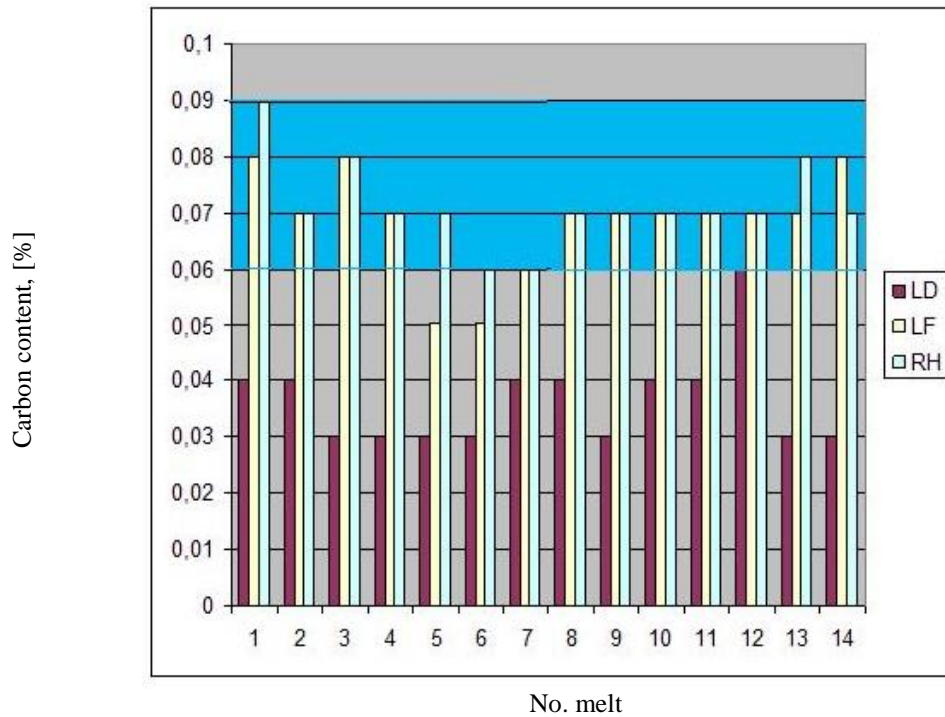
***Fig. 2.** Carbon concentrations of steel X 65*

The hydrogen removal from liquid steel during vacuum degassing was possible (Figure 3).

In the end, the steel has got hydrogen content bellow the limit prescribed of 3.0 ppm. Only an exception was reported.
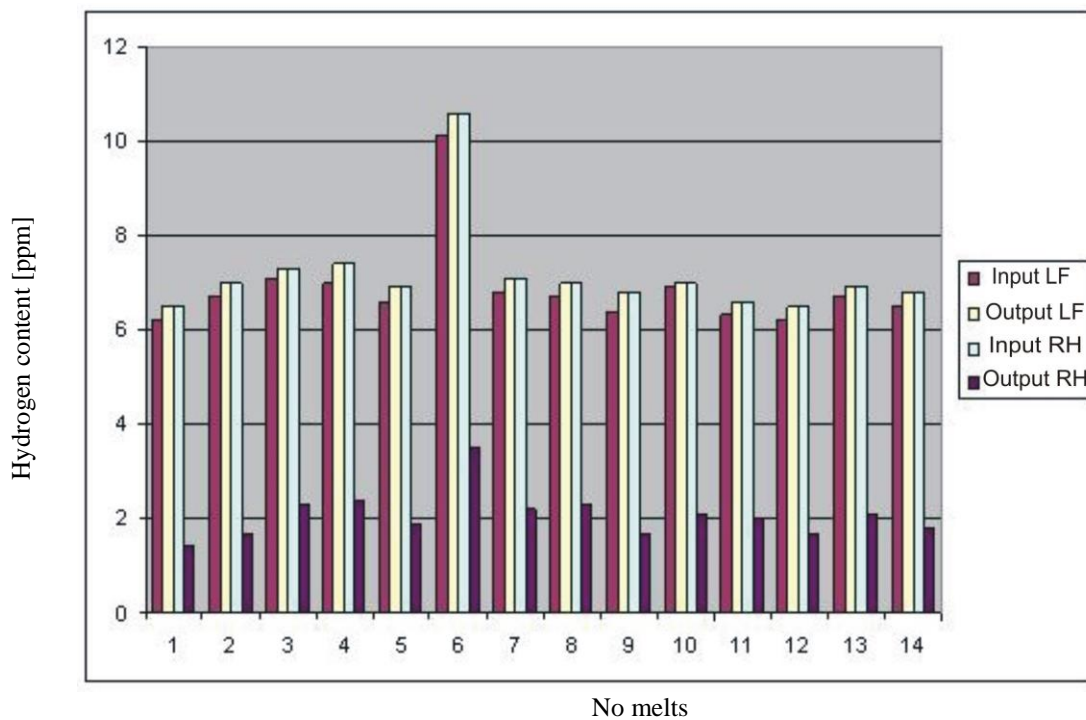
***Fig. 3.** Hydrogen content in molten steel in accordance with refining treatments*

4. Conclusions

The requirements with respect to carbon, oxygen, hydrogen and sulfur (phosphorus) content of the final product make necessary the application of secondary refining treatments. In this case LF refining process and vacuum degassing in RH station were chosen.

The steelmaking technology (BOF steelmaking LF and RH treatments) is able to ensure appropriate temperature conditions for continuous castings. The final temperature of molten steel was in range of 1570 – 1600 ºC. Decarburization rate was satisfactory for the low carbon steel produced in a basic oxygen furnace and refined in a ladle furnace and an RH installation. The carbon content of steel obtained varied within the range of 0.06 – 0.09% required by standards.

The final concentration of oxygen shows that the improvement of metallurgical purity was guaranteed by vacuum treatment at the recirculating degassing system. This has ensured the decreasing of the total oxygen content in steel as in accordance with the application field (between 2.1 and 3.0 ppm). Also, this supplementary treatment proves to be effective for hydrogen removal. The hydrogen removal rates are calculated by relation $\dfrac{[H_i]-[H_f]}{[H_i]}\cdot 100$ $(\%)$, when $[H_i]$ is the initial hydrogen content of the steel measured after tapping from BOF and $\lfloor H_f \rfloor$ is the final hydrogen content of the steel measured after vacuum treatment. These values vary between 65.34 to 77.42 %. They indicate the efficiencies of recirculating systems for the removal of hydrogen from steel.

References

[1]. **J. F. Kiefner, C. J. Trench**, *Oil pipeline. Characteristics and risk factors: illustrations from the decade of construction*, Report, December 2001.
[2]. *******, *Catalogue of international standards used in the petroleum and natural gas industries*, Report no. 362 February 2012.
[3]. **R. J. Fruehan**, *The making, shaping and treating of steel, 11th edition, volume 1 -- steelmaking and refining*, September 15, 1998, ISBN-10: 0930767020.
[4]. **G. J. W. Kor, P. C. Glaws**, *Steelmaking and refining volume, chapter 11 ladle refining and vacuum degassing*, The AISE Steel Foundation, Pittsburgh, PA, p. 681-713, 1998.
[5]. **I. D. Buga, A. I. Trotsan, B. F. Belov, O. V. Nosochenko, I. V. Parenchuk**, *Analysis of refining processes in steel ladle treatment*, Metallurgical and Mining Industry, vol. 2, no. 3, p. 180-185, 2010.
[6]. **Wen Yang, Xinhua Wang, Lifeng Zhang, Qinglin Shan, Xuefeng Liu**, *Cleanliness of low carbon aluminum-killed steels during secondary refining processes*, Steel Research International, vol. 84, issue 5, p. 473-489, 2013.
[7]. *******, *API 5L X52 5L X56 5L X60 5L X65 5L X70, The "universal" steel quality for structural and linepipe applications*, http://www.api5lx.com/.
[8]. **Z. Wcisło, A. Michaliszyn, A. Baka**, *Role of slag in the steel refining process in the ladle*, Journal of Achievements in Materials and Manufacturing Engineering, vol. 55, issue 2, p. 390-395, 2012.
[9]. **A. Radenović, J. Malina, T. Sofilić**, *Characterization of ladle furnace slag from carbon steel production as a potential adsorbent*, Advances in Materials Science and Engineering, vol. 2013, p. 1-6, 2013.
[10]. **Hui-xiang Yu, Xin-hua Wang, Mao Wang, Wan-jun Wang**, *Desulfurization ability of refining slag with medium basicity*, International Journal of Minerals, Metallurgy, and Materials, vol. 21, issue 12, p 1160-1166, 2014.
[11]. **A. Michaliszyn, Z. Wcisło, M. Rydarowicz**, *Production of ultra-pure steel intended for forged elements*, Journal of Achievements in Materials and Manufacturing Engineering, vol. 55, issue 2, p. 742-747, 2012.

RESEARCH ON THE BEHAVIOUR OF THE TOOTH - CROWN ASSEMBLIES MADE OF DIFFERENT METAL MATERIALS IN SOLUTIONS SIMULATING THE ORAL ENVIRONMENT

Elisabeta VASILESCU

„Dunarea de Jos" University of Galati

e-mail: elisabeta.vasilescu@yahoo.com

ABSTRACT

One of the basic principles of restorative dentistry is the conservation of the hard dental structure, while satisfying both aesthetic and functional requirements. Complying with this principle will minimize the harmful effects caused by the diversity of works and materials. There are numerous studies that aim to determine the behavior of different types of materials in the complex environment of the oral cavity, but a small number are those that relate to the changes that occur in the underlying dental hard tissues represented by dental abutments. Experiments were performed on extracted teeth prepared by grinding. On the polished abutments, crowns of three alloy types were made, namely: Cr- Co, Cr-Ni, and copper alloys. The crowns were cemented onto the abutments with a glass ionomer cement and subsequently immersed and maintained in solutions simulating the specific conditions of an oral environment (also called artificial saliva) of the type: Ringer Fusayama-Mayer and citric acid. After a period of six months, the ablation of crowns was achieved and comments were made on the changes in the abutments and also in the crown envelopes.

KEYWORDS: hard dental tissue, dental alloy, artificial saliva, metal crowns

1. Introduction

Progress over time in restorative dentistry art and science can be largely attributed to the dynamics of materials development and evaluation of interaction between material and oral tissues [2, 3, 6]. Numerous research studies are focused generally on the knowledge and enhancement of physical, chemical and mechanical properties of the dental materials, but how they interact with the environment of the oral cavity has yet many unknown aspects. The fixed prostheses, so-called connectives, play a role in the reconstruction of the affected dental crowns and in the replacement of a limited number of absent teeth [3-5].

They are secured by cementing them to the abutments, previously processed by grinding, and are made from metal, acrylics, ceramics or mixed materials.

Micro prostheses of crown cover (envelope) type are all made of materials using different technologies and techniques; the non- physiognomic metal prostheses are made of different alloys and the metallic or physiognomic ones are made of ceramic,

composite materials or acrylic resins [14]. Mixed crowns [11, 12, 14-16, 18, 19] combine the advantages of both materials, are the most often used and, depending on the veneering material, can be metal-ceramic, metal-composite, metal-acrylic or made of ceramic on zirconium support.

The dentist choses between a restorative prosthesis or another, depending on the type of restoration. Moreover, from his dental practice, the dentist notices that there is a significant difference in the macroscopic appearance of the dental hard tissues in different patients, even when prosthetic restoration was done with the same material and at the same time [6, 7, 11].

By removing the prosthetic work, it can be clinically seen that sometimes weaker materials in terms of their general characteristics, such as copper based alloys or acrylic resins, have a greater influence on the dental abutments than others. Therefore, there is the question of taking into account both issues such as the preparation, marginal closing or the type of cement chosen as major factors responsible for the success of prosthetic restorations [12, 19]. Studies on the behavior of different types of metal materials in

the complex environment of the oral cavity are considering how salivary pH requires choosing a particular material for restoration [17, 20]. On the other hand, there are a lot of clinicians, and they should be paid attention to, who noticed that after the ablation of partially fixed dentures, the hard dental structures were affected, putting it on account of the material the prosthetics is made of.

2. Materials and experimental conditions

We used prosthetic restoration materials commonly used for coronary restoration by envelope micro prosthesis restoration. The study conducted over a period of 6 months sought to identify changes in the morphological aspect of the dental hard tissues and alloys in the metal parts under the influence of the oral environment.

Extracted natural teeth were prepared by grinding. After preparing the abutments, metallic crowns (Table 1) were cemented to the abutments and the assembly was then immersed into three types of artificial saliva. After a period of 6 months since the cementing, the crowns were removed and the changes were studied. The morphologic appearance and the surface details of the dental structures and crown envelopes were highlighted using stereo microscope AxioCam ERC5s [6, 7] and microscopy analysis.

Table 1. *Chemical composition of the alloys studied [%]*

Chemical Composition / Alloy	Ni	Cr	Mo	Si	Fe	Cu	Al	Mn	Zn
Ni-Cr (Niadur)	58-64	22-27	10 -12	1.6-2	1.4-1.6	-	-	-	-
Cu alloy (Orcast)	4.5	-	-	-	3	81.5	7	2	2

3. Experimental results and discussion

Microstructural aspects of the alloys studied in their marketing type/state are shown in Figure 1.
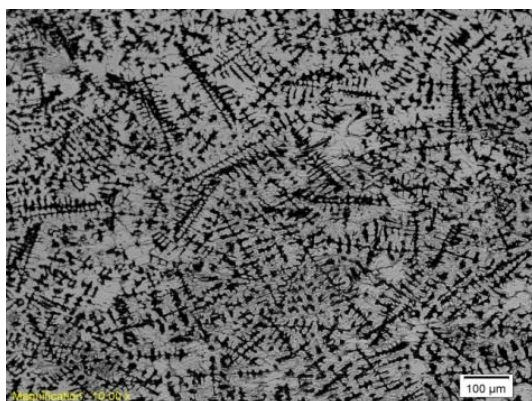
Fig. 1. *Microstructural Aspect of the Ni-Cr Alloy/Niadur (X100)* [6]

Weight %
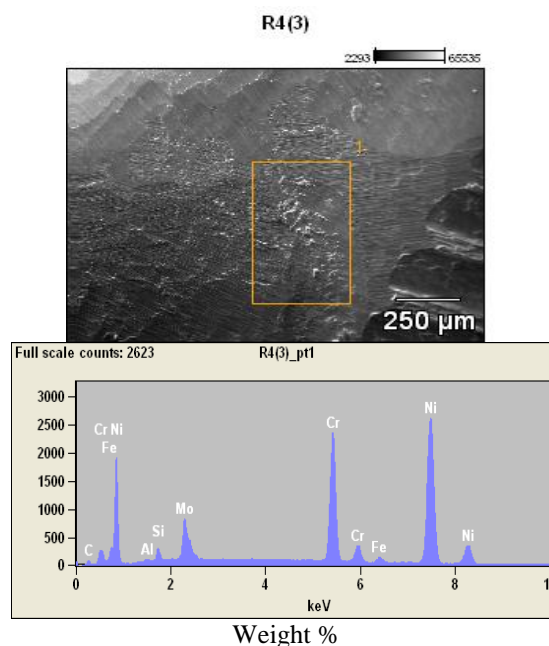
Elements /R4(3)	C-K	Al-K	Si-K	**Cr-K**	Fe K	**Ni K**	Mo L
P. (1)	3,29	0,25	1.04	**24,78**	1,34	**61,91**	7,39

Fig. 2. *X-ray spectroscopic analysis of Ni-Cr Alloy (the marketing state / delivery conditions state)*

After grinding in the dental center, the teeth have been brought to the dental laboratory for the crown envelopes to be made. The abutments and crowns made of metallic materials are shown in the figure below (Fig. 4).
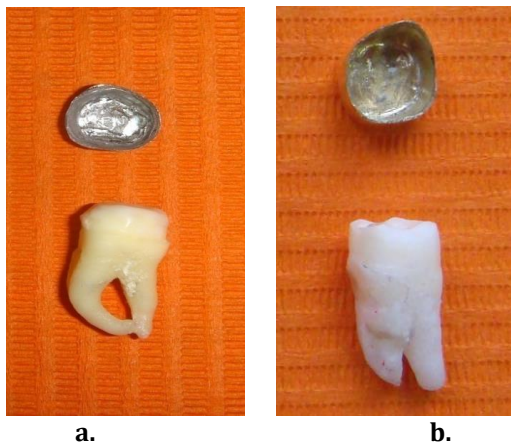
Fig. 4. *The aspect of dental abutments after polishing and crown envelopes of Ni-Cr alloy(a) and copper based alloy(b)* [6]

For cementing purpose, the same type of cement was used, compatible for cementing all types of crowns, namely a glass ionomer, the most common type of cement used in dentistry due to its qualities in cementing metal crowns of Cr-Co, Cr-Ni and copper based alloys and nonmetallic ones of acrylic resin and zirconium oxide.

The ensemble represented by the teeth and metal crowns was immersed into solutions that simulate various conditions of the oral environment (artificial saliva prepared at the Dental Materials Laboratory of the Faculty of Medicine and Pharmacy of UDJ Galati) whose composition and pH are as follows [8]:
- **Saliva Riger (SR)**: pH of 6.6;
- **Saliva Fusayama Meyer (SFM)**: pH of 5.0;
- **Citric Acid (AC)**: 0.5 M $C_6H_8O_7$ (citric acid) with pH of 1.81.

The teeth - crown assembly was maintained for 6 months in the saliva indicated above. The observation after the maintenance of the sediment indicates a slight disintegration, particularly in the citric acid solution. Incidentally, the largest amount of dissolved material derived from dental cement (and maybe from the dental tissue) was obtained as a white precipitate as a result of the chemical reactions between the solution and the components of the tooth - crown assembly occurring in the environment considered to be the most aggressive, namely the citric acid solution.

Discolouration is visible (shading), particularly with copper based alloys, and is higher in citric acid solution.

Fig. 5. *Tooth – crowns assembly after 6 months of maintenance in citric acid solution*

The main modification is the presence of cement film of variable thickness and aspect / consistency according to the type of artificial saliva and the type of crown shell/envelope.

EDS analysis (Fig. 6, 7) of the samples taken from crown envelopes reveals, especially in the case of the copper based alloys, the presence of impurities (mainly oxide inclusions) but they were also highlighted in the case of Ni-Cr or Co-Cr alloys, proof of the long presence of the alloy in contact with the atmosphere during the melting-casting operations.

VB 2(1)
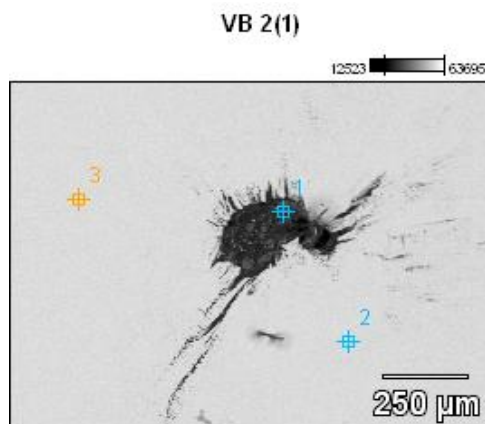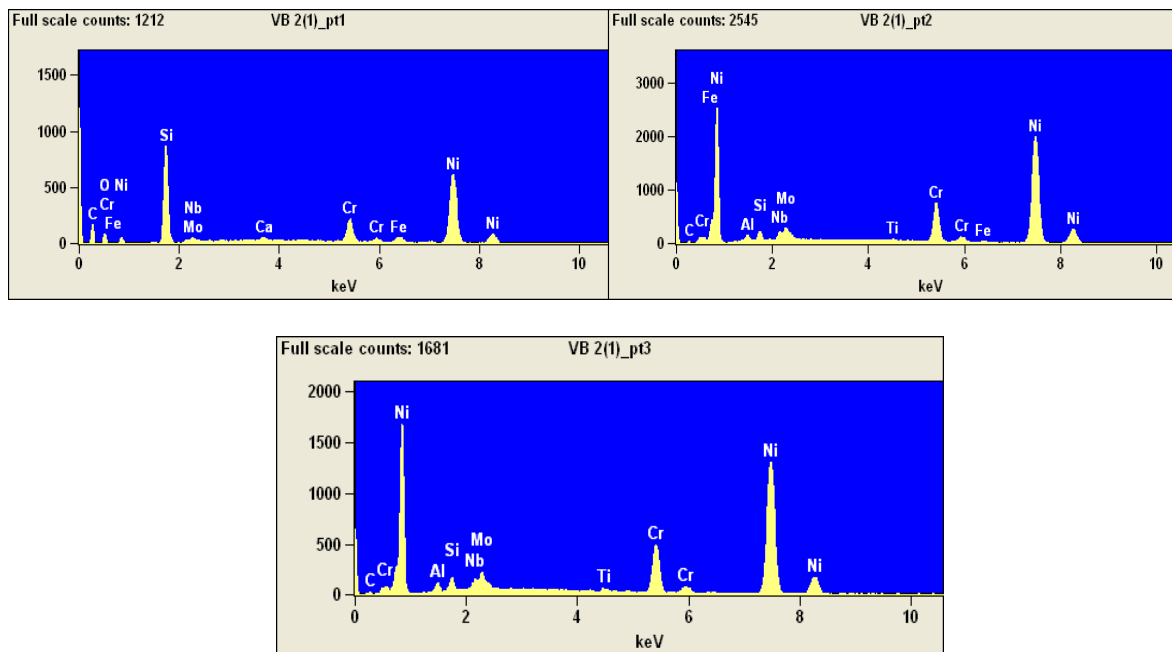
Fig. 6. *X-ray spectroscopic analysis of Ni-Cr Alloy (Samples of metal crown)* [11]
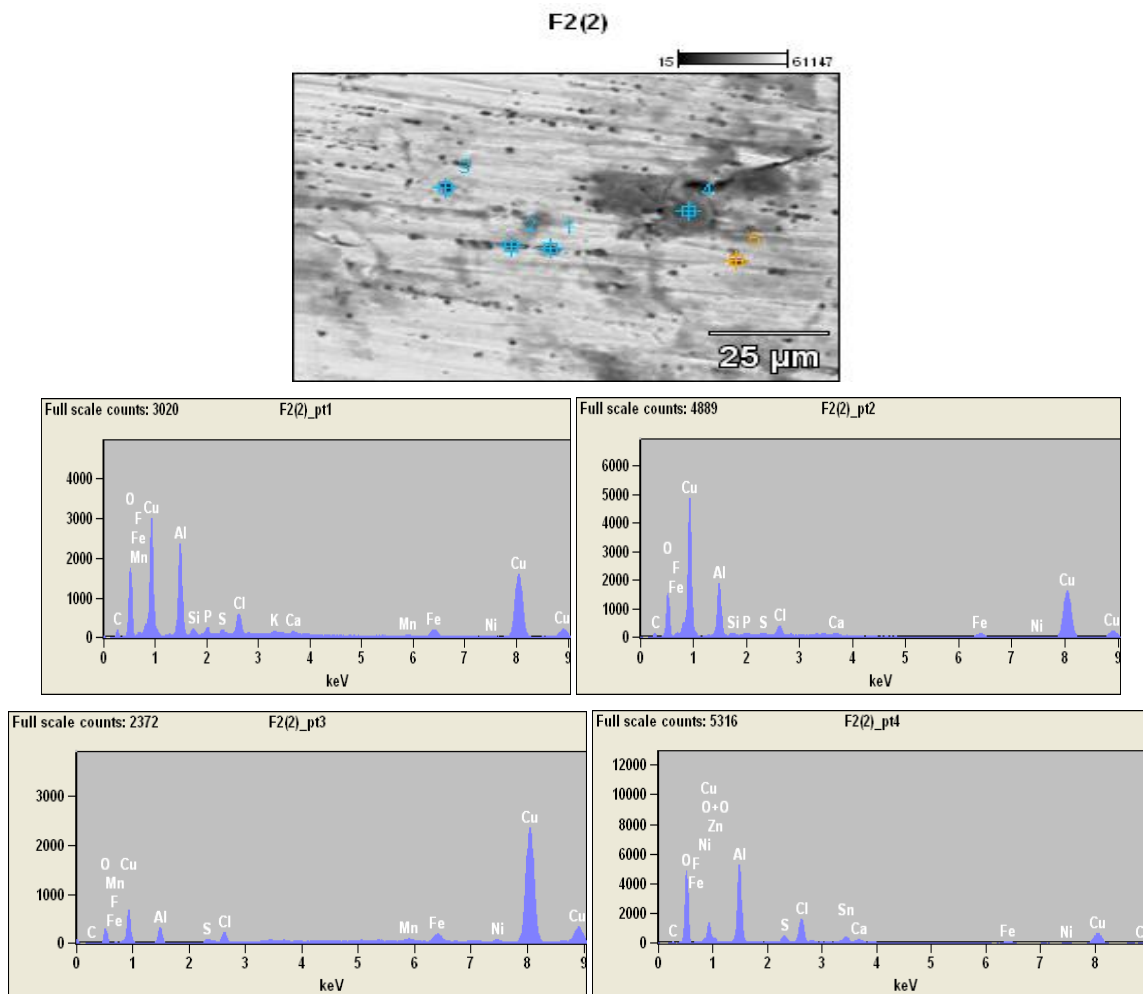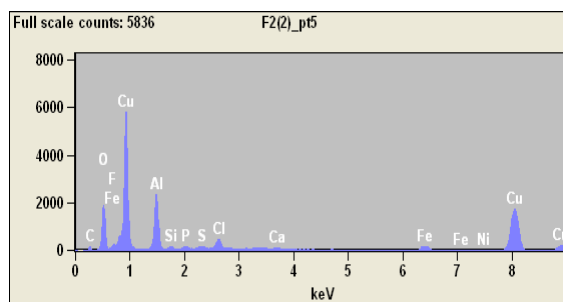
Fig.7*. X-ray spectroscopic analysis of the chemical composition of samples of Cu-alloy
(Samples of metal crown)*

Table 2*. The chemical composition of the Copper Alloy, (%)*

F2(2)	C-K	O-K	F-K	Al-K	Si-K	P-K	S-K	Cl-K	K-K	Ca-K	Mn-K	Fe-K	Ni-K	Cu-K	Zn-K	As-K	Sn-L
_pt.1	6.49	28.69	0.26	10.48	0.72	0.70	0.39	2.19	0.48	0.43	0.37	2.23	0.66	45.92			
_pt.2	5.67	24.94	0.82	10.12	0.39	0.48	0.33	1.45	-	0.40	-	1.85	0.69	52.86			
_pt.3	1.33	6.31	0.11	2.57	-	-	0.37	0.86	-	-	0.65	2.52	0.96	84.33			
_pt.4	2.84	**51.45**	0.95	**15.05**	-	-	1.17	4.89	-	0.36	-	1.57	0.84	**16.20**	**0.84**	0.64	3.21
_pt.5	5.63	**26.74**	0.61	**10.88**	**0.32**	0.35	0.39	1.66	-	0.23	-	2.44	0.75	**49.99**	**-**		

There are also present microporosity and solidification shrinkage voids, casting system defects which are transmitted to the crown envelopes affecting its strength and the assembly as a whole.

EDX spectroscopy analysis (Fig. 6) shows high contents of oxygen, silicon and aluminum (Pt.1) in areas where the proportion of basic elements (Ni and Cr) decreases significantly. The analysis performed within the matrix indicates the initial composition of the alloy in the range indicated by the manufacturer (Pt.2 and pt.3)

4. Conclusions

The paper presents an important subject in restorative dentistry practice. The research studies made show the lack of rigor in the processing of the alloys, by highlighting defects (oxidation) that can affect the quality of conjunct fixed prostheses built from different metal materials. The study of changes recorded on the abutments under prosthetic bridges composed by crowns made from different alloys but also the metal crown, ended with the conclusive results that firstly confirm the influence of oral environment on materials (shading) and secondly the importance of respecting technological conditions of processing for achieving the metal component without defects. It was highlighted the different behavior of restoration materials under the influence of pH saliva (the most acid saliva determined accentuated color changes to metallic materials, particularly visible in copper alloys). EDX spectroscopy analysis on samples taken from the crown, from all alloys (but especially copper based alloys) confirms the presence of impurities (mainly oxides), proof of the long-standing contact with the atmosphere of the alloy during processing.

References

[1]. Graham J. Mount, W. R. Hume, *Conservarea și restaurarea structurii dentare*, Ed. All Educational, Timișoara, p. 69, 78, 80, 1999.
[2]. Kenneth J., Anusavice-Philip`s *Science of Dental materials eleventh edition*, Elsevier, Florida, 2011.
[3]. Craig, R. G., *Restorative dental materials*, Mosby, Chicago, 1993.
[4]. Bratu D., Nussbaum R., *Bazele clinice şi tehnice ale protezării fixe*, Ed. Medicală, București, 2009.
[5]. Roland Strietzel, *Restaurări protetice fixe şi combinate,* Dental Press Hungary, 2013.
[6]. Banu Bujoreanu L. C, *Cercetări privind modificările țesuturilor dure dentare sub lucrări protetice conjuncte din diferite material,* Lucrare de licenta, FMF a UDJ Galati, 2015.
[7]. Banu Bujoreanu Carmen–Laura, *Cercetări privind modificările țesuturilor dure dentarea sub lucrări protetice din diferite aliaje,* Sesiunea Națională de Comunicări Științifice Studențești ,,*Anghel Saligny*", 20-21 mai 2015 – Galați.
[8]. V. G. Vasilescu, L. Benea, E. Vasilescu, *Influence of pH solution on corrosion behavior of cobalt-cromium alloy used in dentistry*, TEME-2nd Edition of the International Conference of Young Researches, 28th-30th October, Galati 2013.
[9]. Daniel Sutiman, Adrian Căilean, Igor Crețescu, Mircea Nechita, Daniel Mareci, *Comportarea la coroziune a biomaterialelor pe bază de Ni-Cr în saliva Rondelli*, Rev. Chim. (București), vol. 59, no. 4, 2008.
[10]. Jung R. E., Sailer I., Hammerle C. H. F., Attin T., Schmidlin P., *In vitro color changes of soft tissues caused by restorative materials*, International Journal of Periodontics and Restorative Dentistry, 27, p. 251-257, 2007.

[11]. Deliu L., *Cercetari privind influența unor factori tehnologici în procesul de realizare a componentei metalice pentru coroane mixte metalo-ceramice*, lucrare de licență, UDJ Galați, 2015.

[12]. Muntean Violeta, *Studii asupra biocompatibilității și bioeconomiei materialelor utilizate în restaurările protetice metalo-ceramice la interfața cu structurile dentare*, Univ. Titu Maiorescu, Teza de doctorat.

[13]. Wen S., Liu Q., *High Resolution Electron Microscopy Investigation of Interface and Other Structure Defects in Some Ceramics*, Microsc. Res. Tech., feb. 1, 40(3), p. 177-186, 1998.

[14]. Floyd A. Peyton, *Materials in restaurative dentristry*, University of Michigan School of dentistry, Annals New York Academy of Sciences, vol. 47, issue 6, p. 100-469, June 1961.

[15]. Flinn R., Trojan P., *Engineering Materials and Their Applications,* 3rd edition, Boston, MA, Houghton Mifflin Co., p. 116-169, 1986.

[16]. Bratu D., Leretter M., Românu M., Negruțiu M., Fabricky M., *Coroana Mixtă*; Editura Signata, Timișoara, 1992.

[17]. ***, *Materiale dentare metalice utilizate în medicină-Biomateriale*, p. 55.

[18]. Duchaye R., Hastings G. W., *Metal and Ceramic Biomaterials,* vol. I & II, Ed. Boca Raton Florida. 1998.

[19]. Pătrașcu I., Ciocan L. T., Frussigniotti S., *Evaluation of Metal-Ceramics Interface for Modern Ni-Cr Alloys*, "BASS2000" Congress of Balkan Stomatological Society, Thessaloniki, Greece, April 15, 2000.

[20]. Vasilescu E., *Research on Influence of Metallurgy Factors on the Quality of Metal Components in Metalceramic Prosthetic Restorations,* The Annals of "Dunarea de Jos" University of Galati Fascicle IX. Metallurgy and Materials Science, No. 1, p. 27, 2015.

THE PROTECTIVE BEHAVIOUR OF TITANIUM NITRIDE COATINGS

Stela CONSTANTINESCU

"Dunarea de Jos" University of Galati, Romania
e-mail: constantinescu_stela@yahoo.com

ABSTRACT

The experiments conducted to obtain a thin layer of nitride through the vapour chemical deposition method have followed an original path to obtain TiN directly in the working room thus avoiding the import of these hazardous substances. In this paper, the protective behaviour of titanium nitride coatings onto hard carbide substrate was investigated using scanning electron microscope (SEM), X-ray diffractometer (XRD) and Knoop hardness. Scanning Electron Microscope was used to investigate the coating morphology and interface structure. X-ray mapping was also performed to characterize the elements in a semi-quantitative analysis. Dron X-ray diffractometer with Mo Kα radiation operating was used for phase(s) identification. Microhardness value (Knoop hardness) measured in the coating layer was 28.000 MPa. CVD TiN coatings usually show only moderate or even poor corrosion protection for hard carbide substrates.

KEYWORDS: thin layer, titanium nitride, protective coatings, corrosion, microhardness

1. Introduction

Titanium nitride coatings find extensive applications in tribilogical, mechanical and even decorative applications. CVD TiN coatings usually show only moderate or even poor corrosion protection for hard carbide substrates. The poor corrosion performance is not due to the intrinsic corrosion behaviour of the nitride coating itself. It results from small structural defects, pores and crack formed during or after deposition, which act as channels for the corrosion of the substrate. We investigated the corrosion tests in water of titanium nitride coatings elaborated by the CVD process.

If the vapour chemical deposition takes place within a tubular continuous reactor, a gas carrying the reacting species is passed over the sub-layer. At the sub-layer surface, the reacting elements undergo a number of chemical reactions leading to product formation. Part of the products are deposited on the sub-layer and part of it goes back to the gas stream [1, 2].

Before examining the vapour chemical deposition reactions, it must be determined if the reaction is possible thermodynamically. The reaction will be possible thermodynamically if the calculated concentrations (partial pressures) of the reactants, under equilibrium conditions, are less than their original concentrations.

The calculation of the equilibrium concentrations from the equilibrium constant involves a good choice of the number of gas spaces which can be higher than two and the number of independent relations. A relation implies the equilibrium expression depending on the free standard reaction energy and temperature.

The other relation consists in that the system pressure is the sum of the partial pressures. If some reactants possess more than one valence state, the reaction should contain the reactant under its most stable valence state [3, 4].

During the corrosion test in water, samples covered with TiN channel are stronger compared to uncoated samples TiN [5, 6].

Hard alloys made out of metallic carbides manufactured at an industrial scale for cutting processing can be divided into two categories, to investigate the coating morphology and interface structure. X-ray mapping was also performed to characterize the elements in a semi-quantitative analysis. Dron X-ray diffractometer with Mo Kα radiation operating was used for phase(s) identification. The microhardness tests show that we have TiN, value $HV_{0,05} = 28\ 000$ MPa is in good agreement with the data from the literature.

2. Characterization

The characterization of the coating deposed by CVD method was done using scanning electron microscope (SEM), X-ray diffractometer (XRD). The TiN coated plates feature higher endurance capabilities than those uncoated for the same cutting speed both for steel and white cast iron.

The parameters of the cutting conditions were chosen in the range of the values used on the working machines at Arcelor Mittal Steel Galati.

Table 1. *Domains of the parameters values of the cutting conditions*

Plate type	Processed material	n [rot/min]	v [mm/min]	s [mm/rot]	t [mm]
SNUN 15.04.08 K20	white cast iron	450	110	0,096	0,5
		500	123	0,096	0,5
		530	130	0,096	0,5
		570	140	0,096	0,5
		610	150	0,096	0,5
		630	154	0,096	0,5

In Table 1 the values of the parameters of the cutting conditions are shown, where: n: rotation speed [rot/min]; v: speed cutting [mm/min]; s: advance [mm/rot]; t: deep cut [mm].

The operation of the latter is based on a housing which cuts the deposited TiN layer. Samples for metallography were prepared by polishing, this prevented damage to the dissimilar interface (strate – substrate) during polishing. SEM was also used.

3. Results and discussion

The optimum layers in the cutting process are the TiN layers. Having thickness within 4-10 μm above these values, the layers lose tenacity and become fragile. As a result of the thermal treatment which means heating up to 1050 ºC degrees for various exposure times, layer thickness within 3.5-10 μm was achieved [7]. The thickness of the thin layers increases with the time of exposure to the working temperature as illustrated in Fig. 1.

The micro-hardness of WC-TiC-Co alloys is affected by a large number of elements connected to the raw material, purity and component dispersion in the alloy and the solid solution quality and grain size of components.
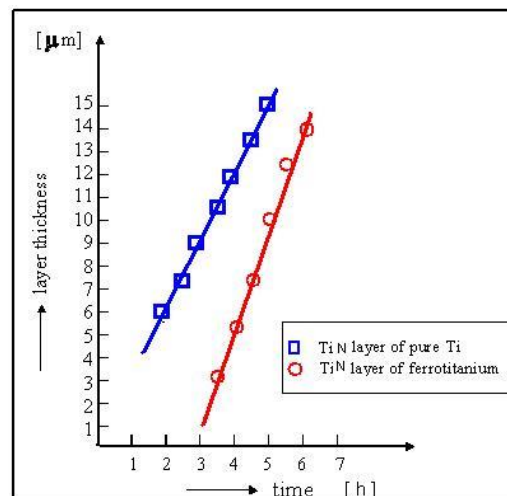
Fig. 1. *The thickness of the thin TiN layers increases with time*

In the factory process, these elements are playing an ultimate role in effective micro-hardness measurement of the material with a given chemical composition (Fig. 2).
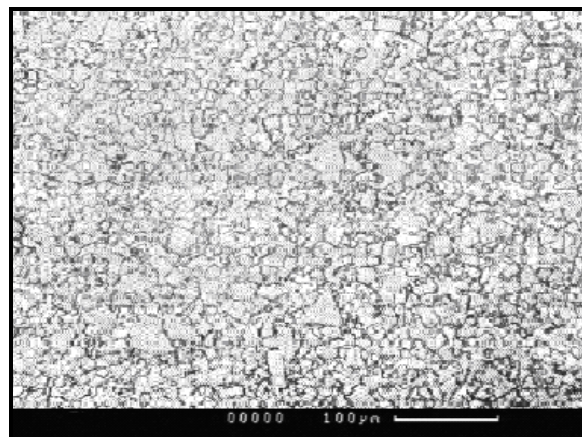
Fig. 2. *Metallographic appearance of alloy with 82%WC, 12%TiC, 6%Co, x1500*

Micro-hardness is not a constant like Vickers hardness, in spite of the geometrical similarity, but decreases with higher testing charges depending on the size of the print.

Measurements were made on TiN covered thin plates whose thickness ranges between 6, 8 and 10 μm [8, 9].

Micrography, Fig. 3-5, shows an adherent layer which is uniform and homogenous over the entire depth [10].
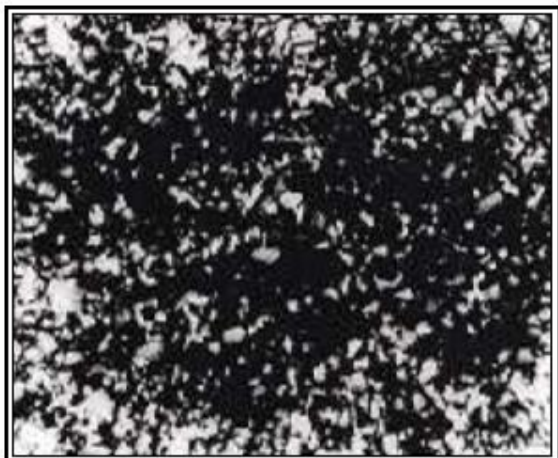
Fig. 3. *Uncoated plate surface appearance - SEM electron microscopy*
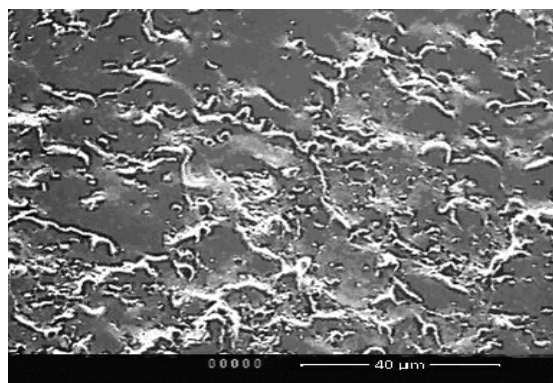
Fig. 4. *SEM image of a monolayer covered surface plate, appearance TiN*

Figures 3 and 4 show the superficial aspects of the CVD deposited layers, compared to TiN monolayer uncovering a plate, classic appearance, studied by electron microscopy. It is a clear difference in crystals, in layer size, uniformity and surface roughness [11].

In Figure 5 metallographic appearance is set for good quality coated plates. TiN coating has uniform thickness and the grain has a crystal columnar layer.
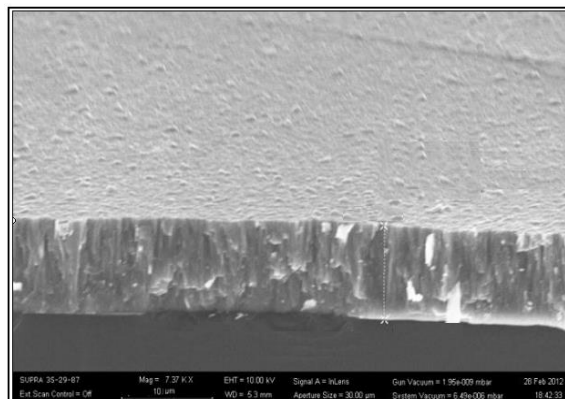
Fig. 5. *SEM images of TiN layer*

The almost uniform grain isomorphic layer and its purity ensure proper behavior at cutting premises. The best results are obtained for layer depth of 8 μm, with homogeneous and even structure, a feature that can be emphasized by means of diffraction pattern analysis, Fig. 6.
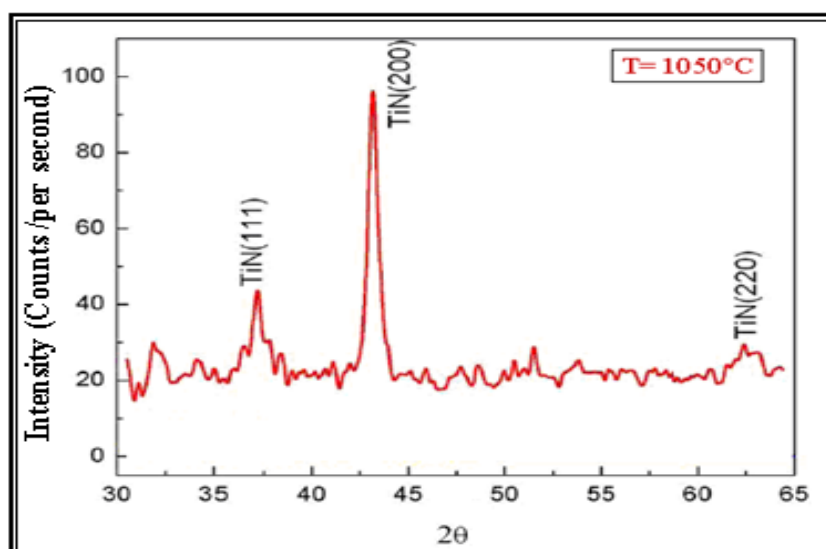
Fig. 6. *X- ray diffraction spectrum of TiN coating*

The titanium nitride coating diagram (Figure 6) presents diffraction lines which are characteristic to the most intense peak of TiN compound and correspond to the (200) diffraction plane [12]. The values of the thin TiN layers as measured by the Kalotest (Fig. 7) device are in good agreement with the values measured by microscopic analysis but slightly lower.

The steel ball diameter is 12 mm. Therefore, the shell diameter is much less than that of the ball.
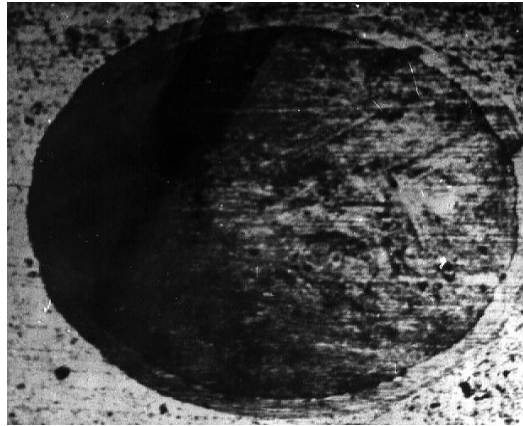
Fig. 7. The sphere shell of TiN by the Kalotest
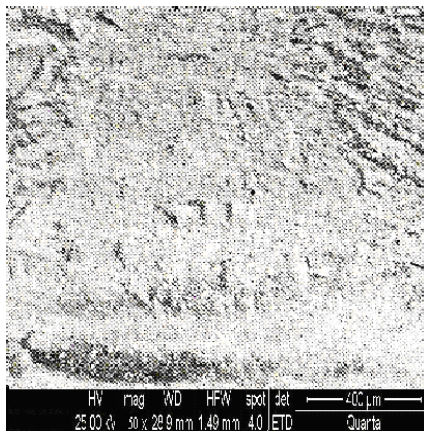
a)   b)

Fig. 8. *Surface appearance of uncoated TiN samples: a) before corrosion, b) after corrosion*
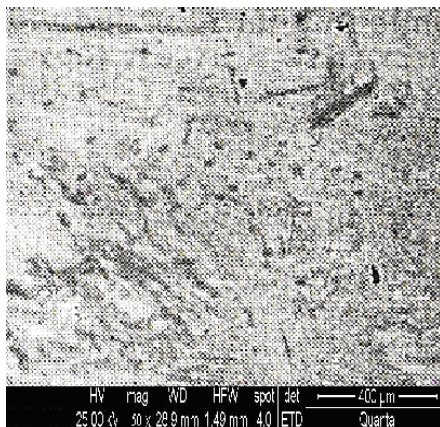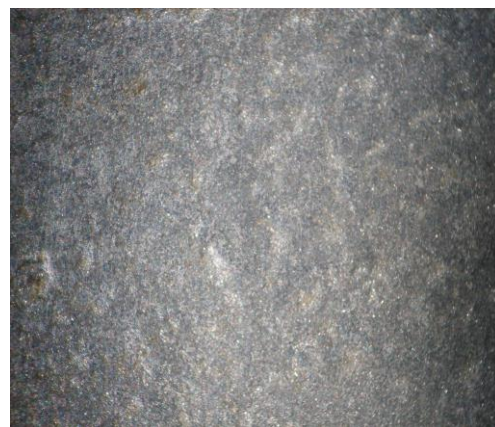
a)   b)

Fig. 9. *Surface appearance of covered TiN samples 6 µm: a) before corrosion,
b) after corrosion*

a)   b)
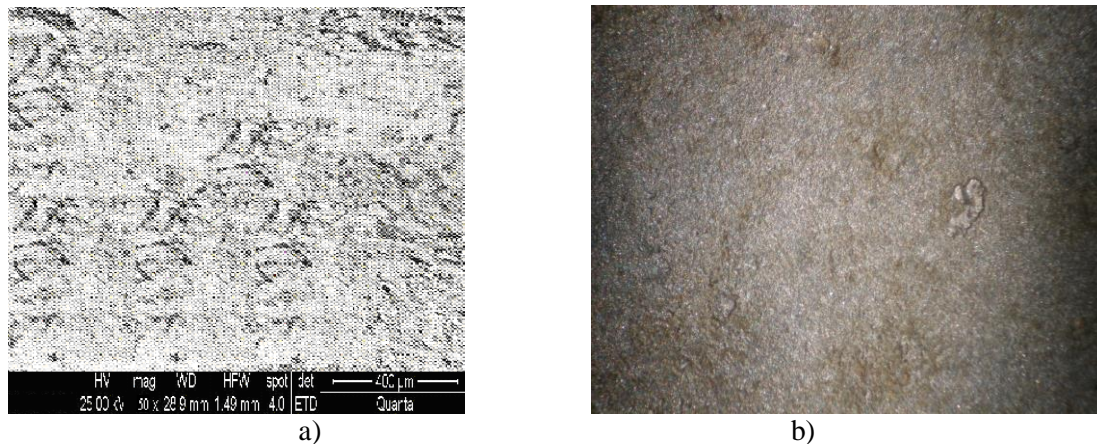
Fig. 10. Surface appearance of covered TiN samples of 8 μm: a) before corrosion, b) after corrosion

As seen in Figures 8-10, uncoated surface TiN samples have surface oxides by 70% if the samples coated with the thickness of 6 μm TiN have slight traces of surface oxides on 5% non-stick surface, and covered with TiN samples with thickness of 8 μm the surface shows no oxides. It is noted that in corrosion test in water samples covered with TiN, channel is stronger compared with uncoated TiN samples [13].

4. Conclusions

These coatings have good wear resistance, abrasion resistance, corrosion resistance and a strong strate-substrate interface. This leads to formation of thick and rough coating. The coating is fine grained, adherent, dense and free from cracks. However, some porosity is observed in the coating layer.

The widia plates coating with thin TiN layers entirely suppresses the inconveniences of a relatively rough topography of the common sintered nitrides while preserving the adequate material mechanical strength.

The layer begins losing its tenacity if its thickness increases considerably, exceeding the thickness of 10 μm mainly due to the lower strength characteristics. This together with the increase in the inner tensions results in cracks and breakings in the layers. This has been attributed to poor wetting characteristics.

During the corrosion test in water, samples covered with TiN channel are stronger compared to uncoated TiN samples.

Reference

[1]. **S. Constantinescu,** *Studies on Thin Carbide and Nitride Layers Deposition on Metal Basis, Based on Chemical Reaction at High Temperatures*, Academic Thesis, Galati, 1998.
[2]. **S. Constantinescu,** *Nitride coatings on widia substrate for mechanical applications*, Journal Surface Engineering, vol. 1, p. 77-81, 2009.
[3]. **S. Constantinescu, T. Radu**, *Advanced methods of obtaining thin coats*, Ed. Ştiinţifică F.M.R. ISBN 973-8151-25-2, Bucureşti, 2003.
[4]. **I. M. Notter, D. R. Gabe,** *Porosity of Electrodeposited Coatings: Its Cause, Nature, Effect and Management*, Corrosion Reviews, 10 (3-4), p. 217-280, 1992.
[5]. **J. Munemasa, T. Kumakiri**, *Effect of the Surface Roughness of Substrate on the corrosion properties of fims coated by Physical Vapour Deposition,* Surface and Coatings Technology, 49, p. 496-499, 1991.
[6]. **L. Orac, V. Grechanyuc**, *Corrosion resistance of the composites Cu-Mo obtained by PVD method*, METAL 2010, Ostrava, Czech Republic, p. 932-937, 2010.
[7]. **A. Zhecheva ,W. Sha, S. Malinov, A. Long**, *Enhancing the microstructure and properties of titanium alloys through nitriding and other surface engineering methods*, Surface and Coatings Technology, vol. 200, issue 7, p. 2192–2207, 2005.
[8]. **K. L. Choy**, *Chemical vapour deposition of coatings,* Progress in Materials Science, 48, p. 57–170, 2003.
[9]. **E. Bemporad , M. Sebastiani, C. Pecchio , S. De Rossi**, *High thickness Ti/TiN multilayer thin coatings for wear resistant applications,* Surface and Coatings Technology, vol. 201, issue 6, p. 2155-2165, 2006.
[10]. **J. C. Caicedo, C. Amaya, L. Yate, O. Nos, M. E. Gomez, P. Prieto**, *Hard coating performance enhancement by using [Ti/TiN]n, [Zr/ZrN]n and [TiN/ZrN]n multilayer system*, Mater. Sci. Eng. B, vol. 171, p. 56-61, 2010.
[11]. **O. Yasuharu, K. Shinya, O. Kazuhide, A. Hideki, N. Hideki, H. Kenji, M. Osamu**, Thin Solid Films, 497, 2006.
[12]. **A. D. Krawitz**- *Introduction to Diffraction in Materials Science and Engineering*, Wiley, New York, p. 165-167, 2001.
[13]. **V. Sista, O. Kahvecioglu, O. L. Erylmaz, A. Erdemir, S. Timur.** *Thin Solid Films*, 520, 1582, 2011.

CORROSION RESISTANCE OF ZINC COATED STEEL IN SEA WATER ENVIRONMENT

Adrian DIACONU, Cătălin SOLOMON, Lidia BENEA*,
Valentin DUMITRAŞCU, Laurenţiu MARDARE

Research (Competences) Centre: Interfaces-Tribocorrosion and Electrochemical Systems (CC-ITES),
Engineering Faculty, Dunarea de Jos University of Galati, 47 Domnească Street, RO-800008, Galati, Romania
*Corresponding author
e-mail: Lidia.Benea@ugal.ro

ABSTRACT

The life time of metallic materials used in naval transport industry is influenced by their corrosion resistance. For utilization in shipbuilding and offshore construction, metallic materials need to be covered with protective coatings, especially, or different anti-corrosion protection methods need to be used. During the last decades a series of inorganic and organic coatings was developed. Among inorganic coatings, the most used ones are the galvanizing treatments. This paper presents a comparative investigation regarding the corrosion resistance of uncoated low alloy steel and galvanizing steel. Both samples have been subjected to corrosion in sea water harvested from the Black Sea, Mangalia harbor. The electrochemical assays were: open circuit potential (OCP), linear polarization resistance (Rp), potentiodynamic polarization (PD) and cyclic voltammetry. The results obtained by in situ determination were confirmed by optical microscopy. The results revealed an improved corrosion resistance of galvanized steel in natural sea water in comparison with low alloy steel.

KEYWORDS: low alloy steel, galvanizing steel, corrosion behavior, marine environment

1. Introduction

Currently, the development of naval transport industry has become a focus point around the world, which provides a huge marketing demand for the metal used in ocean engineering. Therefore, there would be a great potential to develop metals with low cost and outstanding corrosion resistance to seawater [1] and marine environments [2]. Most metal structures used in sea water (ships, oil platforms, piers, pipelines, etc.) and in close proximity to the oceans are traditionally made of mild low-carbon and low alloy steels and are subject to corrosion, especially if unprotected [3, 4].

Nowadays, people have started to pay more attention to the effect of protective layers on corrosion resistant property, especially after the successful development of high-tensile corrosion resistant steel containing different layers with good anti-corrosion properties and low price. Mild low-carbon and low alloy steels surfaces are coated with different types of layers such as metallic (zinc, lead,

chrome, etc.), ceramic (alumina, etc.) or polymeric layers (layers of bitumen, epoxy-based material, etc.) or modified with different passivation treatments (cerium-based [5], tungsten-based [6], tin-based [1] or chromium-based [7], etc.) for protection against rusting.

Galvanized sheet is a type of sheet which consists of mild steel as the base metal but coated with zinc either by hot dip galvanizing process or metallic coating process [8].

Hot-dip galvanized steel is increasingly used in industry as an alternative to non-galvanized cold rolled steel due to its enhanced corrosion resistance. During the last decade, numerous works focused on new galvanized coatings including magnesium and aluminum or a combination of both in the zinc coating [9].

Zinc is widely used for corrosion protection of steel due to its sacrificial aim: its redox potential being more negative (less noble) than that of steel under the same conditions, zinc deposits behave as

sacrificial anodes and thus offer a cathodic protection to the steel substrate [5, 10, 11].

The ability of zinc to galvanically protect mild steel and low carbon steel has made this metal important from an industrial point of view. Therefore, the compactness of galvanized coatings, which provide mild steel with good corrosion protection, is essential for the economic utilization of steel. The composition and structure of the protective layer depend on the kinds of alloying metals and corrosion environments containing various anions such as Cl^-, SO_4^{-2}, CO_3^{-2}, and NO_3^-. The good corrosion resistance of hot dip galvanized steel products in natural environments is due to the formation of a protective basic zinc carbonate film on the surface of the zinc coatings [12, 13].

Studies on the corrosion of galvanized steel revealed that its corrosion behavior consisted of three different stages. In stage 1, the electrochemical behavior of galvanized steel is mainly related to the dissolution of the zinc oxide layer which was formed in the air. In stage 2, the surface of the zinc layer is covered with thick, white rust and the underlying steel begins to corrode. During this stage, the corrosion rate of the zinc coating rapidly decreases, accompanied by a shift in the corrosion potential to a more noble potential. In stage 3, the amount of red rust on the coating surface rapidly increases; the galvanized steel shows almost the same corrosion potential as that of carbon steel, even though the zinc coating is still covering a few parts of the steel reinforcement. The underlying steel corrosion progresses by dissolution of iron and, therefore, at this stage, the zinc coating no longer acts as a sacrificial anode [14].

The aim of this paper was to investigate the corrosion behavior of the low alloy steel and galvanized steel in seawater by electrochemical methods. The attempts are to evaluate the contribution of zinc layer deposited on low alloy steel to the corrosion resistance in seawater environment.

2. Experimental set-up

The corrosion experiments were performed on low alloy steel and galvanized steel, which were purchased from Arcelor Mittal Galati, Romania. The mean zinc coating thickness was 6.5 µm.

All samples were cut to dimensions of 25x25x2 mm. Before any experiments, the samples have been bonded with cooper wire and isolated with epoxy resin to obtain a measurable active surface area. The samples were degreased with acetone and alcohol and rinsed afterwards with deionized water.

The experiments were done using a Potentiostat–Galvanostat PGZ 100 and the data were recorded with VoltaMaster software. In order to perform the corrosion experiments it was used a standard three-electrode cell consisting of the tested samples as working electrode, a Pt-Rh grid used as auxiliary electrode and Ag/AgCl electrode (saturated KCl solution, E = -200 mV vs. normal hydrogen electrode (NHE)) as a reference electrode.

As corrosive environment it was used sea water harvested from the Black Sea, Mangalia port area and its characteristics are shown in Table 1.

Table 1. *Black Sea water characteristics*

pH	Salinity [ppt]	Conductivity [mS]
7.63	12.4	21

The in-situ applied electrochemical methods were: open circuit potential (OCP), linear polarization, polarization resistance, potentiodynamic polarization and cyclic voltammetry.

The surfaces were investigated on an optical microscope type OPTIKA XDS-3MET before and after corrosion tests in order to estimate the corrosive effects. The optical image was performed with software Vision Pro Plus Ver 5.0 on computer connected to an optical microscope.

3. Results and discussions

3.1. Open circuit potential

The evolution of the steady state interface between uncoated steel or galvanized steel and the corrosive environment was evaluated by measuring the open circuit potential of both surfaces during immersion time in sea water. In Fig. 1 there are presented both diagrams obtained during one hour when it was reached a steady state value of free potential explained by an equilibrium of metallic interface and corrosive sea water solution.
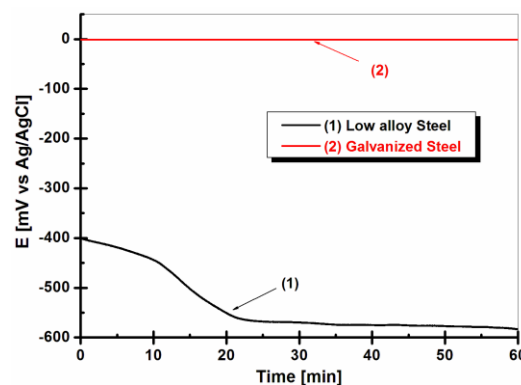
Fig.1. *Variation of open circuit potential during immersion time in sea water: (1) - Uncoated steel and (2) - Galvanized steel*

From Fig. 1. it can be seen that for low alloy steel the potential drops down in the first 30 minutes from -400 mV vs. Ag/AgCl to -575 mV vs. Ag/AgCl and after that it reaches a stable value. This behavior indicates a high instability and changes on its surface because of the corrosion process and corrosion products. This type of potential behavior was observed by S.S. Xin et al [15] when studied the corrosion behavior in hot concentrated sea water of 316 stainless steel.

For galvanized steel the potential remains constant with the value around 0 mV vs. Ag/AgCl, for the same immersion period. This aspect is correlated with an improved corrosion resistance by the zinc layer on the steel surface.

Generally, the steady state potential indicates that the zinc layer remains intact and protective. Comparing the steady state potentials presented in Fig. 1 it can be clearly observed that the galvanized steel offers improved corrosion resistance in comparison with untreated low alloy steel.

3.2. Measuring the polarization resistance (Rp) values during immersion time

The evolution of polarization resistance during immersion time was evaluated by measuring the linear polarization curves around the open circuit potential value with a very small potential amplitude (± 40 mV) to preserve the steady state balance obtained at the interface between metallic samples and corrosive environment. The polarization resistance values of low alloy steel and galvanized steel immersed in sea water are presented in Fig. 2 (a).
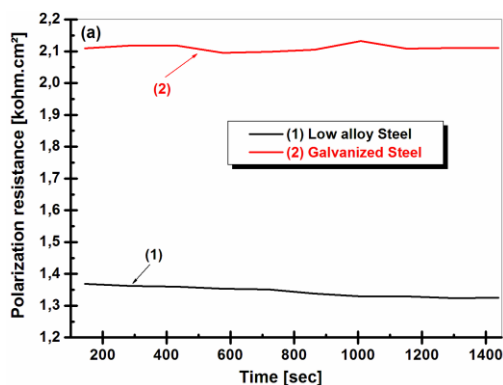
From Fig. 2 (a). it can be observed that the low alloy steel has the lowest polarization resistance (Rp) being equal to *1.35 kohm.cm²*. By applying a zinc layer on the low alloy steel surface, the polarization resistance increases to a mean value of *2.1 kohm.cm²*. By increasing the value of polarization resistance, the corrosion current density decreases and therefore the corrosion rate is lowered, as it can be seen in Fig. 2 (b).

Fig. 2 (b). illustrates the evolution of corrosion rate in time, corresponding to the polarization resistance (Fig. 2 (a)) for both analyzed surfaces immersed in seawater.

According to the data presented in Fig. 2 (b) it can be observed that for the low alloy steel, which has the lower polarization resistance, it corresponds the higher corrosion rate in comparison with the corrosion rate of galvanized steel.
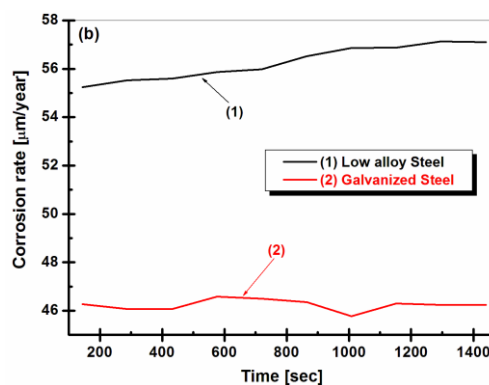
Fig. 2. The evolution of polarization resistance (Rp) values during the immersion time for: (1) uncoated steel and (2) galvanized steel

These results suggest that the zinc layer increases the corrosion resistance of low alloy steel and are in good agreement with the evolution of open circuit potential values.

3.3. Potentiodynamic polarization

The effects of natural sea water environment on the corrosion rate of galvanized and low alloy steel samples were studied using Tafel polarization technique. Fig. 3. presents typical E-log *i* polarization curves which were recorded in a range of potentials starting from -1.5 V vs. Ag/AgCl to -0.5 V vs. Ag/AgCl at a potential sweep scan of 5 mV/s for both samples immersed in natural sea water. The corresponding corrosion potential (E_{corr}), corrosion current density (i_{corr}), anodic slope (b_a) and cathodic slope (b_c) are presented in Fig. 3.

From the data plotted in Fig. 3 it can be observed for both metallic surfaces the anodic dissolution of iron or zinc and the cathodic hydrogen evolution reaction in natural sea water.

The calculation of the Tafel slopes and the current densities (as corrosion rates) from polarization potentiodynamic curves are also presented in Fig. 3

for low alloy steel and galvanized steel. Fig. 3 indicates that the zinc coating shifts the corrosion potential (E_{corr}) to the more negative direction without affecting anodic dissolution, which leads to a significant decrease of corrosion current density (corrosion rate).
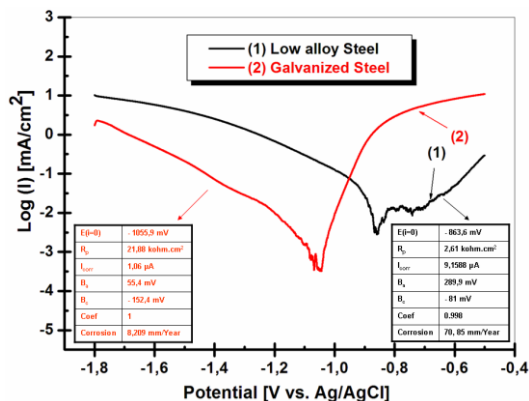
Fig. 3. *Tafel representation of potentiodynamic polarization for uncoated and galvanized steel immersed in natural sea water*

From Fig. 3 it can be also seen that the corrosion current (i_{corr}) of uncoated steel is higher than the corrosion current of galvanized steel which results in a decrease of the corrosion rate from 279.5 μm/year for uncoated steel to 8.24 μm/year for zinc layer over carbon steel, in natural sea water.

3.4. Cyclic voltammetry

The cyclic voltammograms for low alloy steel and galvanized steel were recorded in the potential range from -1.5 V vs. Ag/AgCl to -0.5 V vs. Ag/AgCl at a scan rate of 5 mV/s and then reversed with the same scan rate till the starting potential. The cyclic voltammograms for both studied surfaces are presented in Fig. 4. From Fig. 4 it can be seen that upon the onset of the transpassive region, the current still raises up until the potential is reversed in the case of galvanized steel in natural sea water solution. On the other hand, the current of the transpassive region decreases for low alloy steel, forming a reduced anodic peak and this behavior can be attributed to the rust layer formed on the surface.

The highlighting of the localized corrosion susceptibility in the presence of chloride ions in the sea water of galvanized steel can be seen very well due to the specific hysteresis aspect which is present in the anodic transpassivation part of the plotted curve (1) in Fig. 4.

At the end of the narrow passive region for galvanized steel, the pitting potential breaks down the

passive film and pits initiate on the zinc layer surface. This is indicated by the rapid increase in the passive current density without any sign for oxygen evolution, as a consequence of the passivity breakdown. The low alloy steel has revealed the expanded passive domain due to the formation of a rust layer and the appearance of general corrosion. This type of comportment was observed by K. M. Zhody *et al.* [16] when they studied the corrosion behavior of leaded-bronze in sea water.
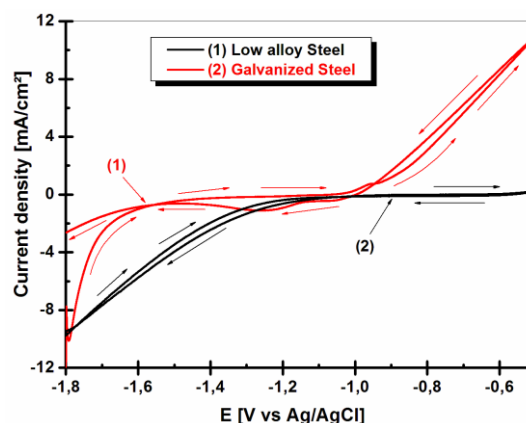
Fig. 4. *Cyclic voltammograms in sea water for: (1) uncoated steel and (2) galvanized steel*

3.5. Optical microscopy

Ex-situ investigations of surfaces were performed with an optical microscope. In Fig. 5 are presented the optical micrograph of low alloy steel and galvanized steel before and after electrochemical assays.

From Fig. 5 (a) it can be observed that the low alloy steel before the corrosion study has a non-uniform surface, the marks of atmospheric corrosion attack being visible, in special pitting corrosion.

For galvanized steel, in Fig. 5 (b) before electrochemical tests there are shown the marks of zinc flow produced in hot dip galvanizing treatment. The low alloy steel after electrochemical tests presents a surface with generalized corrosion (Fig. 5 (c)) and significant amounts of corrosion products (rust). For galvanized steel (Fig. 5 (d)), it can be observed only the pitting corrosion with small diameter pits which confirm the results of cyclic voltammetry tests.

The overall electrochemical corrosion results confirm the improving of corrosion resistance offered by the galvanizing treatment to form a zinc layer on the low alloy steel surface.
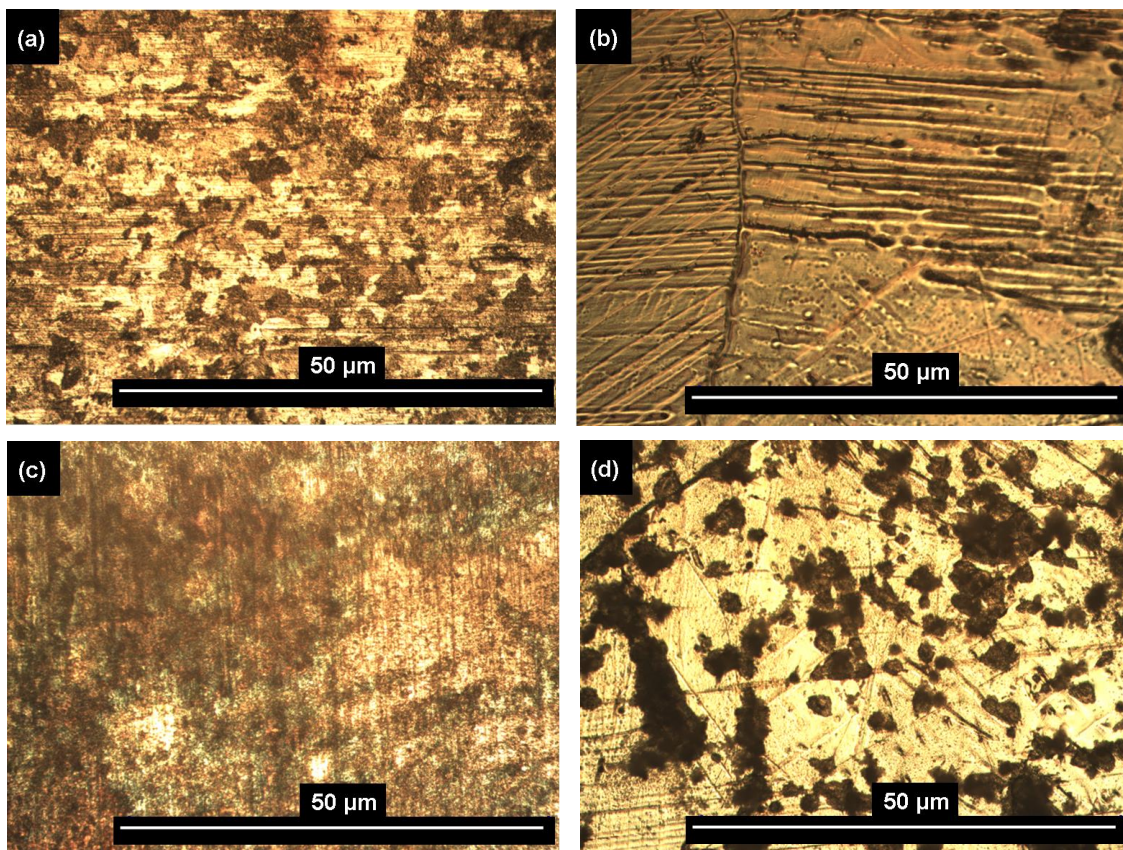
***Fig. 5**. Optical microscopy of low alloy steel: (a) before corrosion and (c) after corrosion and galvanized steel: (b) before corrosion and (d) after corrosion*

4. Conclusion

In this paper it was studied the corrosion behavior of low alloy steel and galvanized steel in natural sea water. From the results offered by the electrochemical methods used in our research, the following conclusions can be drawn:

- the zinc coating improves the polarization resistance of steel comparatively to uncoated low alloy steel suggesting an increase of corrosion resistance. The higher corrosion rate corresponds to low alloy steel as compared to galvanized steel.

- from the Tafel representation of potentiodynamic polarization diagrams, it can be observed that the decrease of current density is associated to the decrease of corrosion rate for galvanized steel.

- the cyclic voltammograms reveal a higher susceptibility to pitting corrosion for galvanized steel as compared to low alloy steel which presents higher general corrosion.

- the zinc coating increases the lifetime for naval steel and this is materialized in lowering maintenance costs.

Acknowledgements

References

[1]. H. Li, H. Yu, T. Zhou, B. Yin, S. Yin, Y. Zhang, *Effect of tin on the corrosion behavior of sea-water corrosion-resisting steel*, Materials and Design, 84, p. 1-9, 2015.

[2]. R. E. Melchers, *The effect of corrosion on the structural reliability of steel offshore structures*, Corrosion Science, 47, p. 2391-2410, 2005.

[3]. D. P. Schmidt, B. A. Shaw, E. Sikora, W. W. Shaw, L. H. Laliberte, *Corrosion protection assessment of sacrificial coating systems as a function of exposure time in a marine environment*, Progress in Organic Coating, 57, p. 352-364, 2006.

[4]. A. H. Al-Moubaraki, A. Al-Judaibi, M. Asiri, *Corrosion of C-steel in Red Sea: Effect of immersion time and inhibitor concentration*, Journal of Electrochemical Science, 10, p. 4252-4278, 2015.

[5]. M. A. Arenas, C. Casado, V. Nobel-Pujol, J. de

Damborenea, *Influence of the conversion coating on the corrosion of galvanized reinforcing steel*, Cement & Concrete Composites, 28, p. 267-275, 2006.

[**6**]. **C.-Y. Tsai, J-S. Liu, P.-L. Chen, C.-S. Lin**, *A roll coating tungstate passivation treatment for hot-dip galvanized sheet steel*, Surface & Coatings Technology, 205, p. 5124-5129, 2011.

[**7**]. **B. Ramezanzadeh, M. M. Attar, M. Farzam**, *Corrosion performance of a hot-dip galvanized steel treated by different kinds of conversion coatings*, Surface & Coatings Technology, 205, p. 874-884, 2010.

[**8**]. **D. T. Oloruntoba, O. O. Oluwole, E. O. Oguntade**, *Comparative study of corrosion behavior of galvanized steel and coated Al 3103 roofing sheets in carbonate and chloride environments*, Materials and Design, 30, p. 1371-1376, 2009.

[**9**]. **E. Diler, B. Rouvellou, S. Rioual, B. Lescop, G. Nguyen Vien, D. Thierry**, *Characterization of corrosion products of Zn and Zn–Mg–Al coated steel in a marine atmosphere*, Corrosion Science, 87, p. 111-117, 2014.

[**10**]. **M. Mouanga, M. Puiggali, B. Tribollet, V. Vivier, N. Pébère, O. Devos**, *Galvanic corrosion between zinc and carbon steel investigated by local electrochemical impedance spectroscopy*, Electrochimica Acta, 88, p. 6-14, 2013.

[**11**]. **A. Pritzel dos Santos, S. M. Manhabosco, J. S. Rodrigues, L. F. P. Dick**, *Comparative study of the corrosion behavior of galvanized, galvannealed and Zn55Al coated interstitial free steels*, Surface & Coatings Technology, 279, p. 150-160, 2015.

[**12**]. **Y. Y. Chen, S. C. Chung, H. C. Shih**, *Studies on the initial stages of zinc atmospheric corrosion in the presence of chloride*, Corrosion Science, 48, p. 3547-3564, 2006.

[**13**]. **F. Rosalbino, G. Scavino, D. Macciò, A. Saccone**, *Influence of the alloying component on the corrosion behavior of zinc in neutral aerated sodium chloride solution*, Corrosion Science, 89, p. 286-294, 2014.

[**14**]. **V. Padilla, A. Alfantazi**, *Corrosion film breakdown of galvanized steel in sulphate–chloride solutions*, Construction and Building Materials, 66, p. 447-457, 2014.

[**15**]. **S. S. Xin, M. C. Li**, *Electrochemical corrosion characteristics of type 316L stainless steel in hot concentrated seawater*, Corrosion Science, 81, p. 96-101, 2014.

[**16**]. **K. M. Zohdy, M. M. Sadawy, M. Ghanem**, *Corrosion behavior of leaded-bronze alloys in sea water*, Materials Chemistry and Physics, 147, p. 878-883, 2014.

CORROSION BEHAVIOR OF Ni-P COATED STEEL STRIPS

Gina Genoveva ISTRATE, Tamara RADU
"Dunarea de Jos" University of Galati, Faculty of Engineering
e-mail: gina.istrate@ugal.ro

ABSTRACT

In addition to high hardness, Ni-P coatings obtained by the electroless method are widely used due to their high corrosion resistance. The corrosion resistance depends on the content of phosphorus in the coating. Various phosphorus contents result from changes in pH in the process of obtaining layers. The layers obtained in different working conditions were tested for electrochemical corrosion. Tests were conducted on a potentiostat PGP 201. There were plotted and analyzed the anodic polarization Tafel curves for different phosphorus contents, pH conditions and time-exposure in the coating bath. Analyzing the anodic polarization curves it is noticed that low phosphorus sample shows an almost continuous corrosion process while samples with high phosphorus content have slow corrosion in the 3.5% NaCl testing medium.

KEYWORDS: coating, electroless method, corrosion

1. Introduction

Ni-P chemical coatings are obtained by means of autocatalytic method using a nickel salt (sulphate or chloride) and a reductant (sodium hypophosphite) [1, 2]. Protective layers of Ni-P have many features such as hardness and high wear resistance, corrosion resistance, acceptable ductility [3, 4]. One of the most common reasons for using chemical coatings of Ni-P in functional applications is their excellent resistance to corrosion.

As shown in Figure 1, 30% of these types of coating applications refer to their increased resistance to corrosion [5].
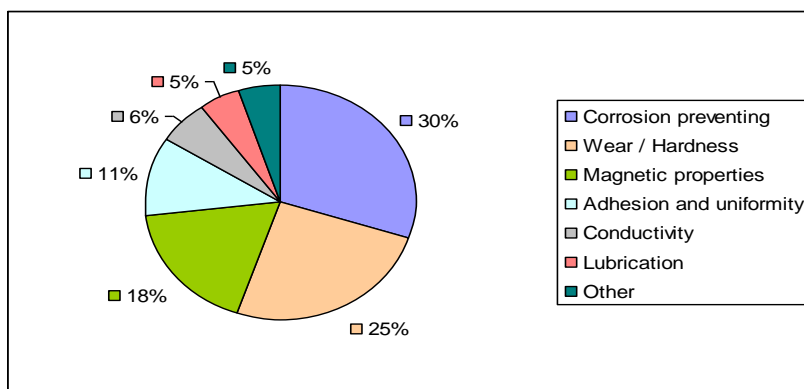
Fig. 1. *Ni-P layer applications* [5]

Compared to electrochemical coatings [6], deposits obtained by the chemical method are usually less porous and more resistant to corrosion (to equal thickness).

In warm highly alkaline solutions, low phosphorus coatings are more resistant to corrosion than those with high content of phosphorus [7].

However, alloys having high content of phosphorous provides increased corrosion resistance in most corrosive environments [8].

The high corrosion resistance of Ni-P coatings is due to the formation of a nickel coating which acts as a barrier to oxygen diffusion onto the metal surface. In general, the corrosion resistance of the Ni-

P coatings is improved by increasing the content of P so that the layers with high phosphorus content and amorphous structures feature a very high resistance to corrosion [9].

2. Experimental research

Corrosion tests were conducted using PGP 201 potentiostat connected to an electrochemical three-electrode cell: working electrode – sample being tested on the surface of which measures were made, counter - electrode of platinum and the saturated calomel electrode, Hg/Hg_2Cl_2, as reference electrode (SCE = + 241 mV/ENH). The system was connected to a computer with VOLTAMASTER 4 software for data analysis. The samples to be tested (working electrode) were isolated on one side prior to immersion into the test solution, i.e. 3.5% NaCl solution.

The corrosion test of each sample begin by monitoring the corrosion potential (open circuit potential – OCP) until this has reached the stationary value.

For potentiodynamic polarization tests, the scanning speed of 2 mV/s was used.

Plotting and interpretation of the Tafel curves give information on the corrosion current density, polarization resistance and the corrosion rate of the systems tested.

Figure 2 illustrates the polarization curves for three coating layers of different phosphorous contents. The Tafel parameters listed in Table 1 show close corrosion behavior for the samples code P1 and P3, P2 having the best resistance to corrosion.
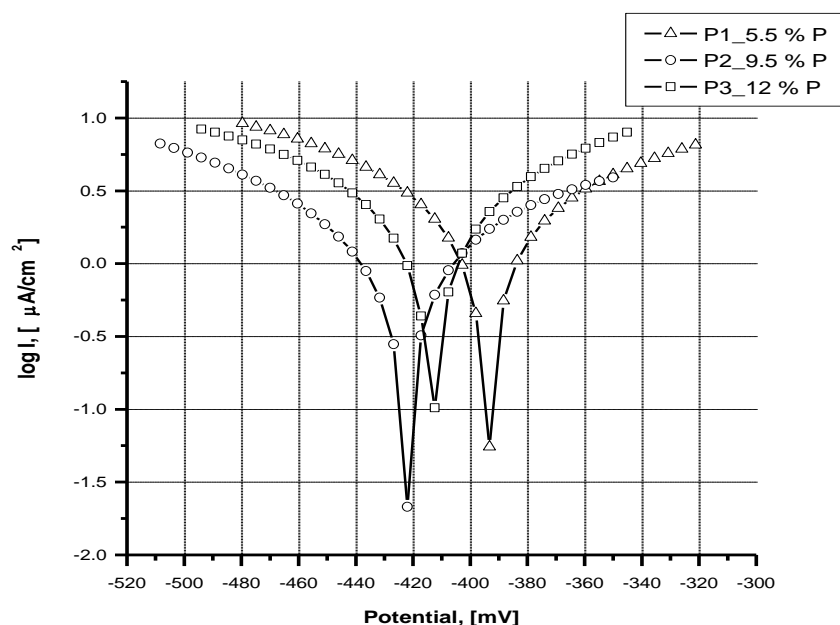
Fig. 2. Comparative polarization potentiodynamic curves for
Ni-P coatings with different phosphorous contents (in 3.5% NaCl solution)

Table 1. Results from the potentiodynamic polarisation curves for Ni-P coatings with different phosphorous contents

Sample	Potential [mV]	Rp [kohm cm^2]	I cor [μA/cm^2]	βa [mV/decade]	βc [mV/decade]	V cor [μm/an]
P1 _ 5.5 % P	-393.4	10.15	2.40	127	-144.5	24.73
P2 _ 9.5 % P	-422.5	16.07	1.35	124.2	-121.5	13.96
P3 _ 12 % P	-413.3	8.96	1.30	127.6	-140.0	23.66

For Ni-P coatings, the lowest corrosion rate in NaCl 3.5% (13.96 μm/year) was obtained with the Ni coating having 9.5% P content and the highest value of the corrosion rate (24.73 μm/year for the Ni coating with low P content (5.5% P).

Since the duration of the coating process affects the layer thickness and this further influences the corrosion resistance, the corrosion behavior was tested on the samples obtained at different times of immersion for obtaining coatings.

Results are shown in Table 2 and Figure 3.

The lowest corrosion rate in NaCl 3.5% (14.35 μm/year) was obtained for the Ni coating achieved in 20 minutes and the highest corrosion rate (83.73 μm/year) for the Ni coating obtained in 10 minutes.

It can be seen that with increasing the time of exposure in the chemical deposition bath, corrosion rate decreases with increasing layer thickness.

Table 2. *Results from the potentiodynamic polarisation curves for Ni-P coatings obtained at different times of immersion*

Sample	Potential [mV]	Rp [kohm cm^2]	i cor [μA/cm^2]	βa [mV/decade]	βa [mV/decade]	V cor [μm/an]
P4_10 minutes	-521.7	2.28	8.1459	68.7	267.8	83.72
P5_15 minutes	-454.4	2.76	6.9861	77.8	199.9	71.80
P6_20 minutes	-392.1	12.22	1.3964	104.8	105.1	14.35
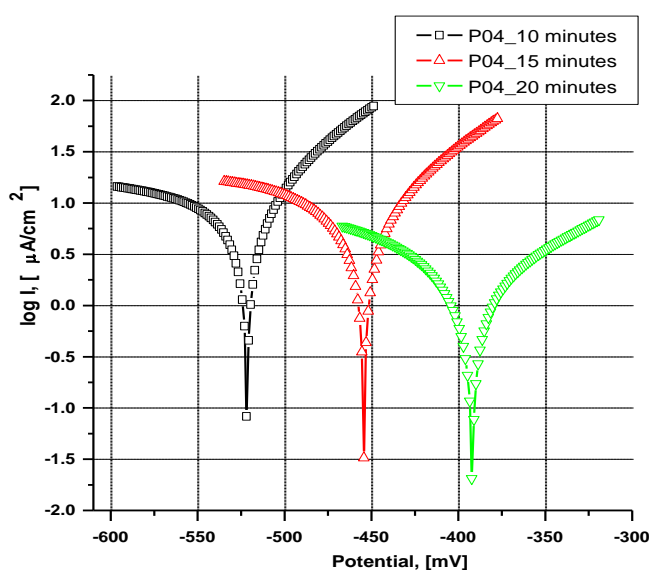
Fig. 3. *Comparative polarization potentiodynamic curves for Ni-P coatings obtained at different times of immersion (in 3.5% NaCl solution)*

Since at different pH of the nickel plating bath different chemical compositions of Ni-P coatings are obtained, the corrosion behavior was analyzed on samples obtained with different values of pH, maintaining the other parameters constant, respectively duration (10 minutes) and temperature (83 ºC).

The best corrosion behavior as resulting from the polarization curves (Figure 4) is to be found with the samples obtained at pH = 5. At this pH value, high phosphorous content is achieved that enriches the nickel, thus increasing the coating corrosion resistance. Also at pH = 5 under the same conditions of temperature and time, thicker layers are obtained as compared to those at pH = 4 and pH = 3.5, respectively.

Table 3 illustrates the Tafel parameters achieved for these samples.

Table 3. *Results from the potentiodynamic polarisation curves for Ni-P coatings obtained at different pH values*

Sample	Potential [mV]	Rp [kohm cm^2]	i cor [μA/cm^2]	βa [mV/decade]	βc [mV/decade]	V cor [μm/an]
P7_ pH ≈5	-357.7	10.86	1.26	86.4	90.7	12.96
P8_ pH ≈4	-347.4	9.09	1.69	99.2	98.9	17.40
P9_ pH ≈3.5	-367.4	16.73	1.39	169.1	119.6	14.37
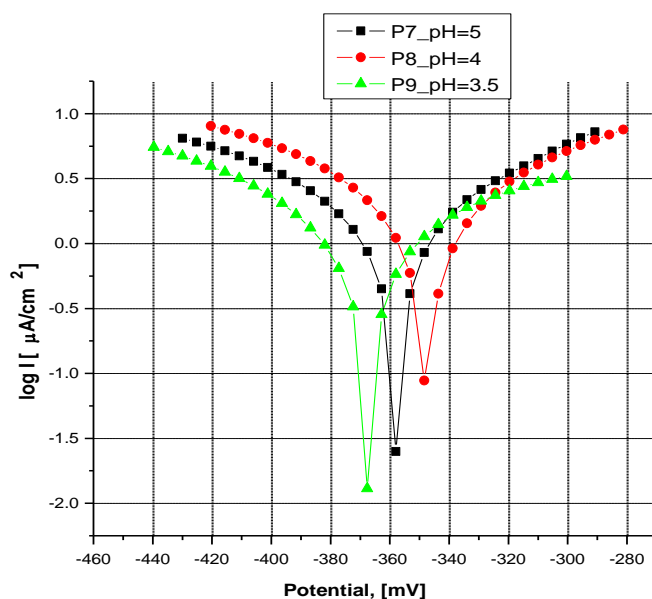
Fig. 4. *Comparative polarization potentiodynamic curves for*
Ni-P coatings obtained at different pH values (in 3.5% NaCl solution)

In order to explain the corrosion behavior of the samples analyzed, it is of interest to study and account for their anodic polarization curves.

Figure 5 shows the anodic polarization curve of the Ni-P layer obtained at different pH's which gives them different contents of P, the concentration of this element being greater as the pH is lower. We can say that P5 sample has the highest phosphorus content

and P10 sample the lowest. By analyzing the curves in Figure 5 it is observed that the sample with a low content of phosphorus (pH = 6) features an almost continuous process of corrosion and high phosphorus-containing samples obtained at lower pH have a slow corrosion, the evolution of oxygen depolarization being virtually constant at P7 sample.
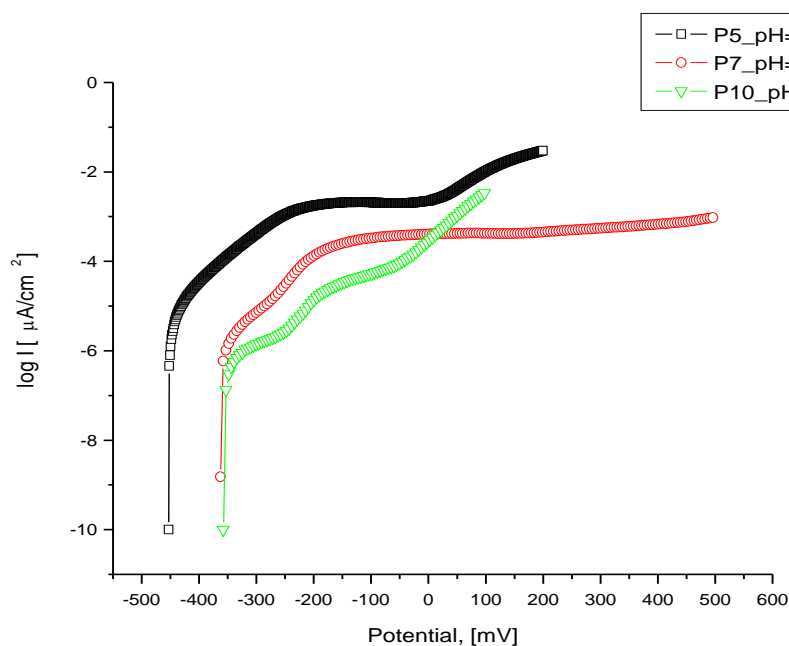
Fig. 5. *The anodic polarization curve of the Ni-P layer obtained*
at different pH values (in 3.5% NaCl solution)

3. Conclusions

The Ni-P layers can be distinguished in terms of their resistance to corrosion based on the content of phosphorus as given by the pH of the nickel plating bath and the coating thickness which varies with the duration of immersion, the temperature and pH of the nickel-plating bath.

The best corrosion behavior is obtained for the Ni-P layers with 9.5% phosphorus obtained at a pH of 5 to a minimum immersion time of 10 minutes at 85 ºC. The highest value of the corrosion rate (24.73 μm/year) resulted by coating with Ni and low P content (5.5%).

The anodic polarization curves indicate for the sample obtained at pH 5 a very slow evolution of the corrosion process as compared to the upward continuous evolution of the sample obtained at pH= 6 with a low content of phosphorus.

References

[1]. A Babanejhad, M Hashemi, Y Rahmatallahpur and SH A Nozad, *Effect of lactic acid on nucleation morphology and surface roughness of electroless Ni-P deposition in nanoscale*, Bull. Mater. Sci., vol. 35, no. 4, p. 561-566, 2012.

[2]. Glenn O. Mallory, Juan B. Hajdu, *Electroless Plating – Fundamentals and Applications,* American Society of Civil Engineers 1990.

[3]. Mordechay Schlesinger, Milan Paunovic, *Electroless deposition of nickel* in Modern Electroplating 5th Edition, ISBN 978-0-470-16778-6, 2010.

[4]. I. E. Ayoub, *Study of electroless Ni-P plating on stainless steel,* The Online Journal on Mathematics and Statistics (OJMS) vol. 1, no. 1, Reference Number: W10-0028 13, p. 13-16.

[5]. F. Reidenbach, *ASM handbook, surface engineering, vol* 5. ASM International, Materials Park, Pages p. 290-310, 1994.

[6]. A. C. Ciubotariu, L. Benea, M. Lakatos–Varsanyi, V. Dragan, *Electrochemical impedance spectroscopy and corrosion behaviour of Al_2O_3 –Ni nano composite coatings*, Electrochimica Acta, 53, p. 4557-4563, 2008.

[7]. Fernando B. Mainier, Maria P. Cindra Fonseca, Sérgio S. M. Tavares, Juan M. Pardal, *Quality of Electroless Ni-P (Nickel-Phosphorus) Coatings Applied in Oil Production Equipment with Salinity,* Journal of Materials Science and Chemical Engineering, 1, p. 1-8, 2013.

[8]. T. S. N. Sankara Narayanan, I. Baskaran, K. Krishnaveni, S. Parthiban, *Deposition of electroless Ni–P graded coatings and evaluation of their corrosion resistance,* Surface & Coatings Technology, 200, p. 3438-3445, 2006.

[9]. K. Hari Krishnan, S. John, K. N. Srinivasan, J. Praveen, M. Ganesan, P. M. Kavimani, *An Overall Aspect of Electroless Ni-P Depositions*-A Review Article, Metallurgical and Materials Transactions A, vol. 37A, p. 1917-1925, 2006.

LASER DEPOSITION OF BRONZE ALUMINUM ON STEEL SUPPORT

Simona BOICIUC
„Dunarea de Jos" University of Galati
e-mail: simonaboiciuc@yahoo.com

ABSTRACT

In order to rise the wear and corrosion resistance of 0.45% C superficial steel layers, a multilayer coating was tested by injection of powder with 88.3% Cu; 9.5% Al; 2.2% Fe in melted bath by CO_2 continuous wave laser. Layers made by different laser conditions were characterized by macro and microstructure analysis, phase quality analysis, by X ray diffractometry and microhardness analysis. Research was carried out regarding the importance of nickel alloy intermediary layer for the rising of cladding quality.

KEYWORDS: laser cladding, aluminum bronzes, microstructure, microhardness, diffractometry.

1. Introduction

Biphasic aluminum bronzes are known for their outstanding wear resistance, cavitation, corrosion etc., widely used in naval, petrochemical, chemical industry, etc. (bearings, rods, valve, pump impellers, and compressor screws and rotors, etc.).

Copper alloys with 9-11% Al feature, in addition to high corrosion resistance, good casting and hot forming properties and heat treatment hardening capacity of martensitic quenching and tempering.

According to the equilibrium diagram, Cu-Al alloys have balanced structure consisting of plastic solid solution α and eutectoid ($\alpha + \gamma_2$), where γ_2 is a solid hard and brittle solution based on the electronic $Cu_{32}Al_{19}$, compound.

Classical quenching consists of [1-3] heating at temperatures of 980-1000 °C in the β solid solution range based on the Cu_3Al, electronic compound, followed by rapid cooling in water. According to the thermal kinetic diagram, at higher cooling rates there is a diffusion transformation, with the solid solution ordering $\beta \rightarrow \beta_1$, after which the diffusion-free transformation of phase β_1 occurs in a needle-type martensite structure β' [1-3].

This structure has a relatively low hardness due to the coarse grain formed at high temperatures and in the presence of phase α. Subsequent tempering at 400-550 °C causes reverse transformations: $\beta' \rightarrow \beta_1$ and β_1 phase decomposition in a dispersed mixture $\alpha + \gamma_2$, having hardening effect.

Thus the CuAl10Fe4Ni4 alloy after quenching from 980 °C in water and tempering at 400 °C, increases its hardness from 170-200 HB to over 400 HB.

In the special Cu-Al alloys there are additions of Fe, Ni, Mn, which change the solubility of aluminum in copper and lead to new phases. Iron polishes granulation and improves mechanical and antifriction properties. In Fe-rich alloys an intermetallic compound $FeAl_3$ may occur with hardening and embrittlement effect. Nickel and manganese increase corrosion resistance and provide further hardening by solid solution alloying.

Laser heating has the advantage that it provides very fast heating rates (over 10^3 °C/s) at high temperatures and similar cooling speed, which allows hardening of aluminum with bronze both in liquid and solid phases while maintaining an ultrafine granulation [4-8]. Laser surface quenching, however, has the disadvantage of relatively small thickness of the hardened layer, a certain variation of the properties of the hardened layer depth and the need for subsequent tempering [9-11].

Multilayer deposition of aluminum bronze powders injected onto the laser melted surface has the advantage of making thick layers with uniform chemical composition and properties throughout the section.

This paper presents laboratory experimental research on multilayer deposit on a steel support by injecting biphasic aluminum bronze powders in a laser molten bath.

2. Experimental conditions

2.1. Sample preparation

For coating, use was made of a two-phase aluminum bronze powder, capable of hardening by quenching. Table 1 shows the origins, chemical composition and particle shape of the addition materials. The powder was aspherical, so that fluid flowing on the surface of processed addition material was stimulated by vibration. Since the coating with aluminum bronze on the steel support indicated a low quality of the deposited layers geometry (rough surface, thin deposit and micro-cracks), its deposition on a buffer layer of nickel alloy was experienced and a very good deposition on steel substrate was found.

Coatings were made on samples of 25 x 25 x 15 mm of 0.45% C normalized carbon steel.

Table 1. Characteristics of the added materials used

Nr. crt.	Type of added material	Chemical composition of added material	Grain shape
1	Nickel alloy „Alliages Speciaux 7569 ALLIAGES FRITTÉS, Franța".	8.9% Cr; 4.5% Fe; 5.1% B; 2.4% Al; 0.6% Cu; rest Ni.	
2	Bronze with alluminum „Rototec Proces FRIXTEC CASTOLIN U.S.A.".	9.5% Al; 2.2% Fe; rest Cu.	
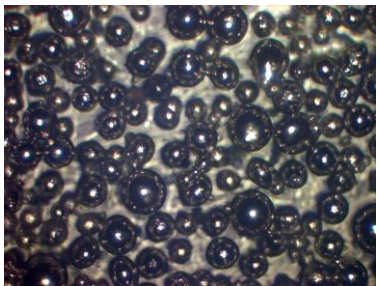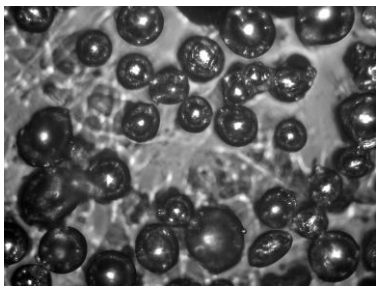
Laboratory experiments were conducted on a CO_2 continuous wave laser facility type GT with power of 1400 W, with coordinate table and computer for the process control, equipped with a powder injection system on the support surface.

Laboratory tests used a 1.8 mm diameter laser beam, which made partially overlapping parallel strips. The final thickness of the layer was achieved by superposition of five layers.

To determine the optimum deposition regime, the added material flow rate was varied, Q, from 53 to 150 mg/s, beam power, P, from 900 to 1200 W, surface scanning speed, v, from 5-7 mm/s and transverse movement step, p, 1 to 2 mm.

The nickel alloy buffer layer was deposited by the superposition of two layers, under the following conditions: Q = 53 mg/s, P = 1100 W, v = 7 mm/s, p = 1-2 mm. Table 2 shows the experimented working regimes and thickness, h, of the deposits obtained. Deposition regime was characterized by energy density factor $K = P / d * v$, which ranged within $79.3 \div 100$ J/mm².

2.2. Structural properties

Initially deposited layers were characterized by macroscopic analysis of the surface layer deposited. Microstructural analysis was performed on samples cross-section, perpendicular to the direction of laser processing.

The microstructure of the samples was observed by optical microscopy Olympus BX 51M.

For the phase qualitative analysis of the surface layer deposited, use was made of the diffractometer DRON 3 with copper anti-cathode, monochromatic diffraction beam, U = 34 kV, I = 30 mA; $F_1 = 2$ mm; $F_2 = 0.5$mm; $\omega = 1°$/min; $v_{strip} = 720$ mm/h for the diffraction angle variation within $2\theta = 20°....75°$.

2.3. Microhardness depth profile measurement

It was determined the microhardness profile HV0,1 (0.98N load) over the depth of the deposited

layers. Microhardness depth profiling measurements were performed using a PMT-3 apparatus.

Vickers microhardness was calculated according to the SR EN ISO 6507-1:2002 standard. Results are presented as a mean of three measurements.

3. Results and discussions

3.1. Structural properties

Macroscopic analysis highlights the deposited layer surface quality, thickness and adhesion to the support.

The macrostructures of the laser deposition of aluminum bronze show a low adhesion to the carbon steel support, which can be explained by the poor metal link due to the low solubility of solid copper in iron.

The surface layer is rough (Fig. 1) and requires subsequent removal by machining of a relatively large layer. Inside the layers, solidification shrinkage cracks have appeared. The coating is hardened and made brittle by diffusion of iron from the base material into the added material and formation of the compound $FeAl_3$.

Table. 2. Experimental conditions and deposited layer thickness

Sample code	Q [mg/s]	P [W]	v [mm/s]	K [J/mm²]	P [mm]	h [mm]	Observations
Bronze aluminum deposition on steel support							
1	86	1000	7	79.36	2	0.38	C
2	86	1100	7	87.30	2	0.5	C
3	110	900	7	71.42	2	0.16-0.54	C, N
4	150	900	5	100.00	2	0.06-0.49	C, N, E
5	150	1100	7	87.30	2	0.13-1.00	C, N
6	119	1100	7	87.30	2	0.08-1.23	C, N
7	119	1200	7	95.24	2	0.14-1.21	C, N
Bronze aluminum deposition on steel support, with middle nickel alloy layer							
8	53	1100	7	87.30	2	0.47	-
9	53	1100	7	87.30	1.5	0.74	-
10	53	1100	7	87.30	1	0.64	-

Note: C-cracks; N-non uniformities of the layer thickness, E-exfoliation

From Table 2 and Figure 1, it can be seen that the non-uniform thickness of the layer deposited under the same conditions and the surface roughness increase with increasing the added material flow rate over 86 mg/s (sample code 2, 5 and 6). This is explained by the increased added material flow rate under the same conditions of laser processing, the molten bath temperature decreases by additional energy consumption for heating and melting the powder, which increases the viscosity of the molten added material. With lower laser beam powers and higher flow rates, there is insufficient melting of the support material and lack of adhesion of the deposited layers (sample code 4). With the same added material flow rate, the layer thickness increases with higher laser beam power, more pronounced at higher flow rates (sample code: 1 and 2, 4 and 5). These macroscopic observations indicate that the samples code 1...7 show no practical interest.

The decrease in the added material flow rate to 53 mg/s and the use of a buffer layer of nickel alloy, unlimitedly soluble as solid in both iron and copper, increased the adhesion to the steel support and to the deposited layer. The layer quality was significantly improved as this becomes uniform, compact, without solidification shrinkage cracks and with practical applicability. Note that when using a 1.8 mm diameter laser beam on the surface being processed, the max. layer thickness is obtained on a step of the transverse movement of the 1.5 mm sample.

Figures 2 and 3 show the microstructure of the deposited layer for samples code 1 and 10. Good support adherence of the deposited layer is visible. At the fusion limit there are no compactness defects or inclusions of metal. When coating is directly performed on steel support, the presence of transverse cracks is initiated at the solidification surface (Fig. 2a), while by using the buffer layer of nickel alloy, the deposited layer is compact and crack-free (Fig. 3a).

The microstructure of the deposited layer results from melting and ultra-fast solidification of the added material, followed by a partial self-tempering in the overlapping area of the strip deposited i.e. sub-layer tempering when an additional layer is deposited.
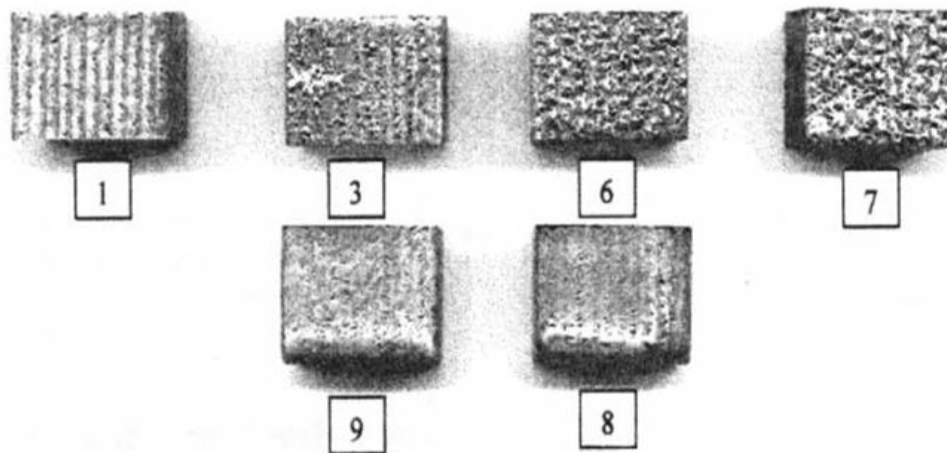
Fig 1. Macroscopic aspect of some thick bronze-aluminium samples
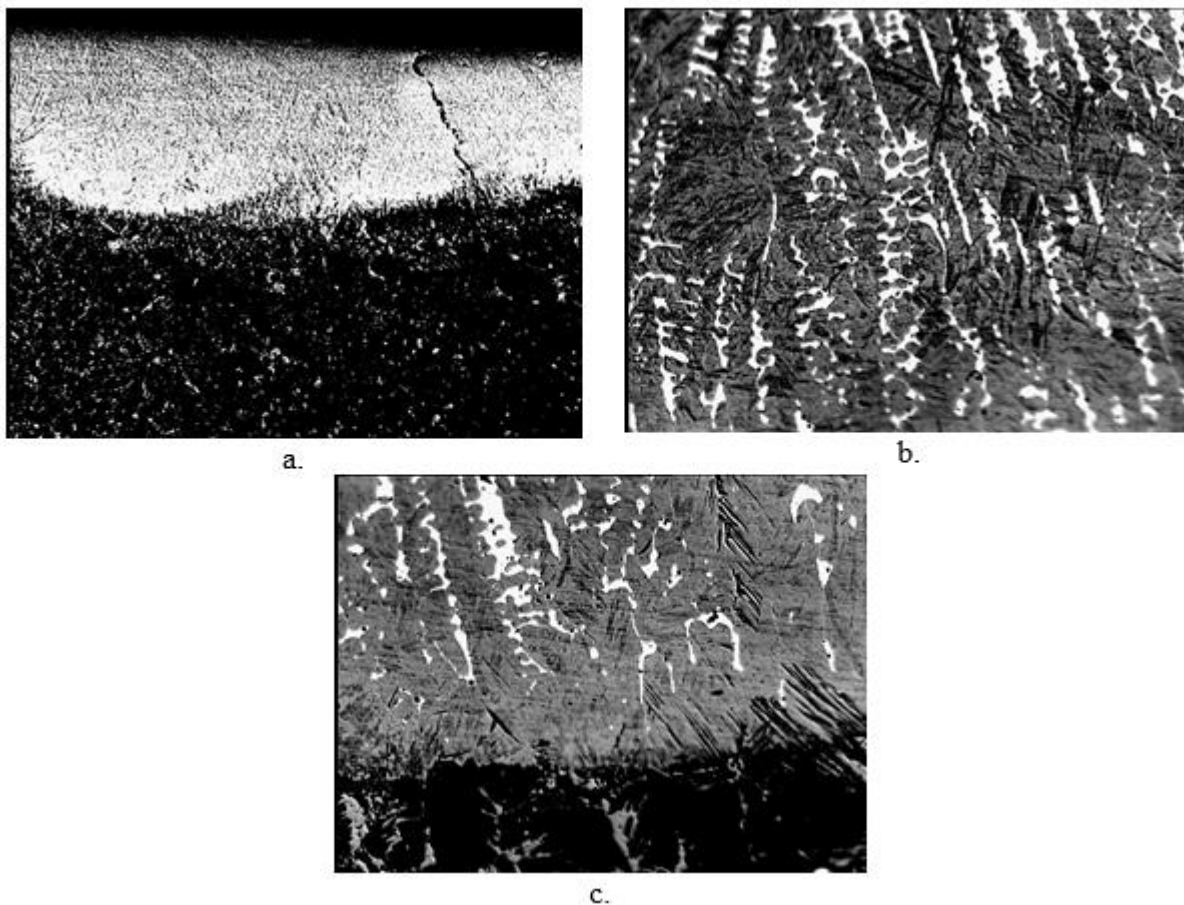
***Fig. 2**. Microstructure of the deposited layer with sample code 1 without Ni alloy middle layer a), general view x500; b). Middle of the deposited layer x1000; c). Base of the deposited layer x1000. Ferric chloride attack*
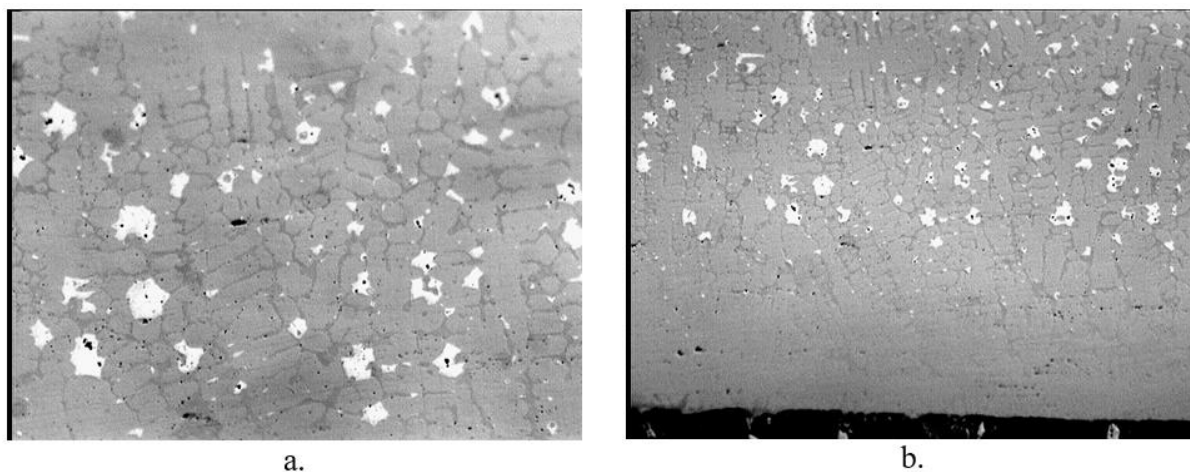
Fig. 3. *Microstructure of the deposited layer with sample code 10 with Ni alloy middle layer a).*
Middle part of the deposited layer x1000; b). Base of the deposited layer x1000.
Ferric chloride attack

For example, with sample code 1, the basic microstructure is fine columnar dendritic, at certain points with needle type appearance specific to hardening martensitic structures with coarse interdendritic separation of an intermetallic compound according to the diffraction diagram for the qualitative phase analysis of the deposited layers (Fig. 4). In the copper-based solid mass solution there is the interdendritically separated compound Fe - Al (Fig. 2b). The occurrence of relatively large quantities of compound is because the 2.2% Fe content in the added material is added to the iron by melting a steel substrate. Initiation and propagation of transverse shrinkage cracks upon solidification can be accounted for by the hard and brittle compound. At the base of the deposited layer there is a small thickness dilution layer which makes the transition to the steel support with a small amount of Fe-Al compound. With the sample code 10, the microstructure is similar to a smaller amount of intermetallic compound – K - phase-intermetallic compound of Fe, Al, Ni (Fig. 5) with rosette aspect, because the layer of molten nickel alloy, which alloys the filler material, had a smaller amount of iron and the nickel presence slows the diffusion processes upon compound separation.

Additional nickel alloying of the added material led to a solid solution of copper, more resistant to metallographic attacks.

The unlimited solubility of copper and the nickel bases of the added material and buffer do not allow for the creation of a buffer zone separating the two deposits.
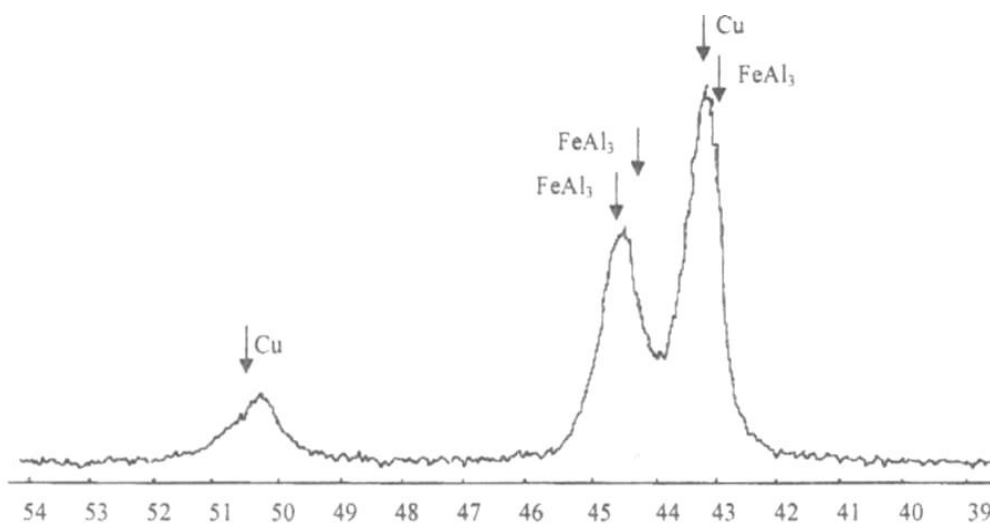
Fig. 4. *Diffractogram for the layer cladded for sample code 1*
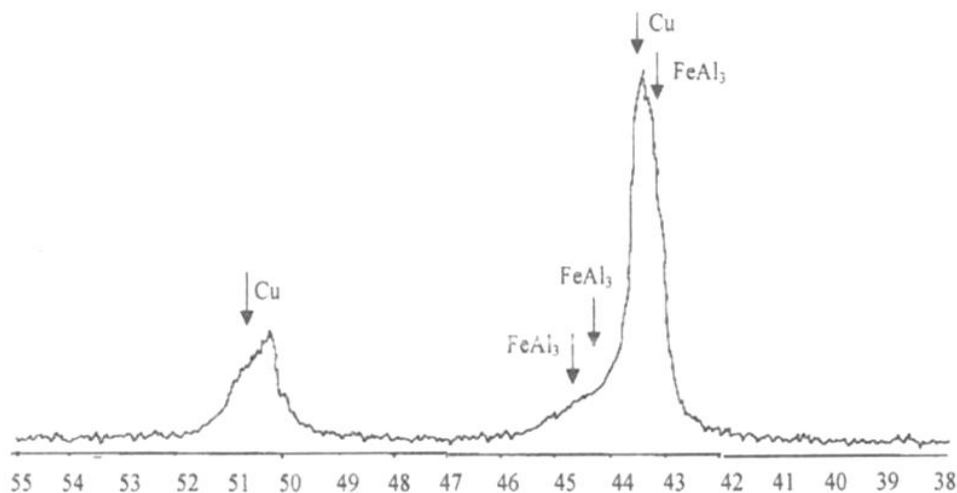
Fig. 5. Diffractogram for the layer cladded for sample code 10

3.2. Microhardness depth profile measurement

Figure 6 shows the variation of microhardness HV0.1 over the depth of the layer deposited on the sample code 1 and 10. Microhardness maximum corresponds to a sample code 1, due to the presence of $FeAl_3$ compound in large amount and due to the stability of the martensitic structure to the quick tempering process.

The layers obtained with nickel alloy buffer layer have less hardness because nickel reduces the amount of intermetallic compound and increases the amount of the additionally alloyed solid solution of copper. Microhardness is maximal in the buffer layer of the nickel alloy with higher thermal stability.
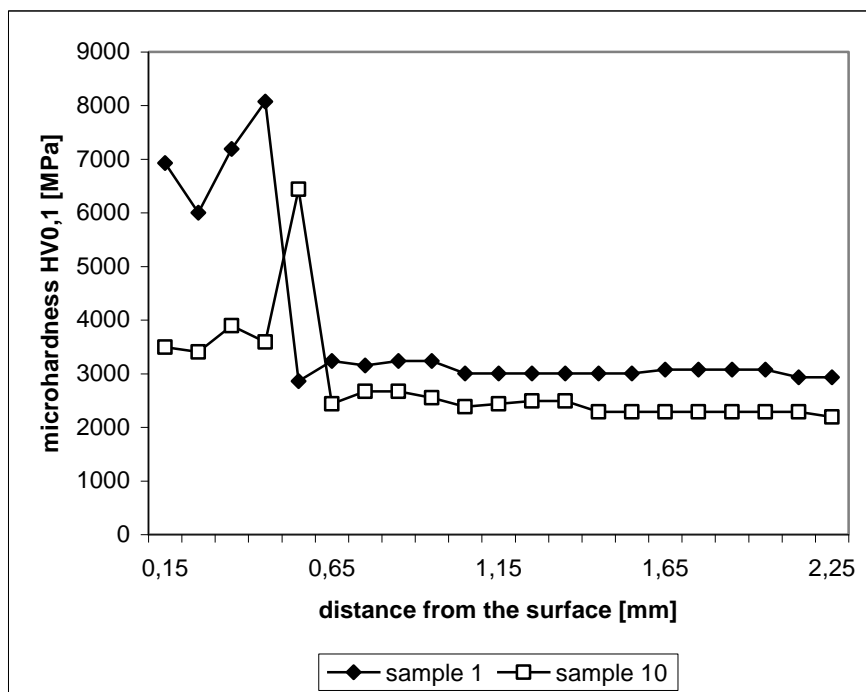
Fig. 6. Variation of microhardness HV0.1 over the depth of the layer deposited on the sample code 1 and 10

Comparing the microhardness of the multilayer deposit by laser with the properties of the aluminum bronzes, laser hardened in the liquid phase and tempering [5-7], it was found that laser deposition

resulted in higher microhardness and greater depths. This is due to alloying bronze with nickel and iron, to the finer microstructure and the self-tempering process.

4. Conclusions

Multilayer deposition by aluminum bronze powder injection into the laser melted bath on steel base presents difficulties because of the poor adhesion of the deposit to the steel support, the non-uniformities of the deposited layer and shrinkage cracks. The coating is hardened and made brittle by diffusion of iron from the base material into the added material and by the formation of $FeAl_3$ compound.

Non-uniformity of the deposition increases with the deposit filler flow rate over 86 mg/s and lower laser beam power, below 1000 W.

Introducing a buffer layer of nickel alloy has improved adhesion, thickness uniformity and compactness of the aluminum bronze deposited layers. The optimum deposition regime was nickel alloy middle layer, regimes 9 and 10, which ensured a 0.64 to 0.74 mm thick layer with a microhardness HV0,1 ranging between 3895 and 3406 MPa.

Multilayer deposit ensures self-tempering of the layer and provides a superior microhardness at depths greater than the liquid phase quenching of aluminum bronzes of similar chemical composition.

References

[1]. **Jan Lodewijk de Mol van Otterloo**, *Surface engineering with lasers*, Thesis, Shell Research and Technology Centre, Amsterdam, 1996.
[2]. **Shi Z, Bloyce A, Sun Y, Bell T.**, *Effect of Processing Parameters on Structure and Properties of Surface Melted Aluminum Bronze*, Eoromat, vol. E+D, p. 365-371, 1995.
[3]. **Levcovoci S. M., Levcovici D. T., Paraschiv M. M.**, *Laser Hardening of Aluminum Bronzes*, Materials and manufacturing processes, vol. 17, p. 13-22, 2002.
[4]. **M. F. Schneider**, *Laser cladding with powder*, Ph. D. Thesis University of Twente, Enschede, Olanda, 1998.
[5]. **H. Gedda**, *Laser surface cladding - a literature survey*, Lulea University of Technology, Division of Materials Processing, Suedia, 2000.
[6]. **D. Salehi**, *Sensing and control of Nd:YAG laser cladding process*, Ph. D. Thesis, Swinburne University of Technology, Melbourne, Australia, 2005.
[7]. **R. P. Martukanitz, S. S. Babu, J. M. Vitek**, *Development of Advanced Wear and Corrosion Resistant Systems through Laser Surface Alloying and Materials Simulation*, Applied Research Laboratory, State College, PA 16804, Oak Ridge National Laboratory.
[8]. **F. Vollertsen, K. Partes, J. Meijer**, *State of the art of Laser Hardening and Cladding*, Proceedings of the Third International WLT – Conference on Lasers in Manufacturing, Munich, 2005.
[9]. **S. Levcovici, D. T. Levcovici, C. Gheorghieș, S. Boiciuc**, *Laser Cladding of Ni-Cr-B-Fe-Al Alloy on a Steel Support*, The International Thermal Spray Conference and Exposition (ITSC), 15-17 may, Seatle, USA, ISBN 0-87170-836-1.
[10]. **S. Boiciuc, S. Levcovici, D. T. Levcovici, C. Gheorghies**, *Characterisation of hard coatings obtained by laser cladding process*, Metalurgia international, 9, p. 32-39, 2008.
[11]. **S**. **Boiciuc, et al.**, *EDX Analysis of Laser Cladding Layers with Ni-Cr-B-Fe-Al Alloy*, Conference UgalMat, Galati, Romania, 2009.

OPTIMIZATION OF THERMAL PROCESSING PARAMETERS OF A HIGH STRENGTH ALUMINUM ALLOY

Marian-Iulian NEACSU, Doru HANGANU

"Dunarea de Jos" University of Galati
e-mail: uscaeni@yahoo.com

ABSTRACT

The work shows a calculation meant to optimize the thermal processing parameters (time and temperature) of a high strength aluminum alloy. The optimization calculation has been done by gradient method which involves multi-step (iteration) calculation of thermal processing parameters in which the values of the mechanical properties meet certain restrictions imposed. Identifying the most economic variants of heat treatment of those resulting from the application of gradient method was carried out by performing calculations of heat balance of the heat-treatment oven.

KEYWORDS: optimization, thermal processing, gradient method, parameters, heat balance

1. Introduction

Among the non-ferrous metals and alloys currently used in the top fields of engineering, aluminium and its alloys have the greatest weight due to the properties and characteristics of this metal and especially due to the classical hardening techniques of these alloys. Aluminium and its alloys occupy a foreground position in the category of metallic materials with great applications in engineering industry through a vast range of uses. The extensive use of aluminium alloys is due to its good mechanical properties which are obtained after thermal and/or thermo-mechanical processing.

By optimisation we understand the operation of studying a problem with a view to obtaining a result which, compared to other possible results at that moment, is the best, the most advisable and the one based on which a technical or economical decision can be made [1].

Optimizing thermal processing parameters allows for the selection of those existent parameters and conditions which will determine the best technico-economic performance of the process (choosing optimal parameters) [3, 5]. At the basis of any technological process, there is a mathematical model which has to express the respective process as precisely as possible. The mathematical model being the main element in running the process, its accurate design is of utmost importance for describing the process as accurately as possible, which means that there should be a high concordance between the

model and the process it describes [4, 5]. By determining some values of the independant variables we can determine the optimal solution so that the best value for the objective function (the function to be optimized) should be obtained [3]. According to each case, the optimum value of the objective function can mean its maximum or minimum value. The optimization methods are usually decreasing methods which express the minimum of a function U of n real variables which is called *aim* or *objective function*. In the case of optimizing the thermal processing parameters of the studied alloy, the objective function is represented by the energy consumption "$Q = f(t, \tau)$", taking into account some restrictions as far as the values of the analyzed mechanical properties are concerned.

2. The gradient method for optimizing the thermal treatment process of the studied alloy

The alloy studied belongs to the Al-Zn-Mg-Cu system and has the composition presented in Table 1.

The optimization calculation was achieved by the gradient method which implies the calculation of the thermal processing parameters in multiple situations (reiterations) which comply with certain conditions (restrictions) required.

The restrictions imposed refer to the values of the mechanical properties according to EN_485-2-2007 and are given in Table 2.

Table 1. *Chemical composition of the alloy studied [mass %]*

Element / Alloy	Zn	Mg	Cu	Si	Fe	Pb	Cr	Mn	Al
AlZn6.5MgCu	6.5	2.70	1.80	0.15	0.20	0.02	0.20	0.15	rest

Table 2. *Values of mechanical properties according to EN_485-2-2007* [11]

Rm, [MPa]	Rp$_{0,2}$ [MPa]	A$_5$ [%]	HB [MPa]
540	470	7	161

Besides the restrictions for the values of the mechanical properties, there are also some restrictions for the variation interval of the thermal processing parameters, the thermal treatment time and the thermal treatment temperature. They must have the following values:

$$120\ °C \le t \le 200\ °C \qquad (1)$$
$$4\ hours \le \tau \le 20\ hours \qquad (2)$$

The mechanical properties studied are:
- Mechanical resistance Rm, [Mpa];
- Yield resistance Rp$_{0,2}$, [Mpa];
- Tensile elongation A5, [%];
- Brinell hardness HB.

The following mathematical equations are used for optimization, which are obtained after carrying out the mathematical modelling for each property analyzed.

$$Y_1 = 664.2589 - 1.1953 \cdot t + 7.6093 \cdot \tau - 0.0292 \cdot t \cdot \tau, \qquad (3)$$

$$Y_2 = 627.371 - 1.262 \cdot t + 8.25 \cdot \tau - 0.032 \cdot t \cdot \tau, \qquad (4)$$

$$Y_3 = 7.25 + 0.014 \cdot t - 0.1 \cdot \tau + 0.00031 \cdot t \cdot \tau, \qquad (5)$$

$$Y_4 = 169.5357 - 0.2906 \cdot t + 4.687 \cdot \tau - 0.019 \cdot t \cdot \tau, \qquad (6)$$

Where: Y_1 = Rm; Y_2 = Rp$_{0,2}$; Y_3 = A$_5$; Y_4 = HB.

The gradient method is an iterative method which by multiple iterations facilitates finding the optimal complex of properties which comply with the restrictions simultaneously.

Partial derivatives of the function Y1 (t, τ) were calculated, (Y1 is the main mechanical feature for which the maximum value is imposed in the given circumstances):

$$\frac{\partial Y_1}{\partial t} = -1.195 - 0.029 \cdot \tau \qquad (7)$$

$$\frac{\partial Y_1}{\partial \tau} = 7.609 - 0.029 \cdot t \qquad (8)$$

The gradient vector for Y1, which is the traction resistance, is:

$$grad\ Y_1 = (-1.1953 - 0.029 \cdot \tau;\ 7.609 - 0.029 \cdot t) \qquad (9)$$

As starting point is chosen the point having the coordinates: t1 = 120 °C, τ_1 = 20 hours, the point where the calculation of the minimum starts after the gradient direction.

Replacing the values of t1, τ_1 in the gradient expression of Y1 we have: grad Y$_1$(1) = (-1.079; -4.129.).

The next stage is checking the boundary conditions in the initial point and it indicates that the properties of resistance as well as those of malleability are satisfied:

Rm(1) = 602.9289 MPa;
Rc(1) = 564.131 MPa;
HB(1) = 182.8037;
A$_5$(1) = 7.674 %.

In order to find the optimal point(s), we proceed as follows:
- the variation step h = - 0.4 is chosen;
- a useful step for carrying out the transformation at the initial point is shown by a vector of the form [9]:

$$-\quad x_{i(N+1)} = x_{i,N} + h \cdot \frac{\partial Y_{i,N}}{\partial x_{i,N}},\quad i = 1,2,...k \qquad (10)$$

- the relationship: $x_{i(N+1)} = x_{i,N} + h \cdot \dfrac{\partial Y_{i,N}}{\partial x_{i,N}}$ (11)

is calculated:

i = 1,2,...k, the coordinates of point 2, where x_i represents the heat treatment variables (t, τ):

t$_2$ = 120.71 ºC; τ_2 = 18.348 ore;

- Rm, Rp$_{0,2}$, A$_5$ and HB are calculated with the help of the mathematical models, and replacing t, τ, with t$_2$, τ_2 we obtain:

Rm(2) = 619.056 MPa;
Rc(2) = 572.081 MPa;
A$_5$(2) = 7.011 %;
HB(2) = 180.148.

The restrictions are checked by iteration 2. t, τ calculated with the relation (11) are replaced in the relationship (10) and we obtain: grad Y1 (2) = (-

1.727; 4.108) which is important for calculating the variables t_3, τ_3 at the next iteration.

Using the same calculation algorithm, which is edited in MATLAB program package, 40 iterations were solved for finding those values which comply with the conditions imposed by the restrictions.

The mechanical properties of the studied alloy, obtained by calculation by applying the gradient method for the 40 iterations, are represented in figures 1, 2, 3.
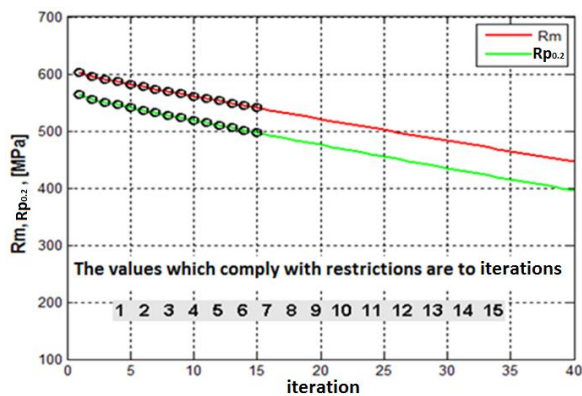
Fig. 1. Graphical representation of the values of mechanical and yield resistance obtained by calculation using the gradient method for the 40 iterations (the marked ones are those which comply with the imposed conditions)
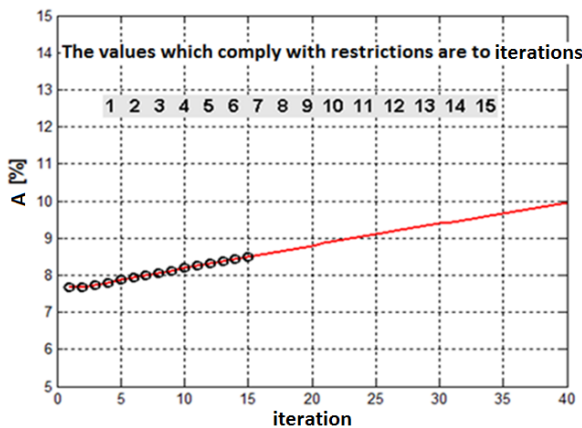
Fig. 2. Graphical representation of the values of tensile elongation obtained by calculation using the gradient method for the 40 iterations (the marked ones are those which comply with the imposed conditions)

For the iterations 1, 2, 3, 4, 5, 6, 7, 8, 9, 10, 11, 12, 13, 14, 15, it results from the calculation that the values of the mechanical properties studied as well as for the thermal treatment parameters t, τ are in accordance with the conditions imposed by the restrictions (Table 1 and relationships 1 and 2). The values imposed for the properties by the Euro norm in use are reached for temperature values between 120 °C and 123.5 °C, while the time values range between 6 and 20 hours. In order to establish which of these values is optimum economically as well, the calculations for energy consumption were made.
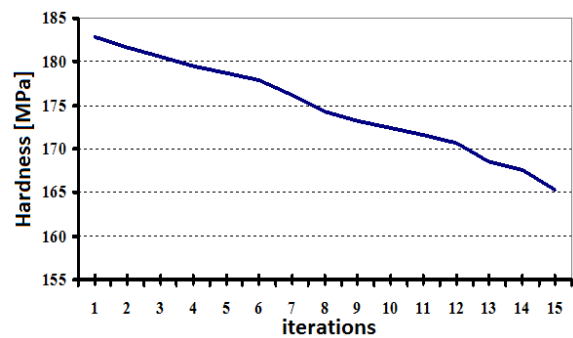
Fig. 3. Graphical representation of the values of the values of Brinell hardness obtained by calculation using the gradient method for the 15 iterations

3. Calculation of thermal energy consumption Q, [kWh]

In order to find out which of the 15 variants of thermal treatment is the optimum variant from the economic point of view, the calculation of the thermal energy consumption Q, [kWh] is made.

The calculation of the energy consumption under the form of heat (thermal energy) means the calculation of the total energy consumed at the thermal treatment oven where the artificial ageing is made according to the thermal processing variant and the relationship below:

$$Q_{total} = Q_{total\ oven} \qquad (12)$$

$Q_{total\ oven}$ – the quantity of heat necessary for attaining and maintaining the treatment temperature over the whole period of the thermal treatment.

The oven on which the thermal treatment was carried out is an electrically heated oven with silit bars made of chamotte refractory brick, lined with mineral wool and having steel sheet on the outside. The energy consumed for performing the thermal heat treatment will be determined after carrying out the thermal balance of the treatment oven.

The energy consumption will be expressed by the quantity of heat necessary to maintain the treatment temperature while the thermal treatment is applied (Figure 4), according to the relationship:

$$Q_{total\ oven} = Q_A + Q_B \qquad (13)$$

Q_A – the quantity of heat consumed (energy) during heating the oven;

Q_B - the quantity of heat consumed (energy) during maintaining the heat treatment temperature;
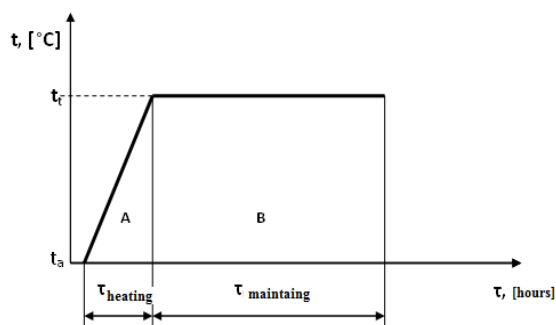
Fig. 4. *Thermal treatment diagram*

A – oven heating time from the ambient temperature to the thermal treatment temperature;

B – period of maintaining the heat treatment temperature inside the oven;

$\tau_{heating}$ – oven heating time, [hours];

$\tau_{maintaining}$ – time of maintaining the oven at the treatment temperature, [hours];

t_a – ambient temperature, [ºC];

t_t – thermal treatment temperature, [ºC].

The heat necessary to raise the temperature inside the oven from the ambient temperature to the heat treatment temperature is [37]:

$$QA = Q_{ac\ sample\ A} + Q_{ac\ zid\ A} + Q_{pierd\ zid\ A} \qquad (14)$$

Qac pies A- the heat accumulated in the pieces (samples) during the oven heating.

$$Q_{ac\ sample\ A} = m_{sample} \bullet c_{sample} \bullet \Delta t1, [kJ] \qquad (15)$$

m_{sample} – sample mass, [kg];

$$\Delta t1 = tt - ta, [°C]$$

Δt_1 – the difference of temperature between the treatment temperature and the ambient temperature.

The samples (pieces) subject to artificial ageing heat treatment have the dimensions of 150x60x3 mm.

$$Q_{ac\ zid\ A} = (m_{cs} \cdot c_{cs} + m_{vm} \cdot c_{vm} + m_t \cdot c_t) \cdot \Delta t_1, [8, 9], [kJ], \qquad (16)$$

$Q_{ac\ zidarie\ A}$ – the heat accumulated in the oven walls during heating;

c_{cs} – specific heat of the chamotte brick;

c_{vm} – specific heat of the mineral fibre;

c_t – specific heat of the steel sheet;

m_{cs} – mass of the oven chamotte refractory brick;

m_{vm} – mass of the mineral fibre used for oven covering;

m_t – mass of the steel sheet used for oven coating;

$m_{cs} = V_{cs} \cdot \rho_{cs}$;

V_{cs} – volume of the chamotte refractory brick used to build the oven;

ρ_{cs} – density of the chamotte refractory brick;

$Q_{pierd\ zidarie\ A}$ – the heat lost through the oven walls during heating which is calculated using the heat flow, Φ_A;

$$Q_{pierd\ zidarie\ A} = \Phi_A \cdot \tau_A, [Wh] [37, 38] \qquad (17)$$

τ_A – heating time for the inside of the oven, [h];

Φ_A – the heat flow during the heating period A is:

$$\Phi_A = k_1 \cdot S \cdot \Delta t_2, [W] \qquad (18)$$

$\Delta t_2 = t_m - t_a, [°C]$

Δt_2 – difference of temperature between the average temperature and the ambient temperature [37, 38].

$$\Phi_A = \Phi_{orizA} + \Phi_{vert\ A} [37], [W] \qquad (19)$$

Φ_{orizA} – the heat flow through the horizontal walls of the oven during heating;

Φ_{vertA} – the heat flow through the vertical walls of the oven during heating;

$$\Phi_{oriz\ A} = k_{1oriz} \cdot 2 \cdot S_{oriz} \cdot \Delta t_2 [37, 38] [W] \qquad (20)$$

k_{1oriz} – global coefficient of heat transfer through the horizontal walls of the oven during oven heating up to the thermal treatment temperature;

S_{oriz} – surface of a single horizontal wall of the oven;

$$\Phi_{vert\ A} = k_{1vert} \cdot 2 \cdot S_{vert} \cdot \Delta t_2 [W], [8] \qquad (21)$$

k_{1vert} – global coefficient of heat transfer through the vertical walls of the oven during its heating up to the thermal treatment temperature;

$$S_{vert} = S_{vert\ 1} + S_{vert\ 2} \qquad (22)$$

S_{vert} – surface of all vertical walls of the oven;

Q_B, the heat necessary to maintain the samples inside the oven at the heat treatment temperature, equals the heat lost through the oven walls during this whole period.

$$Q_B = Q_{pierdere\ zidărie\ B}, [kJ] \qquad (23)$$

This can be expressed using the heat flow Φ_B:

$$\Phi_B = k_2 \cdot S \cdot \Delta t_1 [W], [8] \qquad (24)$$

Φ_B – heat flow during maintaining the samples at the thermal treatment temperature;

$\Phi_B = \Phi_{orizB} + \Phi_{vertB}$ [W], [8];

Φ_{orizB} – heat flow through the horizontal walls of the oven during maintaining the samples at the thermal treatment temperature;

$$\Phi_{oriz\,B} = k_2 \cdot 2 \cdot S_{oriz} \cdot \Delta t_1, \text{ [W], [8]} \qquad (25)$$

Φ_{vertB} – heat flow through the vertical walls of the oven during maintaining the samples at the thermal treatment temperature;

$$\Phi_{vert\,B} = k_2 \cdot S_{vert} \cdot \Delta t_1 \text{ [W], [37]} \qquad (26)$$

$$k_2 = \frac{1}{\dfrac{\delta_1}{\lambda_1} + \dfrac{\delta_2}{\lambda_2} + \dfrac{\delta_3}{\lambda_3} + \dfrac{1}{\alpha_2}} \text{ [W/m}^2\text{·K], [8]} \qquad (27)$$

K_2 – global coefficient of heat transfer during maintaining the oven at the thermal treatment temperature;

$$\alpha_{2oriz} = \beta_{oriz} \cdot \sqrt[4]{t_t - t_a} + \frac{\varepsilon \cdot C_0}{t_t - t_a} \cdot \left[\left(\frac{t_t + 273}{100} \right)^4 - \left(\frac{t_a + 273}{100} \right)^4 \right]$$

[kJ/m²·h·K], [8]   (28)

$$\alpha_{2vert} = \beta_{vert} \cdot \sqrt[4]{t_t - t_a} + \frac{\varepsilon \cdot C_0}{t_t - t_a} \cdot \left[\left(\frac{t_t + 273}{100} \right)^4 - \left(\frac{t_a + 273}{100} \right)^4 \right]$$

[kJ/m²·h·K], [8]   (29)

α_{2vert} – coefficient of convection and radiation heat transmission through vertical walls during the maintaining period;

α_{2oriz} – coefficient of convection and radiation heat transmission through horizontal walls during the maintaining period;

$$Q_{\text{pierdere zidărie B}} = \Phi_B \cdot \tau_B, \text{ [kWh], [8]} \qquad (30)$$

τ_B – sample maintaining time at the heat treatment temperature, [h].

After making the energy consumption calculations for the 15 situations (Appendix 2), when the values prescribed for the mechanical properties are obtained, the following variation of the energy consumption was obtained, according to Fig. 6.
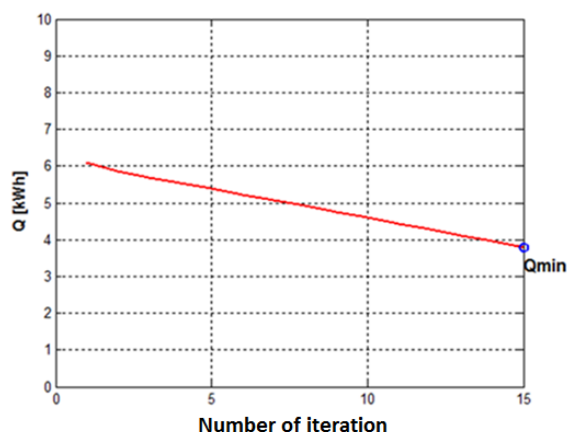
Fig. 5. *Variation of energy consumption for the 15 iterations*

4. Conclusions

From the data presented in Fig. 5, we can conclude that the optimum regimen that ensures the simultaneous accomplishment of the values of the mechanical properties imposed at the lowest energy consumption is the one given by iteration 15, having the following technological parameters:

- artificial ageing temperature t = 123.52 ºC;
- ageing time τ = 6.021 hours;

The values of the mechanical properties obtained for these parameters are:

- mechanical resistance Rm = 540.7 MPa;
- yield resistance $Rp_{0,2}$ = 496.78 MPa;
  - tensile elongation A_5 = 8.49 %;
  - Brinell hardness HB = 165.35.

By applying the gradient method as a calculation variant for the thermal treatment optimization, the following aspects could be noticed:

- the artificial ageing temperature for complying with the properties restrictions imposed ranges between 120 °C and 123.5 °C.

- the values of the thermal treatment time are between 6 and 20 hours.

References

[1]. **Ciucă I. Dumitriu S**., *Modelarea şi Optimizarea Proceselor Metalurgice de Deformare Plastică şi Tratamente Termice*, Editura Didactică şi Pedagogică, Bucureşti, 1998.
[2]. **Cosmeleaţă G., ş.a.,** *Fundamental principles of Physical Metallurgy*, Editura. Printech, Bucureşti, 2000.
[3]. **Taloi D. ş.a**., *Optimizarea proceselor metalurgice*, Editura Didactică şi Pedagogică, Bucureşti, 1983.
[4]. **Taloi D.,** *Optimizarea proceselor tehnologice – aplicaţii în metalurgie*, Editura Academiei, Bucureşti, 1987.
[5]. **Şerban R., Dumitrescu T.,** *Metode de optimizare*, Editura Matrix Rom, Bucureşti, 1998.
[6]. **Şerban V., Raduţă A**., *Ştiinţa şi ingineria materialelor*, Editura Politehnica Timişoara, 2010.

[7]. Firețeanu V., Ghinea M., *MATLAB. Calcul numeric. Grafica. Aplicații*, Editura Teora București, România, 1995.
[8]. Popa B., Man E., Popa M. *Termotehnică, agregate și instalații termice*, Editura tehnică, București, 1979.
[9]. Leca A., Prisecaru I., *Proprietăți termofizice și termodinamice: solide, lichide, gaze*, vol. 1, Editura Tehnică, București, 1994.

[10]. Dulamita T. Florian E., *Tratamente termice si termochimice*, Editura Didactica si Pedagogica, Bucuresti, 1982
[11]. ***, *Aluminium Asociation - SR-EN 485/2/2007 – Aluminium and aluminium Alloys - Sheet strip and plate - Mechanical Propertis.*

DEPOSITION TECHNOLOGIES FOR OBTAINING THIN FILMS WITH SPECIAL PROPERTIES

Cătălin-Andrei ŢUGUI[1], Petrică VIZUREANU[1], Carmen NEJNERU[1]
Manuela-Cristina PERJU[1], Mihai AXINTE[2], Simona-Mădălina BĂLŢATU[1]
[1]"Gheorghe Asachi" Technical University of Iasi, Romania, Department of Technologies and Equipments for Materials Processing, 51 Mangeron Blvd., 700050, Iasi, Romania
[2]"Gheorghe Asachi" Technical University of Iasi-Romania, Department of Materials Science,
41 Mangeron Blvd., 700050, Iasi, Romania
e-mails: tzugui.andrei@yahoo.com, peviz2002@yahoo.com

ABSTRACT

The properties of metallic materials can be improved by deposition of materials. The coating has a tear strength and better hydro-abrasive corrosion. The thin layer deposition has a thickness of less than 10 micrometers.

When speaking about deposition technologies, it is not just about deposited thin layers, but the whole assembly (layer / substrate), therefore the degree of adherence and the costs of making such a substrate have to be taken into account and the whole must be much more powerful than anything taken separately.

In this paper we presented several methods of thin film deposition. We also highlighted some of the advantages and disadvantages of several deposition methods.

Keywords: Deposition method, thin layers, substrate, SEM

1. Introduction

The surface is the most important part of all components, as the most defects appear here, especially those caused by corrosion.

The surface may also have important functional attributes, it is not limited to chemical and mechanical properties, but also features thermal, electronic, magnetic and optical characteristics, influencing the choice of the material.

Depositions of thin films are used worldwide in various technologies. These deposition technologies have been successfully applied for a long time, specifically since 1400 when their first use is registered [1].

Along with traditional technologies for obtaining thin layers, we witness the development, improvement and expansion of deposition, a modern technique of the physical and physico-chemical methods, which ensure high purity and strong adhesion through a wide variety of processes for coatings [1].

The involved technologies are based on vacuum processes, with a low environment impact.

Also, from the economic point of view, these technologies have an increased efficiency, compared to the traditional methods.

Therefore, in recent years there has been a dramatic increase in using these technologies in industrial applications.

2. Theoretical contributions

Thin layers can be produced by mechanical, chemical procedures, and by condensation of the gaseous phase. The work environment is one of the basic factors of depositing, which strongly influences the composition and structure of the deposited layers.

The environment necessary for the gas-phase condensation method is vacuum or pressure controlled atmosphere, reducing the average deployment submission process that ensures the achievement of reproducible layers unaffected by impurities.

Thin films vacuum deposition methods are classified as follows:
➢ Physical vapor deposition methods (PVD) by pulse laser deposition (PLD);
➢ Chemical vapor deposition method (CVD):

• CVD deposition method at high temperatures (HTCVD);

• CVD deposition method based on organ metallic compounds (MOCVD);

• CVD deposition method of assisted plasma (PACVD).

2.1. Physical vapor deposition methods (PVD)

2.1.1. Pulsed laser deposition

Pulse laser deposition is the technique where a high power pulsed laser beam is focused inside a vacuum chamber in order to hit a target of the material that is to be deposited (Figure 1).

This material is vaporized from the target, in a plasma plume, which deposits it as a thin film on a substrate.
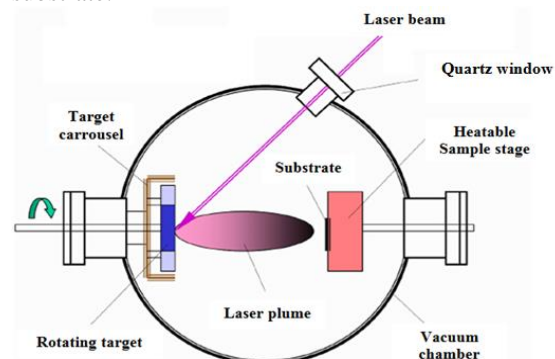
Fig. 1. *Schematic diagram of the pulse laser deposition* [2]
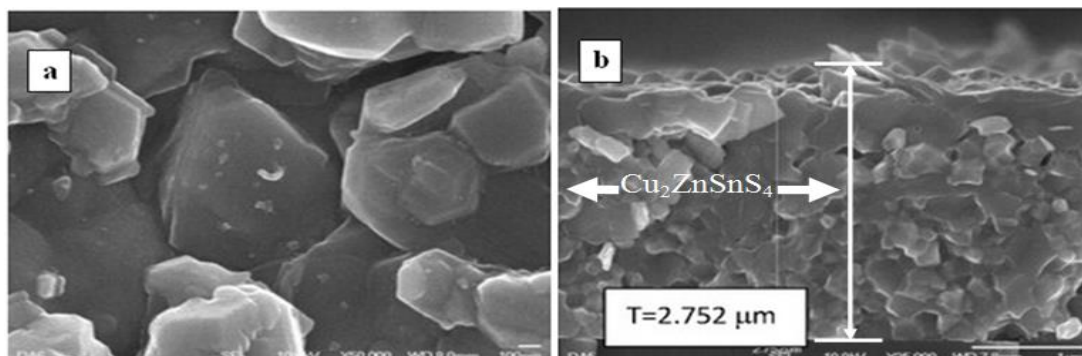
Fig. 2. *SEM images of Cu$_2$ZnSnS$_4$ thin layers obtained by using the coated PLD method: a) surface image for the thin layer; b) cross sections through coating and substrate layer* [3]

Figure 2(a) shows the SEM image of the annealed Cu$_2$ZnSnS$_4$ thin films for various deposition times. It is observed that, due to recrystallization with annealing, the resulting grain size is increased, compared to the as-deposited film.

Figure 2(b) shows the cross-sectional FE-SEM image of the annealed Cu$_2$ZnSnS$_4$ thin films.

The thickness of film is found to vary between 0.525 and 2.902 µm, which indicates that deposition time is a vital parameter to increase thickness indirectly, and to increase efficiency [2].

2.2. Chemical vapor deposition method (CVD)

2.2.1. High temperature chemical vapor deposition

The thin layer deposition methods work at high temperatures in the range of 2100-2300 ºC and a schematic diagram of this method is shown in Figure 3. With HTCVD, crystals can be produced with high

quality, large SiC diameter and costly efficient, opening new markets and applications.
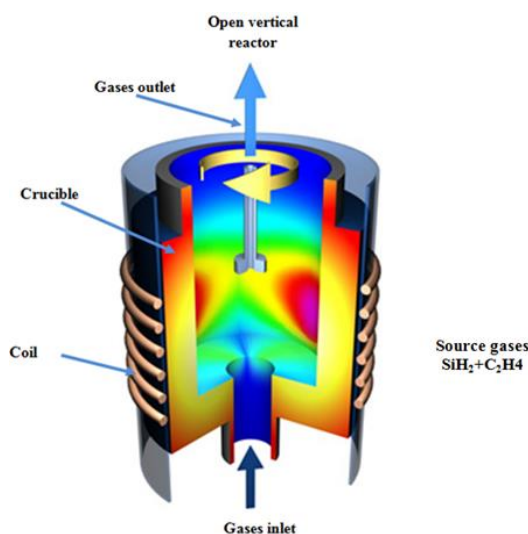
Fig. 3. *Schematic diagram of the method of high temperature CVD (HTCVD)*
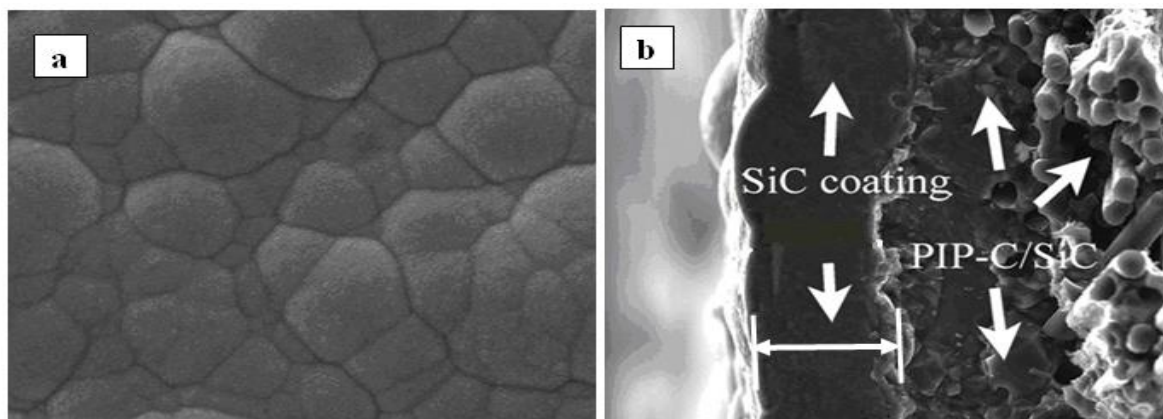
Fig. 4. *SEM images of SiC thin layers obtained by using the coated HTCVD method: a) surface image for the thin layer; b) cross sections through coating and substrate layer* [4]

Figure 4 shows the cross-section and surface morphology of HTCVD coated samples. The SiC coating has a thickness of about 30 μm and a good adhesion to C/SiC composites, Figure 4(a).

No obvious interlinear or impenetrate cracks can be observed.

The high magnification image in Figure 4(b) shows that the surface is closely stacked by spherical grains, with grain size in a range of 10-30 μm.

The coating shows a dense surface with no visible micro cracks. The SiC layer can improve the compactness of the coating and provide good oxidation protection for C/SiC composites at high-temperature [3].

High temperature, specific to HTCVD process, is a major drawback, it adversely affects the structure of the substrate, especially when it is steel. To eliminate the negative effects, both prior and subsequent heat treatments are required to reduce the negative effects of overheating [4].

2.2.2. Metalorganic chemical vapor deposition

The MOCVD method is quite simple and it consists in dissolving the organic metal compound in an organic solvent. Fig. 5 shows the diagram of the principle of this method.
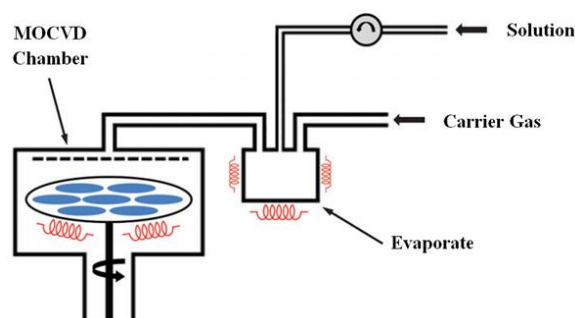
Fig. 5. *Schematic diagram of MOCVD deposition method* [5]
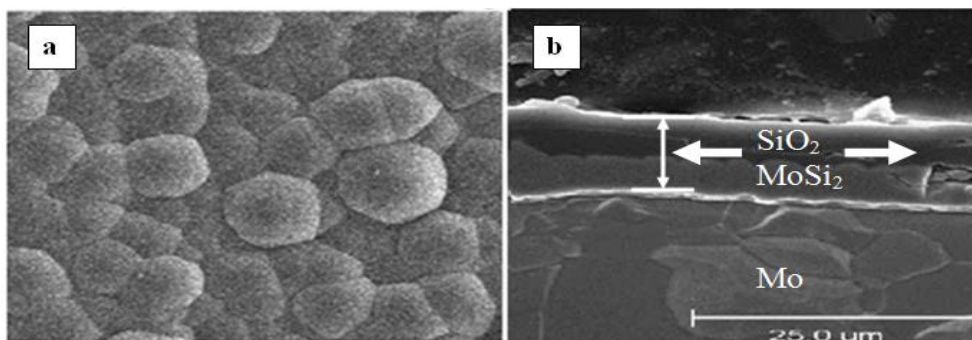
Fig. 6. *SEM images of MoSi$_2$ thin layers obtained by using the coated MOCVD method: a) surface image for the thin layer; b) cross sections through coating and substrate layer* [6]

The micrographs were obtained by a scanning electron microscope (SEM).

Figures 6(a) and (b) show the surface morphology of the specimens before and after the different stages of coatings.

The original surface of the substrate appeared to be smooth. Several cracks on the surface of the $MoSi_2$ coating were observed from high magnification SEM. The observation was not unusual as $MoSi_2$ films produced by CVD of Si on a Mo substrate are often characterized by cracks and voids [7, 8].

On further coating with silica, the surface adopted equiaxed grain morphology. Cross-sections of the coating after 3 h at 620 ℃ were analyzed by SEM.

As shown in figure 6(b), this micrograph reveals that the coating thickness was about 7.5 µm at 620 ℃ [6].

An advantage of this method is the replacement of some donors using metal organic metal compounds.

By this replacement with metal organic compounds, the deposition temperature will be greatly decreased, reaching 400 ℃.

2.2.3. Plasma assisted chemical vapor deposition

In this method, gas phase reactions are catalyzed by the CVD process specific to the presence in the reactor of cold plasma, produced by the glow discharge luminescence similar to the luminescence produced by the ion nitriding.
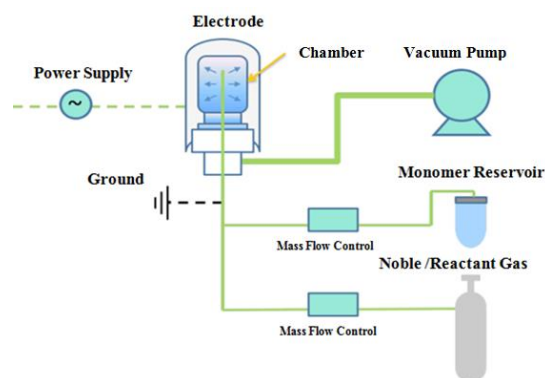
Fig. 7. *Schematic diagram of deposition method* [9]
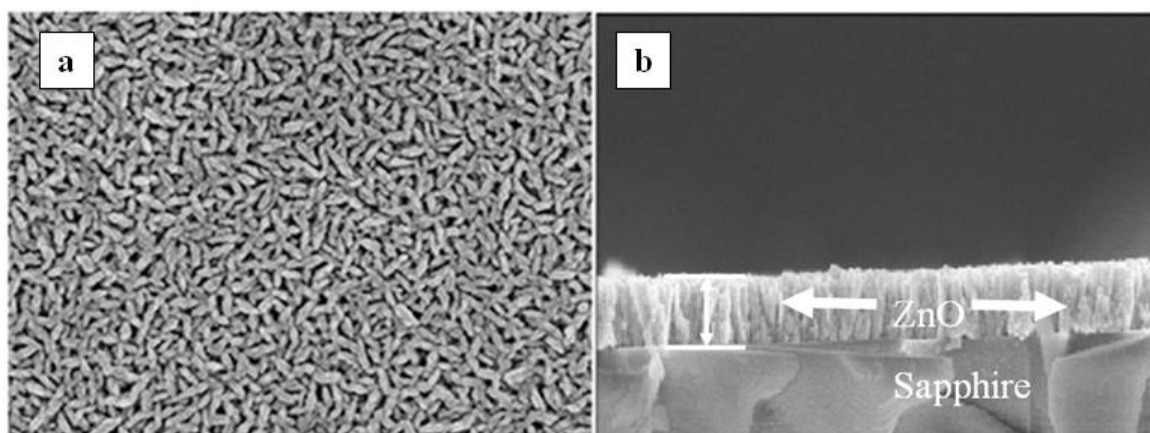
Fig. 8. *SEM images of ZnO thin layers obtained by using the coated PACVD method: a) surface image for the thin layer; b) cross sections through coating and substrate layer* [10]

Figure 8(a) represents the cross-section of the scanning electron microscopy (SEM) image for ZnO thin film grown at 185 °C.

Figure 8 (b) shows the top view of SEM image for ZnO thin films grown at 160 °C. The thickness of ZnO thin film is about 200 nm and a pillar-like structure can be found [11] in Figure 8(a).

During deposition, the atomic kinetic energy is primarily determined by the deposition temperature. Figure 8(b) exhibits a collapsed pillar structure due to the low kinetic energy and weak intensity.

3. Conclusions

From this study of layers, which presents different methods for obtaining thin films and some surfaces and depth morphology, we can conclude the following:

1. By the PLD method, high quality coatings with a wide variety of properties can be obtained.
2. The quality of ZnO thin layers is improved when increasing the sputtering power.

3. The HTCVD deposition method is not much used as high temperature affects the substrate.
4. The MOCVD method is used for the deposition of thin films when the deposition temperature is low so it affects the layer.
5. The PACVD deposition method is an advanced and widely used method.

Therefore, the choice of the method of submission shall consider both the nature of the deposited layer and the base material.

Acknowledgements

References

[1]. G. Vermesan, E. Vermeasan, *Introducere in ingineria suprafetelor (Introduction to surface engineering)*, Ed. Dacia Cluj-Napoca, 1999.
[2]. G. Subramanyam, M. W. Cole, N. X. Sun, T. S. Kalkur, N. M. Sbrockey, G. S. Tompa, X. Guo, C. Chen, S. P. Alpay, G. A. Rossetti Jr., K. Dayal, L. Q. Chen, D. G. Schlom, *Challenges and opportunities for multi-functional oxide thin films for voltage tunable radio frequency/ microwave components*, Journal of Applied Physics 114, 191301, 2013.
[3]. A. V. Moholkar, S. S. Shinde, A. R. Babar, Kyu-Ung Sim, H. K. Lee, K. Y. Rajpure, P. S. Patil, C. H. Bhosale, J. H. Kimb, *Synthesis and characterization of Cu2ZnSnS4 thin films grown by PLD: Solar cells*, Journal of Alloys and Compounds, 509, 2011.
[4]. X. Yang, L. Wei, W. Song, Z. Bi-feng, C. Zhao-hui, *Microstructures and mechanical properties of CVD-SiC coated PIP-C/SiC composites under high temperatur*, Surface & Coatings Technology, 209, p. 197-202, 2012.
[5]. G. Subramanyam, M. W. Cole, N. X. Sun, T. S. Kalkur, N. M. Sbrockey, G. S. Tompa, X. Guo, C. Chen, S. P. Alpay, G. A. Rossetti Jr., K. Dayal, L.Q.Chen, and D. G. Schlom, *Challenges and opportunities for multi-functional oxide thin films for voltage tunable radio frequency/ microwave components*, Journal of Applied Physics 114, 191301, 2013.
[6]. E. K. Nyutua, M. A. Kmetzc, S. L. Suiba, *Formation of $MoSi_2$–SiO_2 coatings on molybdenum substrates by CVD/MOCVD*, Surface & Coatings Technology 200, p. 3980-3986, 2006.
[7]. H. O. Pierson, *Handbook of Chemical Deposition*, Noyes publications, Park Ridge, NJ, 1999.
[8]. J.-K. Yoon, J.-K. Jee, J.-Y. Byun, G.-H. Kim, Y.-H. Paik, J. S. Kim, Surf. Coat. Technol., 160, 2002.
[9]. ***, http://www.sio2med.com/technology-plasma-deposition.html.
[10]. P.-H. Lei, H. M. Wu, C.-M. Hsu, *Zinc oxide (ZnO) grown on flexible substrate using dual-plasma-enhanced metalorganic vapor deposition (DPEMOCVD)*, Surface & Coatings Technology, 206, p. 3258-3263, 2012.
[11]. I. Volintiru, M. Creatore, B. J. Kniknie, C. I. M. A. Spee, M. C. M. van de Sanden, *J. Appl. Phys.*, 102, 043709, 2007.

MANUSCRISELE, CĂRŢILE ŞI REVISTELE PENTRU SCHIMB, PRECUM ŞI ORICE
CORESPONDENŢE SE VOR TRIMITE PE ADRESA:

MANUSCRIPTS, REVIEWS AND BOOKS FOR EXCHANGE COOPERATION, AS WELL
AS ANY CORRESPONDANCE WILL BE MAILED TO:

LES MANUSCRIPTS, LES REVUES ET LES LIVRES POUR L'ECHANGE, TOUT AUSSI
QUE LA CORRESPONDANCE SERONT ENVOYES A L'ADRESSE:

MANUSCKRIPTEN, ZIETSCHRITFTEN UND BUCHER FUR AUSTAUCH SOWIE DIE
KORRESPONDENZ SID AN FOLGENDE ANSCHRIFT ZU SEDEN:

After the latest evaluation of the journals achieved by National Center for the Science and Scientometry Politics (**CENAPOSS**), as recognition of its quality and impact at national level, the journal is included in B$^+$ category, 215 code (http://cncsis.gov.ro/userfiles/file/CENAPOSS/Bplus_2011.pdf).

The journal is indexed in:

EBSCO: http://www.ebscohost.com/titleLists/a9h-journals.pdf

Copernicus: http://journals.indexcopernicus.com/karta.php

The papers published in this journal can be visualized on the "Dunarea de Jos" University of Galati site, the Faculty of Engineering, pages: http://www.sim.ugal.ro/Annals.htm, http://www.imsi.ugal.ro/Annals.html.

AFFILIATED WITH:
- **ROMANIAN SOCIETY FOR METALLURGY**
- **ROMANIAN SOCIETY FOR CHEMISTRY**
- **ROMANIAN SOCIETY FOR BIOMATERIALS**
- **ROMANIAN TECHNICAL FOUNDRY SOCIETY**
- **THE MATERIALS INFORMATION SOCIETY**
  (ASM INTERNATIONAL)

Edited under the care of
FACULTY OF ENGINEERING
Annual subscription (4 issues per year)